PHYSICS AND PSYCHOACOUSTICS OF PLUCKED-STRING INSTRUMENTS

Wiliam H. Roberts

A thesis submitted to Cardiff University
for the degree of Doctor of Philosophy

4/8/2015

Acknowledgements

Firstly I must thank my parents for their tremendous support, guidance and patience throughout my education, particularly during this doctorate.

Thanks to Bernard for engrossing conversations and guidance over the past seven years or so, for introducing me to the fascinating world of musical acoustics and for having faith in my abilities. Many thanks too to Ian Perry for his help with admittance and wire-break measurements, for the use of his sound-field data and for general chats on the subject of musical acoustics. Thanks to Rob Mcleod for various chats on the subject of psychoacoustics and for a few pointers on conducting listening tests.

I would also like to express my gratitude to everyone who took listening tests, especially to those who sat through a number of them. This work would not have been made possible were it not for your kindly giving up your time to listen to my sounds. Thanks to Rhys for the use of his folk guitar, and Eugene, Ben and Rhodri for the use of their banjos.

A special mention goes to the musicians I've played alongside over the past few years, who have constantly fuelled my interest in this subject; cheers Sam, Heledd, Tara, Rhys, Huw, Daf, Laura, Guto, Rhodri, Rhys, Robin, Simon, Jimmy and Winskill!

Also special thanks to Tara for making the final year of my doctorate the best it possibly could have been.

Yn olaf, diolch arbennig i fy holl deulu am fod yn gyfeillion a chefnogwyr mor frwd, ac yn enwedig i Nain am edrych drosta i.

Summary

The overall goal of this work is to help classical guitar makers to have better control over the potential sound of their instruments. This is done by correlating changes in the vibrational behaviour of an instrument with perceivable changes in its radiated sound. Three strategies have been employed in this thesis in an attempt to accomplish this goal.

An investigation is carried out on the vibrational properties and radiated sound of a classical guitar, steel-string folk guitar and a five-string banjo. The aim here is to demonstrate how large constructional differences in plucked-string instruments lead to their unique acoustical characteristics. Results demonstrate that effective masses of low-order body modes relative to higher-order ones, internal damping of strings and amount of coupling between strings and the body of an instrument are responsible for the main characteristics of these instruments' acoustical signatures.

The problem of over-coupling a string to the body of a classical guitar is then addressed. Over-coupling creates an uneven tone quality between notes, an effect known as wolf notes. Knowledge of the perceptual threshold of over-coupling, which is found using psychoacoustical tests, can help instrument makers build a strongly radiating instrument without wolf notes. Simple remedies are suggested to minimise the effects of wolf notes on existing guitars in the most effective manner.

Finally, the smallest perceivable changes are found in the parameters of a physical model of a classical guitar. The parameters that are responsible for the most perceptually obvious changes are likely to be the most important ones for the maker to control because these are the parameters to which our ears are most sensitive. The effective mass and effective area of low-order modes are studied in detail because these parameters have been identified previously as having a strong influence over the radiated sound from the instrument.

Contents

Chapter 1 Introduction

1.1 Aims

The overall goal of this work is to help classical guitar makers to have better control over the potential sound of their instruments. This is done by correlating changes in the vibrational behaviour of an instrument with perceivable changes in its radiated sound. The design-evolution of the classical guitar has reached an impressive stage without modern scientific intervention, but applying the tools of a scientist could further the understanding of the type of constructional changes that lead to perceivable changes in the radiated sound from a musical instrument.

Three main strategies have been employed in this thesis in an attempt to accomplish the above goal. First of all an investigation of the vibrational properties and radiated sound of similar instruments to the classical guitar is carried out; these instruments are a steel-string folk guitar and a five-string banjo. The aim here is to identify the key features of an instrument's acoustical signature and then to highlight those mechanical and acoustical properties that are associated with aiding us to distinguish between the sounds of different plucked-string instruments. This demonstrates how large constructional differences affect the perceptual characteristic of these instruments. Secondly, the problem of over-coupling a string to the body of a classical guitar is addressed. A model is developed that demonstrates the effects of strong string-body coupling. Then psychoacoustical work aids in finding an acceptable upper boundary for the strength of the coupling. Knowledge of this over-coupling limit can help instrument makers build a strongly radiating instrument without sacrificing even tonal qualities between notes. Finally, the smallest perceivable changes are found in parameters that describe the acoustical function of the classical guitar. Parameter changes that are responsible for the largest perceivable changes are likely to be the most important ones for the

instrument maker to control, because these are the parameters to which our ears are most sensitive.

There are a number of different aspects to this work including some theoretical work, experimental measurements, signal analysis, physical modelling and psychoacoustics. This introduces difficulties in bridging the gap between the language used in physics, music, engineering and psychology. It also raises issues with organising the work in a coherent manner. Although the work is multidisciplinary, it is aimed to be presented to the physicist.

1.2 Brief history and anatomy of the guitar and banjo

This section is mainly concerned with the origin and construction of the classical guitar, but the main differences between some other types of guitars are also given before a brief account of the history and anatomy of the banjo. The reason for choosing to study the banjo as part of this work is that its anatomy and acoustical function draw many similarities with that of the guitar, but the sound quality of the banjo is distinctly different.

1.2.1 Guitar

Although the ancestral home of the classical guitar lies in Spain, the guitar actually came to Spain from across the Mediterranean (Sloane 1976). Its origins date back to probably more than 3000 years ago in Egypt, and its ancestors include the Arabic ud, the lute and the Spanish vihuela (Rossing et al. 2002). From the late thirteenth century guitar making was a refined art in the Andalusian region in southern Spain, and in the mid-nineteenth century this era culminated in the developments from possibly the most famous guitar luthier of all, Antonio de Torres Jurado. From experimenting with the instrument's tonal possibilities and power, Torres's innovations included enlarging the body cavity, refining the outline, he fixed the string length and devised a system of bracing the soundboard to enhance tone.

Today the guitar is one of the most popular of all musical instruments, with an estimated 20 million guitars in the United States alone. A guitarist accustomed to playing a factory-made instrument will always be amazed by the brilliance, power and ease of play of a hand-made instrument. However, as the demand is too high for luthiers to handle, low-quality instruments from production lines are sold in large numbers. This unfortunately results in many poorly-made instruments being sold for a

flattering price, and the work of the craftsman is not as celebrated as much as it perhaps should be.

There are four main categories of acoustic guitars; classical, flamenco, flat-top (or folk) and arch-top. The first two listed above have nylon strings and the latter two have steel strings. Figure 1.1 shows a blown-up picture of a classical guitar with a traditional (Torres) fan bracing.

The classical guitar differs from the flamenco guitar because of the different requirements needed to play classical and flamenco music. The flamenco guitar is usually of lighter construction and has tapping plates attached to its body so that the player can introduce a percussive element to the music. The coupling between the string and the body of the classical guitar must be finely tuned so that the instrument is responsive to the player's touch but not have an overly percussive tone. Flat-top guitars are probably more popular than arch-top guitars. As the name suggests, the arch-top has an arched top-plate or soundboard similar to the plates of a violin or cello. The strings of an arch-top guitar are usually fastened to the tail piece rather than the bridge. Modern arch-tops are usually fitted with electric pick-ups making it an electro-acoustic hybrid.

The strings of a guitar are usually fastened to the bridge, which is attached to the front of the soundboard usually at the centre of the lower bout. They run over the saddle, a piece of bone or ivory on top of the bridge, up the fret-board and over the nut at the top of the instrument. They are then wound up to playing tension using tuning machines. Classical and flamenco guitars historically used gut strings, but these were replaced because of the ease of production of more uniform nylon strings. The lowest-pitch strings on acoustic guitars are wound with a metal wire to add mass to the strings. Usually the three lowest strings on a classical guitar and four lowest string of a folk guitar are wound. Using a thicker monofilament nylon or steel to add mass to the string would make the string more difficult to bend and increase the inharmonicity of the string (see Section 2.1.1).

The bracing on the soundboard of a guitar is put in place to increase the stiffness of the plate making it stronger to withstand the force of the strings pulling on it and to have some control over the vibrational properties of the soundboard. In order to enhance the amount of sound radiated from the instrument, the maker aims for high stiffness and low density (Richardson 1994). A guitar maker will spend a long time on the soundboard of the instrument employing such techniques as tap tones; the soundboard is held lightly with one hand, the centre of the lower bout is tapped using a finger on the other hand and the maker listens to the pitch and decay of the sound. Finding the right tone for the soundboard is an important skill for a guitar

maker and comes only with experience. Every soundboard is slightly different, even if they are made of wood from the same tree, therefore a different thickness and amount of bracing is needed on each soundboard in order to find the correct tone. Note that giving a guitar an arched-top is a way of increasing the stiffness of the soundboard without adding mass, therefore the maker can minimise the bracing and achieve a higher ratio of stiffness to density. The back is also braced with cross struts to add stiffness against the grain of the wood. The bracing of the back-plate is generally thought to be of less importance than that of the soundboard.

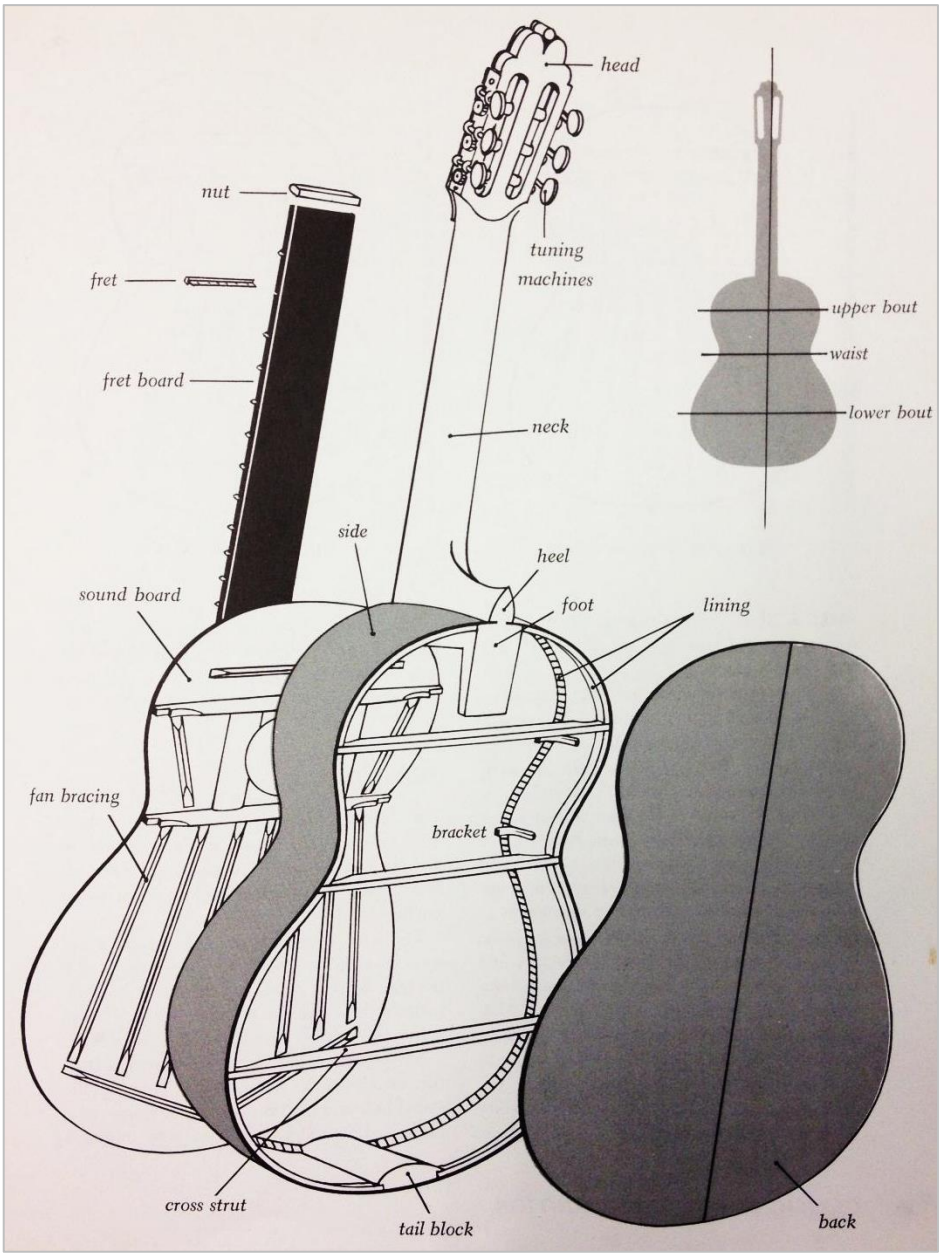

Figure 1.1: Exploded view of a guitar with fan bracing. From Sloane (1976).

Steel-string guitars are built in a more robust manner because of the higher tensions needed in the strings to bring them up to playing pitch. The soundboard therefore usually has a strong X-shaped bracing and a thicker soundboard to

withstand the pulling of the strings on the bridge. The neck is also built with a steel rod running through it to add strength against the high tension of the steel strings.

The soundboard of a guitar is usually made out of spruce or cedar, the former is denser, which some makers say gives a brighter tone. In reality, the ratio of density to Young's modulus is the important factor, which is very similar in these two types of wood. The soundboard is planed down to a thickness of about 2.4-2.8 mm, depending on the density of the particular piece of wood. Historically, the wood of choice for the back and sides, or ribs, is Brazilian rosewood, which is a very dense hardwood. However, over-harvesting and the depletion of Brazilian rainforests mean that this wood is now endangered and its trade is heavily regulated. Nowadays the back is usually a hardwood such as a different rosewood, mahogany or maple and is again about 2.5 mm thick. The struts are usually made from spruce or cedar, like the soundboard.

A guitar has six strings usually tuned to E_2, A_2, D_3, G_3, B_3 and E_4, giving open-string fundamental frequencies ranging from 82.4 Hz to 329.6 Hz. The strings are numbered from one to six starting with the highest frequency string and ending with the lowest frequency string. The classical guitar has a playing length of 0.65 m and the steel-string guitar can be longer or shorter, depending on the model.

1.2.2 Banjo

The origin of the banjo lies in instruments made using hollowed out gourd fruit by enslaved Africans in the New World in the seventeenth century. The modern five-string banjo reached its pinnacle of American popular culture on the turn of the twentieth century (Gura and Bollman 1999).

Figure 1.2 shows a labelled picture of a modern five-string banjo. The first four strings have a playing length of roughly 0.68 m. The fifth string is shorter and starts at the fifth fret of the instrument giving it a playing length of about 0.51 m. The strings are usually tuned to the notes D_4, B_3, G_3, D_3, and G_4 from string one to five, giving the open strings fundamental frequencies in the range 146.8 Hz to 392.0 Hz. Only the lowest-frequency string, D_3, is wound with a metal wire to add mass to the string without overly increasing its inharmonicity.

The banjo's equivalent to the guitar's soundboard is a membrane called the head. The head is held under an adjustable tension by hooks or tension rods pushing down on a hoop that holds the head in place. The head is tuned to an even tension, which is usually checked by lightly tapping the head around the edge with the finger

and listening for an even pitch. An arm rest is put in place so that players do not rest their arm on the head, which would affect the vibration of the light-weight skin.

The flange of the instrument aids in attaching the back onto the body, the holes in the flange are analogous to the sound hole of a guitar. The detachable back, often called the resonator, enables the instrument to be played without the back, or the player can put a cloth inside the instrument resting against the head to act as a 'mute', which decreases the loudness of the instrument. On some banjos the flange can be raised or lowered with respect the back, effectively increasing or decreasing the volume of the internal cavity (Rae 2010).

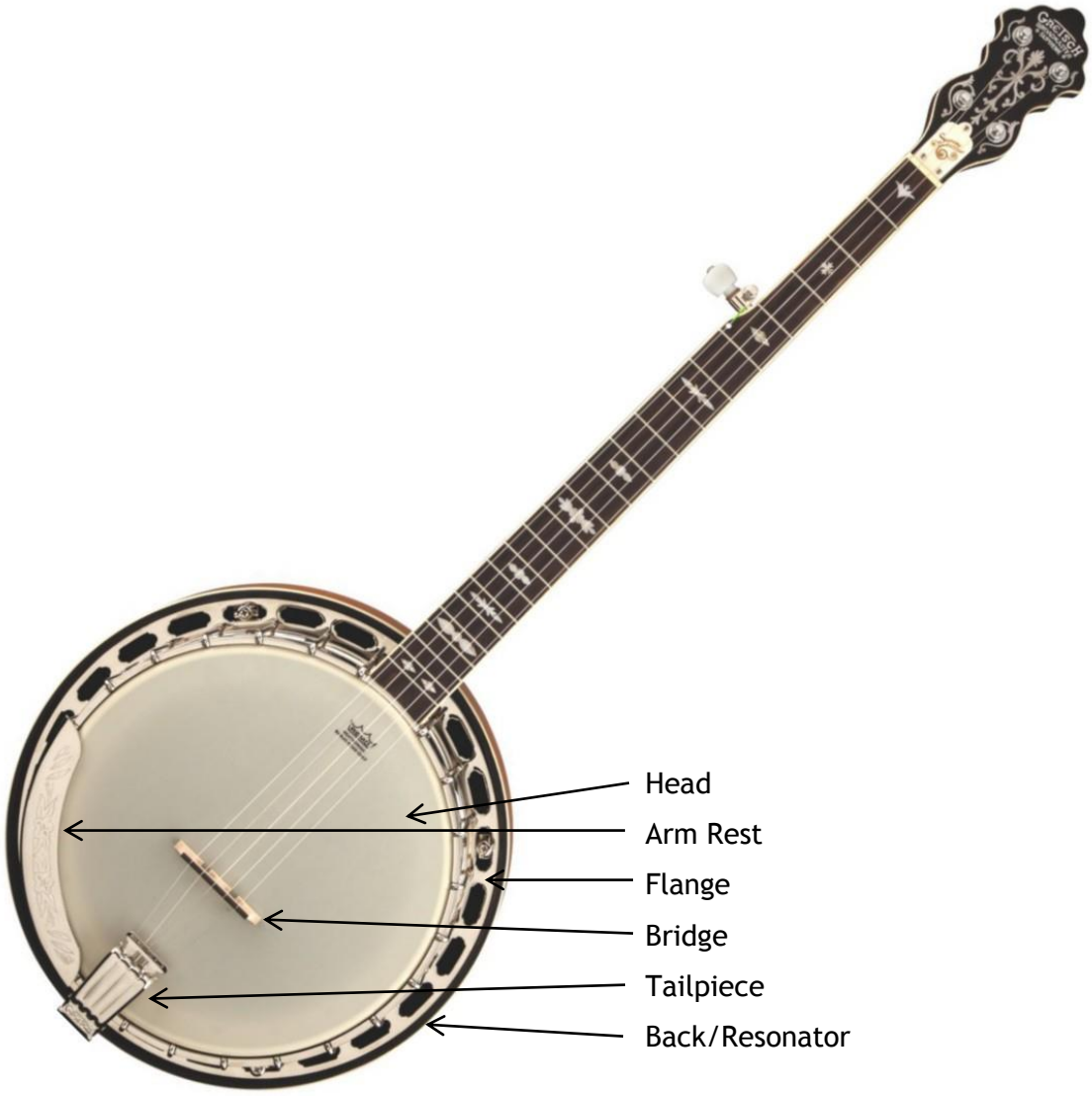

Figure 1.2: Picture of a Gretsch Broadkaster Supreme banjo.

It is possible to get a large variation in sound from a single instrument depending on the instrument's particular 'setup'. The main variable of this complex system is the tension of the head. Once the head is tuned the bridge is positioned

usually about a fifth of the head radius from the centre of the head towards the tailpiece (Dickey 2003). The strings are then brought up to playing tension and small adjustments are made to the position of the bridge, making sure that each open string is indeed an octave below the notes played on the 12th fret. Changing the head tension can give the desired loudness, brightness and decay (Dickey 2003), although trade-offs are an inevitable occurrence.

One important design feature that is similar to instruments from the bowed-string family but different from the guitar (apart from arch-top guitars) is that the strings of the banjo are fastened to a tailpiece at the bottom of the instrument. This means that the tension of the strings do not exert a twisting force on the soundboard like on the guitar and so the head does not need to be strengthened by bracings. The small change in angle of the strings at the bridge keeps the bridge in place with a downward force.

1.3 Basic function of a plucked-string instrument

Now that the reader is familiar with the constituent parts of the guitar and banjo, this section describes the function of their components and how the components interact with each other. This interaction is important in understanding how sound is generated and radiated by the instrument. Figure 1.3 is a schematic of the function of a guitar, where lines with arrowheads on both ends signify an interaction. A similar diagram could be constructed for the banjo without the interaction with the back-plate. In the case of the banjo the back is very heavy and is not intended to vibrate and interact with the rest of the body.

Although the player is mentioned in this diagram, the work in this thesis does not take into account the player's role in affecting the sound from the instrument. The player can change the pitch by moving the finger on the fretboard, adjust loudness by plucking harder or softer and change the tone quality by plucking at different angles or at different positions along the string. Other effects such as vibrato can also be employed by the player, but none of these variables are considered as part of this work.

The strings of a stringed instrument are often said to be the 'musical' part of the instrument. Deconstructing the complex vibration of a plucked string into its constituent components reveals a set of vibrations that are *nearly* harmonic. The ear is well accustomed to detecting such signals because the spectrum of the voice reveals a similar pattern. In fact, in the case of the voice the components *are*

harmonic. The similarity in harmonic content between the voice and a vibrating string explains why strings are useful in harmonic musical instruments. Also, as humans, it is important for us to be able to gather lots of information from harmonic sounds to be able to communicate effectively with one another. As well as using words, one can convey all kinds of extra information by making small changes in tone, pitch and loudness whilst talking. It therefore follows that we are also capable of detecting relatively small changes in the sound generated from a vibrating string.

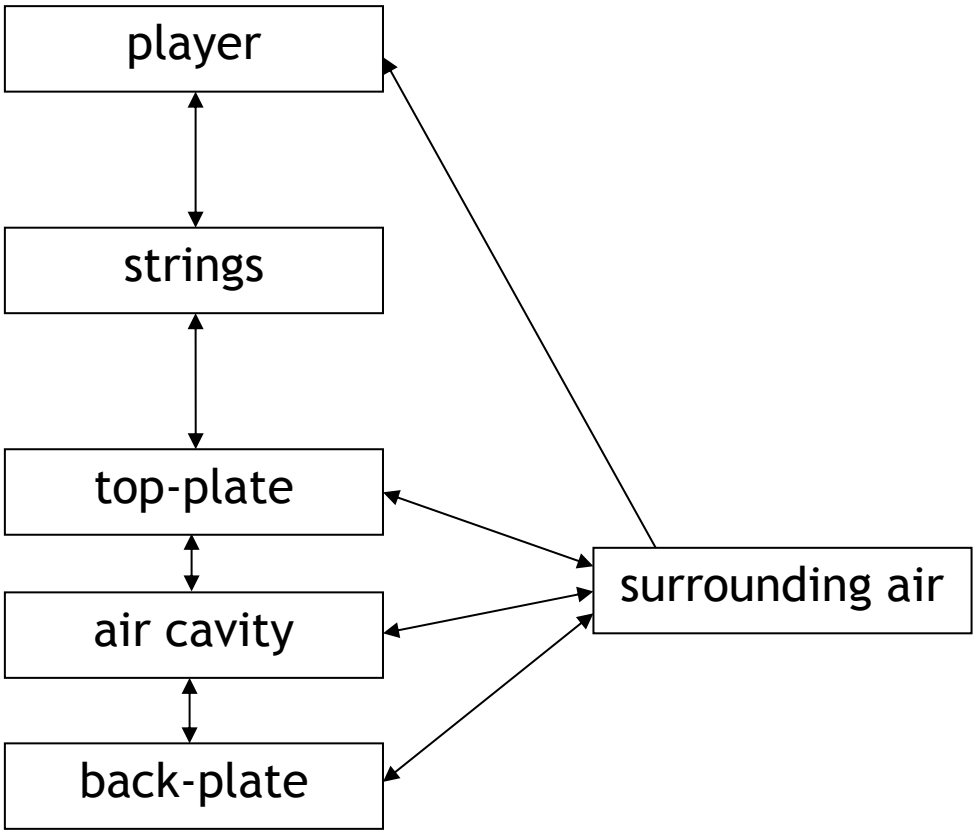

Figure 1.3: Schematic of various interactions associated with playing a guitar.

Strings do not radiate sound very well because they do not move a large volume of air as they vibrate. The 'musical' vibrations of the string are therefore coupled to an efficient sound radiator, which comes in the form of the body of the instrument. The top-plate or soundboard, air cavity and back-plate make up the body of a guitar. The displacement of the soundboard might be small (in the order of microns) but its large area ensures efficient coupling to the surrounding air (Richardson 1994). The body of the instrument therefore has the job of communicating the vibrations of the string to the surrounding air so that we can hear them clearly.

The body does not radiate the sound of each component of the vibrating string by the same amount; it will radiate some components more strongly than others thus having great influence over the overall tone quality of the instrument. The exact

detail or shape of this apparent 'filter' of the body is complex and is governed by the vibrational modes of the body. Therefore in order to control the tone quality of a plucked-string instrument, the maker must understand the nature of the body modes.

Controlling the modes of the body is made much more complex by the interaction, or coupling, of the soundboard, air cavity and back-plate. Due to the nature of coupled vibrating systems, the vibrations of one sub-system will affect the vibration of its coupled sub-systems. The extent of this effect depends on the strength of the coupling. The instrument maker must also be aware of the coupling between the strings and the body. Strong string-body coupling means an efficient transfer of vibrational energy from the string to the body resulting in a loud and relatively short-lived sound, but it also means that the vibration of the body will affect the musical vibrations of the string (see Section 2.3.1).

1.4 Previous work

This section is intended to give the reader an account of some of the previous research carried out that is relevant to the goals of this thesis as stated in the opening section. Many more authors, scientific papers and books will be referred to throughout the work.

1.4.1 Modelling

Christensen (1984) developed a model for the sound pressure response from a guitar by representing a small number of low-order body modes as damped harmonic oscillators. Each mode has its own resonant frequency, Q value and amplitude, which Christensen denotes A/m. The A is the effective area associated with a mode; a larger area means that the mode moves more air whilst vibrating, therefore radiating sound more strongly. The effective mass, m, indicates how well the strings communicate with the body. Christensen did not measure these individually so they are lumped together. A large A/m tells us that a particular mode will be a strong radiator of sound. To get the overall sound pressure response, the individual responses of each mode are summed together. In Christensen's model all modes were assumed to be point sources radiating sound equally in all directions; this is known as a monopole source.

Following on from Christensen's model, Hill *et. al.* (2004) published a paper showing that the sound pressure from a guitar can be modelled more accurately by

including dipole radiation of sound. Hill also measured the effective area and effective mass separately, giving a total of five parameters per mode. The inclusion of dipole radiation was made possible following the work of Weinreich and Arnold (1980), who developed a scheme for dividing the radiated sound from a single source into a monopole source strength and three orthogonal dipole components. Hill also found that the response from a finite-sized source described the sound pressure from a guitar better than a point source. This work demonstrated a scheme of accurately recreating the sound pressure response of a guitar up to about 600 Hz.

Woodhouse wrote two papers on synthesis methods for guitar tones; the first was on comparing some different methods of synthesis (Woodhouse 2004a), and the second was on the accuracy of the models in modelling the acceleration response at the bridge of the instrument from a step function of force applied to the string (Woodhouse 2004b).

In the first paper Woodhouse presents three types of modelling methods, which are frequency-domain, time-domain and modal superposition methods. Within each synthesis group there are further options to choose from and the strengths and weaknesses of these options are discussed in some detail. All of the models include two polarisations of string vibration and go up to a frequency of 5 kHz. Woodhouse concludes that the time-domain methods gave unsatisfactory results, the modal superposition method was a little time consuming, and therefore the frequency-domain method was the recommended method of choice.

In the second paper by Woodhouse he compares the results from the most suitable model from the first paper with measurements of the structural response from a real instrument. To model the instrument up to 11 kHz, the response of low-order modes were initially modelled using a standard method, then he used a computer to randomly choose numbers from certain distributions to generate modal parameters for modes from 1.4-11 kHz.

Woodhouse goes on to say that the model was only moderately successful at reproducing the detailed behaviour seen in measured plucks and that the inclusion of the second polarisation of string motion makes rather little difference to the result of the model. He then stresses the need for an accurate model for string damping in order to accurately reproduce the decay rates in the radiated sound.

1.4.2 Psychoacoustics

Fritz published two papers on perceptual experiments on the violin that are relevant to the work carried out in this thesis (Fritz et al. 2007; Fritz et al. 2012).

Other authors named on these papers include Ian Cross, Brian C.J. Moore and Jim Woodhouse, demonstrating a multidisciplinary collaboration between musician, psychologist and engineer.

The first of these papers, Fritz et al. (2007), was on finding the smallest perceivable changes in the frequency and amplitude (referred to as effective mass in this thesis) of the modes of a violin. The purpose of this work was to find the amount of change needed to produce a perceivable change in the sound of a violin as judged by musicians and non-musicians. Interestingly the results from this study showed that musicians had significantly lower thresholds than non-musicians.

As part of this study, Fritz tried different stimuli for her listening tests. A musical phrase was used as well as short notes that were hardly notable as the sound of a violin. The short notes were favoured because they obtained lower thresholds. The reason for this was said to be due to allowing 'echoic memory' to assist discrimination. Echoic memory is the apparent ability for us to store lots of information about auditory stimuli that occur within a short amount of time, optimally within 1.5 s. Thus, if the test stimuli were presented within 1.5 s, the task would be easier and lower thresholds would be achieved. This effect diminishes with time up to around 4 s, which is the upper limit of echoic memory (Darwin et al. 1972).

The second paper published by Fritz et. al. (2012) that is relevant to this study was on making links between adjectives used by musicians to describe the tonal qualities of a violin and the mechanical properties of the instrument. To split up the mechanical response into frequency bands they used the same bands as Dünnwald (1991), which were five one-octave bands that start at 190-380 Hz and finish with 3040-6080 Hz. The results of the investigation showed that a moderate increase to the two bands between 1520-6080 Hz resulted in an increased brightness and clarity (slightly lower frequency band to that found by Dünnwald), whereas a strongly increased level in the band 1520-3040 Hz resulted in harshness of the violin sound. Although this work cannot be directly related to the guitar, it is reasonable to assume that an instrument that radiates high-order overtones strongly is generally perceived to have a bright tone quality and an instrument that radiates high-order overtones more weakly has a dull or dark tonal quality.

Note that throughout the work published by Fritz, the test stimuli were always in the form of the velocity at the bridge rather than the sound pressure at a point a certain distance away from the instrument.

Meyer (1983b) published work on the links between 19 objective criteria of the sound pressure response of 15 guitars with the subjective opinions of 40 people on

the quality of the instruments. The objective criteria included frequency, peak level (a mix of effective mass and Q value) and Q value of the first three resonances, distance between the modal frequencies and nearest note frequencies and the interval between the first and second resonance. The guitars were chosen such that there was a mix of so-called “good” and “poor” instruments. The subjective opinions of the listeners were graded by asking each listener to choose their preferred guitar from a pair of instruments playing the same piece of music, then a different pair of guitars were presented to the listener, this process was repeated until the 15 guitars were listed in order of tonal preference.

This is a very impressive catalogue of results for evaluating the quality criteria for a musical instrument, and Meyer goes on to analyse the results in great detail. After collecting the results Meyer correlated the 19 quality criteria with the subjective tests. No correlation was found for six parameters, these parameters were concerned with high-frequency observations or distance between low-order modal frequencies to their nearest notes. Seven parameters had a correlation value of less than 0.5, suggesting that these parameters have not a great deal to do with the quality of a guitar. The highest degree of correlation was found to be 0.73, which was the peak level of the third resonance (around 400 Hz). In fact, the top six parameters that had the highest degree of correlation with a high quality instrument were to do with parameters concerning the lowest 500 Hz of the sound pressure response.

There are weaknesses in this investigation that taint the value and credibility of the results. The fact that a low value of correlation was achieved for most parameters is disappointing; one would have hoped that such a vast investigation would have resulted in more clear findings. Also, Wright (1996) is quick to point out that in Meyer’s sound pressure measurements, only one driving position was chosen, and that driving different points along the bridge will result in different responses.

In the second part of this investigation, Meyer (1983a) investigated the effects to the sound pressure of a guitar as the top plate went under some constructional changes. He used a rigid frame in the shape of a guitar and glued a variety of top plates having different bracing patterns and different bridge designs to the frame. He then tracked the resulting changes in the sound pressure, and related these changes to the quality criteria from his earlier work (Meyer 1983b). It seems that the most obvious result from this investigation was the effect of using a bridge with the smallest mass possible. This change resulted in a positive effect in seven out of nine chosen quality criteria. The bridge with the lowest mass increased the overall level of the sound pressure response. Although a louder instrument with a bright tone seems to be advantageous, this investigation did not take into account the coupling

between the body and the strings. A bridge with a low mass will result in an instrument with strong string-body coupling. If the coupling is too strong then the vibration of the body will perturb the natural vibration of the string resulting in an unpleasant sound.

In Meyer's work a parallel measurement of the mechanical response of the instrument as well as the pressure response would have been worthwhile as an intermediate step. Because tracking the changes from excitation to sound pressure is a big leap, and an intermediate step would have perhaps shed some more light on the effects of these constructional changes.

Following progress in the modelling of guitars, Woodhouse (2012) published a paper using a frequency-domain model to carry out psychoacoustical work on the guitar. This work was in a similar nature to that of Fritz et. al. (2007), as Woodhouse mentions using the same software for the listening tests. The focus of this work was to find the just noticeable difference (JNDs) in a few parameters of the guitar model. These parameters included bending stiffness and damping parameters of the string, and modal frequencies and Q values of the body. The JNDs were then compared with data gathered from 15 guitars to assess whether the changes in frequency and Q value of the body modes can account for the perceptual differences between guitars.

The results from Woodhouse's listening tests showed that the most sensitive parameter change was the frequencies of the body modes, achieving a JND of just a 1% shift to all modes up to 5 kHz. This change is small compared with the actual variation among real guitars. The JND in Q value was about 20%, which is just within the variation seen in modal damping of real instruments. This result means that modal Q values are minor contributors to tonal perception in comparing the sound radiated by different guitars.

In his doctoral thesis written here at Cardiff, Wright (1996) aimed to correlate the vibrational behaviour of the classical guitar with subjective judgements in the instrument's tone quality. Wright used a physical model of a string attached to a guitar body, which was modelled up to 700 Hz, to generate tones for the use of listening tests. Wright recognised that in order to make an initial evaluation of the different parameters of his model, standard psychoacoustical listening tests, such as those used by Fritz and Woodhouse, were too restrictive and time consuming. It is also unrealistic to obtain masses of data from subjects who are not paid for their time. Therefore, Wright wrote his own listening tests that asked listeners to rate certain subjective changes due to a given change in a single parameter. Although this type of test involved generating many test tones prior to carrying out a test, it most probably saved many programming hours of a standard psychoacoustical test.

Nevertheless, this method proved useful as an initial investigation into the perceptual changes due to modal parameter changes. In discussing his results, Wright emphasises that compromise is the fundamental concept when considering tone quality. Achieving a perceivable change in the radiated sound by changing a single parameter without affecting any other is highly improbable.

Four experiments were carried out to evaluate subjective judgements of listeners. The first experiment involved changes to all parameters of low-order modes. Modes associated with the top-plate were found to be the most influential, and the Q value was deemed the least important parameter. In the second experiment Wright showed that the effective mass has a greater influence on tone quality than resonance frequency, both on low and high register notes. This also showed that effective mass can be characterised as a global parameter because it affects string partials well above the resonance frequency of the mode. On the other hand, resonance frequency is a local parameter because it only affects notes with fundamentals in the mode's vicinity. The third and fourth experiments investigated the nature of the changes in tone due to parameter changes. Increasing A/m resulted in an increased loudness and brightness, changes to the resonance frequencies affected the 'evenness' of the sound and changes to Q values resulted in virtually no change.

1.5 Structure of thesis

As mentioned at the start of this chapter, the aim of the work is to correlate changes in the vibrational behaviour of a guitar with perceivable changes in its radiated sound. It is therefore important for the reader to firstly be familiarised with the background theory of the vibrational behaviour of the constituent parts of the guitar, their interaction, and a theoretical mechanism for the instrument to radiate sound. This is covered in Chapter 2.

There are several types of measurements that can be carried out to compare the vibrational behaviour of the classical guitar with the steel-string guitar and banjo. The radiated sound from these instruments is studied firstly, then measurements of characteristic impedance of the instruments' strings, mechanical response of the instruments' bodies and mode shapes of the bodies. The methods used to carry out these experiments are discussed in Chapter 3.

In Chapter 4 results are given for the above mentioned experiments. Firstly, the radiated sound from a classical guitar, steel-string guitar and banjo is analysed. Then

the characteristic impedance of the strings of these instruments are compared. The mechanical response of a classical guitar, folk guitar and banjo are then compared as well as the level of coupling between the strings and body of each instrument. Then results are presented for mode shapes of two classical guitars, two steel-string guitars and a banjo.

Chapter 5 is on psychoacoustics. The first section of this chapter presents the basic principles of signal detection theory that lead to the procedures of the listening test used in this thesis. A short section is then given on auditory masking and the theory of critical bands. The latter section of Chapter 5 shows results from some basic listening tests using modified guitar tones that give some insight into the amount of change needed in the sound of a guitar tone to produce a perceivable change.

Over-coupling a string to the body of a plucked-string instrument can lead to some notes sounding dead or out-of-tune, these notes are usually referred to as wolf notes. Although the origin of the effect is well known, the perceptibility of wolf notes on plucked-string instruments has not been assessed. In Chapter 6 the theoretical treatment of the coupled system is advanced and this model is used in conjunction with some listening tests to reveal the perceivable wolf notes on a classical guitar.

In Chapter 7 two physical models of plucked-string instruments are outlined giving the velocity response at the bridge from a step function of force applied to the string. The results of the two models are compared, and the model best suited for the use of listening tests is chosen to proceed with the modelling process. The model of a classical guitar is then coupled to its surrounding air to obtain the sound pressure from a string pluck up to 5 kHz. This is done to obtain the most detailed model possible in order to carry out meaningful psychoacoustical work. The last section of this chapter shows that the same modelling method can be used to synthesise tones for the steel-string guitar and banjo. This also highlights some differences in the modelling procedure that is important for the acoustical signature of these instruments.

The model of the classical guitar outlined in Chapter 7 is used to carry out listening tests in Chapter 8. These tests are designed to measure the smallest perceivable differences in selected parameters from the model. Two investigations are carried out; the first is to compare the significance of monopole and dipole radiation of the instrument, the second is to assess the influence of modes below 400 Hz and above 400 Hz on the perceived sound of low notes and high notes played on the classical guitar.

A closing discussion of the results and findings from Chapters 4, 6, 7 and 8 is given in Chapter 9 along with the conclusions of the thesis and proposed future work.

Chapter 2 Background Theory

This chapter is in four sections. The first two sections discuss the dynamics of strings and instrument bodies respectively. The third section is on the interaction between the strings and the body of a plucked-string instrument. This is discussed in terms of local string-body coupling that affects the low-frequency function of an instrument and global string-body coupling that could be used to characterise different plucked-string instruments. The final section is concerned with the theoretical framework of instrument bodies radiating sound.

2.1 String vibration

2.1.1 Dispersion and damping

After exciting a string it will vibrate in a superposition of its natural modes. In an 'ideal' flexible string the frequency of the natural modes are integer multiples of the fundamental component; in this case the overtones are harmonic. However, a real string has a finite stiffness that must to be taken into account. This stiffness introduces dispersion in the string and causes the frequencies of the natural modes to be stretched from their harmonic values, hence introducing inharmonicity into the string. The string components are therefore called partials rather than harmonics

(Kinsler et al. 2000). The frequency, f_n, of a partial, indexed n, is related to the fundamental frequency, f_0, by the equation (Fletcher and Rossing 1998)

$$f_n = f_0 n(1 + Bn^2)^{1/2}, \tag{2.1}$$

where B is the inharmonicity constant. The inharmonicity is usually greater in plain nylon strings than plain steel strings, with a value of around 6×10^{-5} and 4×10^{-5} respectively, but for wound strings the opposite is true with values of around 2×10^{-5} and 8×10^{-5} for wound nylon and wound steel strings respectively (Woodhouse et al. 2012).

There are three main damping mechanisms in a string on a musical instrument. One form of damping is referred to as internal damping that accounts for the heat loss due to internal processes as the string bends. Examples of the processes are movement of kinks in polymer chains in nylon strings, movement of dislocations in steel strings and internal friction between the windings of wound strings. This form of damping affects higher-order partials more than lower ones. The second form of damping is air damping due to the friction between the string and the surrounding air as the string moves through the air. This damping mechanism affects lower-order partials more than higher-order partials. The third damping mechanism is losses to the body of the instrument; some of this is responsible for the generation of sound as the vibration of the body moves the surrounding air and some of this energy is lost through the body's internal damping. A more thorough analysis of the damping mechanisms in strings can be found by Valette (1995).

2.1.2 Peak heights of string partials

Figure 2.1 shows the spectrum of the radiated sound of a plucked D_3 note on a classical guitar showing the first 30 partials of the string. The general trend of the heights of the partials is often referred to as the formant of the sound. The word formant comes from the trend of peak heights in the spectra of vowel sounds made by the voice. In the case of the voice, the tongue, lips and soft palate move to produce a certain formant for a given vowel sound (Rossing et al. 2002). For a note on a guitar, the formant of the partials can be altered by plucking the string in a different way; changing the plucking position along the string, plucking angle and plucking using the different parts of the finger (Fletcher and Rossing 1998).

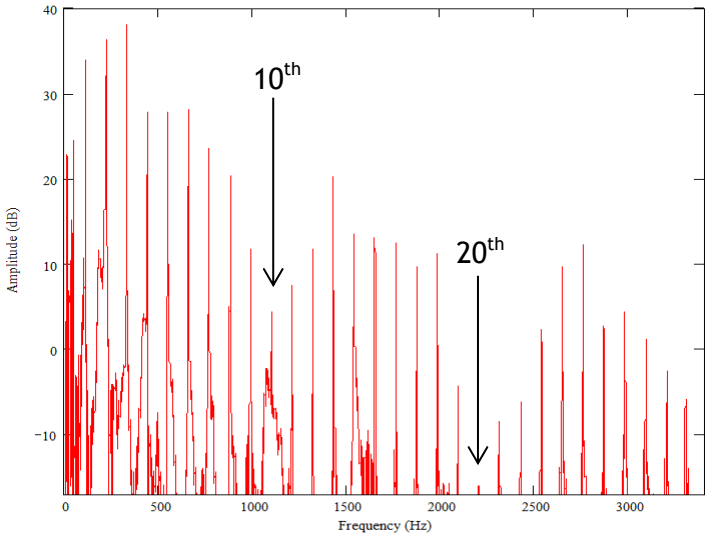

Figure 2.1: FFT of a plucked guitar string D_3 showing the first 30 partials with a fundamental frequency of 146.8 Hz. The time window of the FFT is 6 s and the sampling frequency is 44.1 kHz.

The plucking position for the note in Figure 2.1 was one-tenth of the length of the string, which is evident by inspection of the spectrum as there is a dip in the height of every tenth partial. The plucking angle may be utilised by a guitar player to either play quiet or loud notes; this is because string vibration in the plane parallel to the soundboard is not generally as strongly coupled to the instrument's body as the string vibration in the perpendicular plane. Using a fingernail or plectrum to pluck a string will put more energy into higher-order partials than using the fleshy part of the finger. The rounder edge of the finger will give the string a rounder profile at the point of contact than the sharper edge of a fingernail. Theoretically, the width of the finger is a cut-off point for smaller wavelength modes to be excited, which corresponds to a high-frequency cut-off.

2.1.3 Characterising string decays

In a simple model of a plucked string, the partials are simple exponentially decaying sinusoids. Such waveforms are characterised using four parameters, namely frequency in Hz, f, initial amplitude, A, which is usually normalised in an FFT of the waveform, Q value, Q and phase, φ. The latter is of secondary importance in this work because it depends on the initial plucking conditions of the string rather than the vibrational behaviour of the body of the instrument. Therefore the phase is not included in this basic model. Note that the Q value is related to the damping factor, γ, by $Q = \omega/\gamma$. The time varying amplitude of each component in the radiated sound from a plucked-string instrument can then be described by the equation

$$a(t) = A\sin(2\pi ft)\exp\left(\frac{-\pi ft}{Q}\right), \tag{2.2}$$

where t may be replaced by n/f_s for a discrete waveform indexed n using a sampling frequency of f_s. The initial amplitude in Equation (2.2) is usually replaced by $IA = 20\log_{10} A$ for the initial amplitude in dB.

On a real instrument there are examples where string partials show a more complicated decay profile, which suggests they are generated by more complex physical processes. Figure 2.2 shows examples of three types of decay profiles of string partials from the radiated sound of a classical guitar plotted on a dB scale; a simple exponential, beating exponential and a dual exponential decay. The method of obtaining these graphs is described in Section 3.1.

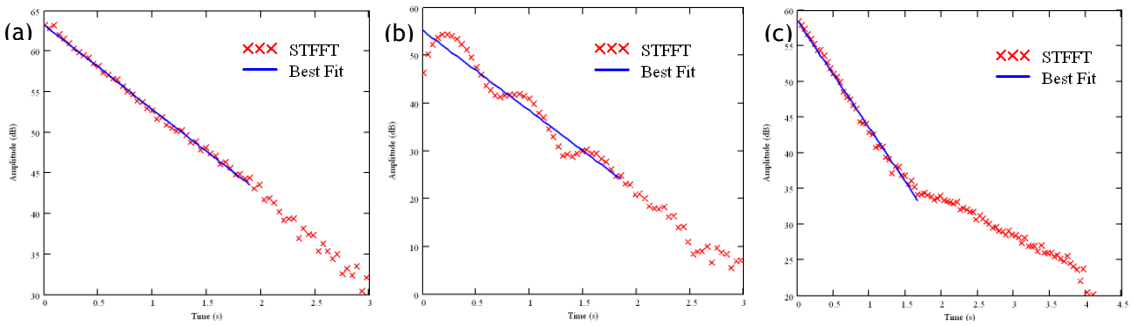

Figure 2.2: Examples of three types of decays on guitar BR2. (a) 2nd partial of the open 6th string- well behaved exponential decays produce a straight line when plotted in dB; (b) 11th partial of the open 4th string- beating decay approximated to a straight line; (c) 5th partial of the open 4th string- a dual decay with a fit to the first portion.

To explain the origin of these more complicated decays two transverse string polarisations and longitudinal vibrations must be considered along with the introduction of some non-linearity into the system. The degeneracy of the two transverse vibrations is removed due to the way the string is attached to the body at either end, meaning that the vibration in the plane parallel to the top-plate and the vibration in the perpendicular plane have slightly different frequency (Gough 1981). The two transverse modes are also coupled to each other through the longitudinal vibration of the string (Morse and Ingard 1968). This can be envisaged as a single transverse plane of vibration being subject to precession as energy is exchanged between the two polarised planes (Gough 1984). The string is usually coupled more strongly to the soundboard in the direction perpendicular to the soundboard meaning that vibration in this plane will have a larger amplitude and faster decay in the radiated sound. Therefore, a fast precession rate can lead to a beating decay (Figure 2.2b), whereas a slower precession rate can lead to a dual decay (Figure 2.2c). Dual decays are a more familiar characteristic in notes played on the piano as unison

strings are tuned to slightly different frequencies by the piano tuner to yield a loud and prolonged note (Fletcher and Rossing 1998).

Woodhouse (2004b) reported that nearly all 'string' components on a classical guitar are split into pairs corresponding to two transverse string polarisations with slightly different frequency, although their perceptual significance has not been formally established. Also, higher-order partials are split into more complex clusters involving four or more peaks whose frequencies correspond to multiples of lower-order partials. This is explained by the radiation of longitudinal string vibrations, because every longitudinal vibration has twice the frequency of its corresponding transverse mode (Fletcher and Rossing 1998). These pairs and clusters are difficult to find in low-order partials because the smaller peaks are consumed by the larger components, but a large FFT with sufficient frequency resolution can make out the closely-spaced pairs and clusters of higher-order partials. This effect is accentuated at large string amplitudes.

In this thesis, a regime for resynthesizing partials is needed for the purpose of psychoacoustical work. An important step is to decide on the amount of detail needed in the synthesis model in order to fulfil the requirements of the listening test. Beating string decays have been shown to be an audible effect in guitar tones (Richardson et al. 2008) but their inclusion in the synthesis model used here is not necessary as they are not a necessary feature of a guitar tone. It is sufficient to use Equation (2.1) to find the expected frequencies of the partials, then find the strongest component near these frequencies and approximate the decay to a simple exponential as described by Equation (2.2). This means that the vibrating string is assumed to be linear. Beating decays will be approximated by a straight line as shown in Figure 2.2b and only the first portion of a dual decay will be fitted, shown in Figure 2.2c.

2.2 Instrument body

The most important part of the body is the soundboard because this radiates the majority of the sound that we hear from a plucked-string instrument. The rest of the body (including the ribs, back-plate and enclosed air cavity) helps increase the efficiency of the instrument. As the soundboard compresses air on one of its sides as it vibrates the enclosure prevents the positive air pressure (relative to ambient pressure) to be cancelled out by the negative air pressure on the opposite side. Incorporating a sound hole is even better because the cavity acts like a bass-reflex

enclosure of a loudspeaker; if the Helmholtz resonance of the cavity is at a lower frequency than the first soundboard resonance, the radiation from the back of the soundboard is added in phase with that from the front (Kinsler et al. 2000). It is assumed in this work that the amplitude of vibration of the instrument body is small enough such that non-linear behaviour can be ignored.

2.2.1 Dynamics of the body and the oscillator model

For the guitar, coupling between the Helmholtz resonance and first soundboard mode splits the soundboard resonance into two peaks in the body's mechanical response. This has been explored theoretically as a two-mass-oscillator model (Christensen and Vistisen 1980). Coupling to the back-plate further splits this peak to make a resonance triplet, each with the two plates and air moving in different phases relative to each other, this constitutes the three-mass model (Christensen 1983).

This mode coupling also extends the response of the body to lower frequencies (Caldersmith 1978). Although this is also true for most plucked-string instruments, it is not the case for the harp. The harp has large holes in the back of the cavity, or 'soundbox', in order to feed the strings through their respective holes in the soundboard. As a consequence of these large holes, the Helmholtz resonance is at a higher frequency than the first soundboard mode resulting in a poor bass response in most harps (Le Carrou et al. 2007).

The vibrations of the soundboard of a guitar are coupled to the air cavity and the back-plate via the ribs and motion of the air inside the cavity. This means that excitation of the body, say, near the bridge, produces a set of natural modes that are a complex mixture of soundboard, air-cavity and back-plate modes that can be seen in the mechanical response of the body in the form of individual peaks. The peaks tend to be well distinguishable at lower frequencies but start to overlap towards higher frequencies, this is called modal-overlap and occurs somewhere around 1 kHz.

A measurement of the mechanical response comes in many different forms, but all involve measuring the input force and the output vibration at carefully chosen positions on an object. The form of mechanical response measured in this thesis is the input admittance. This is defined as the velocity divided by the excitation force measured at the same point.

The mechanical response of the body of many stringed instruments is modelled well as a set of damped harmonic oscillators, this is well documented in the

literature (Christensen and Vistisen 1980; Hill et al. 2004). Each well-defined mode is therefore assigned a natural frequency, ω_0, Q value, Q, and an effective mass, M_{eff}. The latter parameter is related to the amplitude of the mass-normalised mode shape at the measurement position on the bridge, $u = 1/\sqrt{M_{eff}}$ (Woodhouse and Langley (2012)). Close to an antinodal area of a mode the effective mass will be of the order of the actual vibrating mass, but as the measurement position approaches a nodal line the effective mass increases without limit.

The above parameters are combined to give the admittance of a single mode and the expression is summed over all modes of interest to give the response of the instrument in a given frequency range,

$$Y(\omega) = \sum \frac{i\omega}{M_{eff}(\omega^2 - \omega_0^2 + i\omega\gamma)}, \tag{2.3}$$

where $\gamma = \omega_0/Q$.

2.2.2 Mode shapes

Each mode of the body has its own vibrational pattern, called the mode shape. These are similar to modes of the string; a superposition of the individual mode shapes gives the overall vibration of the system. However, the modes of the body are more complex than that of a string because they involve movement of the soundboard, air cavity, back-plate and ribs. Mode shapes can be studied in a number of ways, using basic Chladni patterns, holographic interferometry (like Figure 2.3) or using laser Doppler vibrometry (see Section 4.5). Guitar mode shapes have been studied at Cardiff for a long time (Richardson 1982) and this work has brought success in learning more about the dynamics of the instrument's body. Some examples are given in Figure 2.3.

The modes are classified using a system of counting anti-nodal regions, first in the horizontal direction, then the vertical direction. For example, mode (a) in Figure 2.3 is a T(2,1) mode, where the T refers to the top-plate. Alternatively, a 'B' instead of a 'T' would refer to a mode that is mainly associated with a resonance of the back-plate. The fundamental top-plate mode is split into three because of the coupling to the air cavity and back-plate. In this case the mode with lowest frequency is labelled $T(1,1)_1$, the next mode higher up in frequency $T(1,1)_2$, and the highest frequency mode of the resonance triplet $T(1,1)_3$.

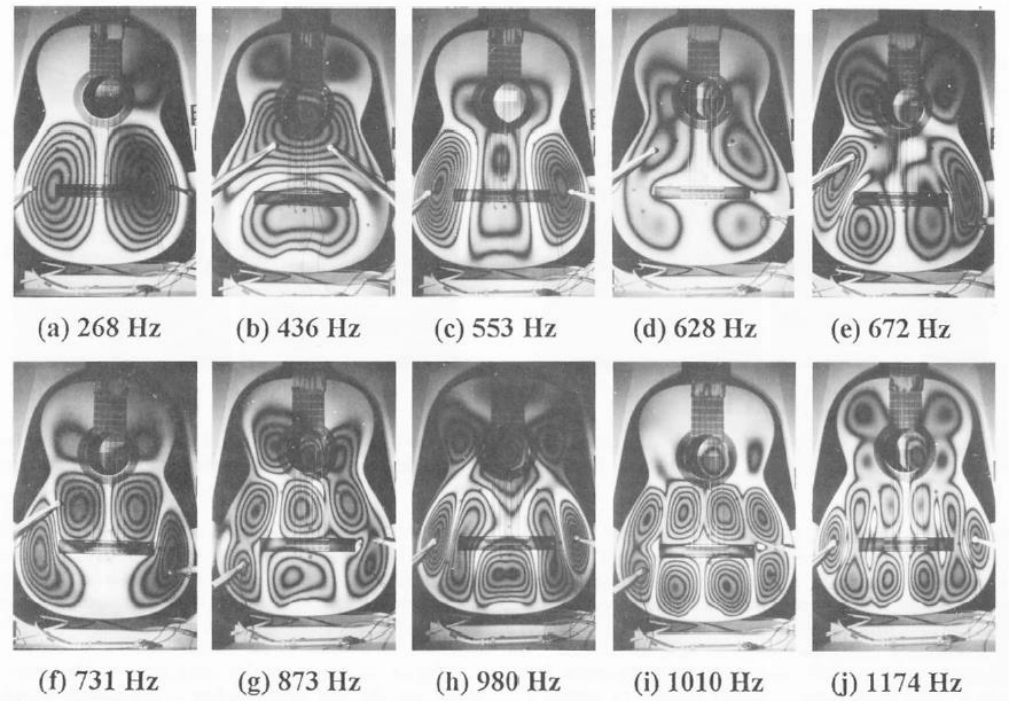

Figure 2.3: Various mode shapes measured on a guitar soundboard using holographic interferometry. Figure taken from Richardson (1994) with permission from the author.

Knowledge about the location of nodal lines and anti-nodal regions can be very insightful as will be shown later in this thesis. This is because they show why some strings will interact strongly with a certain mode, they also show the size and number of in-phase anti-nodal regions on the top-plate indicating the effective radiating area of the mode. Modal shapes will be used later in this thesis to show why the peak height of some modes in the input admittance of the body can change so dramatically between string positions along the bridge of a guitar. They will also be used to show the influence of different bracing patterns on the vibrational characteristics of the body of a plucked-string instrument.

2.3 String-body interaction

The interaction between the string and body will be discussed in two regimes. First of all the narrowband, or local, coupling between a single string mode and single body mode will be discussed. This local string-body coupling has received some attention in the past in the context of wolf notes, on the cello (Firth 1978), violin (Gough 1980) and the guitar (Woodhouse 2004a; Richardson et al. 2012). One can also talk about the broadband or global coupling level between a string and body,

which is characterised by the impedance ratio of the string to the body. This global coupling level has interesting implications for the characterisation of different plucked-string instruments.

2.3.1 Local coupling strength

In this thesis the local coupling strength refers to the problem of wolf notes in plucked-string instruments. The annoyance of the wolf note on the classical guitar is that it yields uneven playing qualities. That is, a wolf note will stand out from other notes on the instrument as sounding slightly out-of-tune or having a dull thud (with a loud fundamental that dies out quickly). The origin of the wolf note lies in frequency and Q value perturbations as a result of strongly coupled modes between the string and body.

The coupling between two vibrational modes was investigated by Weinreich (1977) in the context of coupled piano strings showing typical characteristics of a pair of coupled modes. Gough (1981) came to a similar result by describing the interaction between a string mode and a body mode showing the frequency and Q value perturbations associated with this coupling. Gough went on to characterise the coupling strength using the parameter,

$$K = \frac{2Q_B}{n\pi}\left(\frac{2m_s}{M_{eff}}\right)^{\frac{1}{2}}, \tag{2.4}$$

where Q_B and M_{eff} are the Q value and effective mass of the body mode, n is the partial number and m_s is the mass of the vibrating portion of the string. Consider a string mode and body mode tuned to the same frequency. For weak coupling, when $K < 1$, the coupling does not perturb the frequencies of the coupled modes, but the Q values are perturbed somewhat. For strong coupling, $K > 1$, the frequencies of the coupled modes are split evenly about the unperturbed frequency, and the Q values of the coupled modes are equal, with a value of $2Q_B$.

The work by Gough was an important development in the theory of this phenomenon applied to stringed musical instruments and a similar result was reached by Woodhouse (2004a) using a different formulation. Predictions using Gough's model have been made for perturbations on the guitar (Richardson et al. 2012), but the application of the model to the guitar has not been validated by comparing results from the model with real measurements. A further step is to carry out listening tests to find out whether these perturbations are perceivable; this is done in Chapter 6 of this thesis.

2.3.2 Global coupling level

The global coupling level is given by the ratio of impedances of the string to the body, analogous to impedance matching in electrical circuits (Schelleng 1962). This mechanical impedance matching indicates how well the vibration of the string is transmitted to the body, or the rate at which vibrational energy is transferred from the string to the body. A low coupling level indicates a quieter note with a relatively long sustain, whereas a high coupling level is likely to produce a louder note with a shorter sustain.

Here the input impedance of the string is assumed to be that of an infinite string, which is the characteristic impedance of the string and is given by $Z_0 = \sqrt{T\mu}$, where T and μ are tension and mass per unit length respectively. This is a decent approximation for the input impedance of a finite string, as the correct impedance is purely reactive (Fletcher and Rossing 1998), and therefore imaginary. Since impedance is the reciprocal of admittance the coupling level is equivalent to $Z_0 Y(\omega)$. The input admittance at the bridge should be measured and multiplied with the mean of the characteristic impedances of the strings to plot the global coupling level for various instruments. This was done by Woodhouse (2004b) to compare a set of classical or flamenco guitars and a set of violins.

This is an interesting parameter to use to compare different instruments in this study as there is relatively little difference in the strings on the folk guitar and banjo but there is a clear difference between the soundboard of the guitar and the head of the banjo. The thin membrane head of the banjo is lighter and significantly less stiff (more flexible) than the wooden plate soundboards used for guitars. This means the impedance mismatch in the banjo is relatively small and energy is transferred from string to head at a fast rate. For the heavier and stiffer (more rigid) soundboards of the other instruments studied here, the string-body coupling is weaker resulting in a lower rate of energy transfer and a longer sustain.

A higher global coupling level is also likely to yield more instances of strong local coupling. It is therefore expected that the banjo, for example, has many wolf notes.

2.4 Sound radiation

For the purpose of modelling the radiated sound from an instrument it is necessary to employ a mathematical formulation of how the instrument interacts with its surrounding air. Woodhouse et al. (2012) opted for a severely simplified approach, where the acceleration at the bridge was simply filtered as a function of

frequency until it gave satisfactory-sounding results. A slightly more detailed approach would be to apply this basic filter to the response of each mode, similar to adding a formant to the response function of the body. In actual fact the strings, body and surrounding air should, in theory, be coupled together for an accurate description of the sound pressure at a point in space near the instrument as one of its strings is plucked.

The coupling between the body and the air is important because the air damping on the structure effectively decreases the Q value of the structural modes so that a strongly radiating mode will tend to have a reduced *Q*. However, this problem is rectified to some extent by the fact that the admittance measurement is carried out with air loading on the body already (Wright 1996).

At the time of writing this thesis there is no simple way of coupling these three sub-systems together in the frequency-domain. We are left to simplify the three-way coupling; firstly describe the string-body coupling, then define a monopole and dipole source strengths for each body mode of interest that effectively couples the body to the surrounding air. This method is consistent with previous work at Cardiff (Richardson 2001; Hill et al. 2004).

Weinreich and Arnold (1980) showed that the sound pressure from a spherical sound source can be decomposed into monopole, dipole and higher-order spherical harmonics. This is done by measuring the sound pressure at many different points around the object using two microphones at different radii, therefore enabling separation from incoming and outgoing waves and creating an image of how the object radiates sound in any direction. A calculation called spherical-harmonic decomposition (SHD) separates the sound pressure into a monopole component, three orthogonal dipole components and higher-order spherical harmonics. The sound pressure can then be modelled for each of these components and finally summed together to get the overall pressure response. Hill et al. (2004) showed that the contribution to the radiated sound from sources of higher order than dipoles is negligible, and so are ignored in this thesis.

2.4.1 Monopole radiation

The simplest sound radiator is a pulsating sphere with a sinusoidal-varying radius with time, generating spherically-diverging sound waves, i.e. a monopole source of sound. The simplest example is a monopole point source, but Hill et. al. (2004) showed a much improved fit between model and measurement of the sound pressure of a guitar using finite-sized sources rather than point sources. The

condition for approximating the source as a point source is that the source radius should be small compared with the wavelength of the radiated sound (Morse and Ingard 1968). For the guitar this means that the theoretical framework would hold up to about 500 Hz. Although describing the source as having a finite size extends the validity of the theory to higher frequencies, it is unlikely that the theory holds particularly well up to the frequencies studied here. The reader will be reminded of this issue and reassured of its application in Chapter 7.

The goal in deriving the response of this finite-sized monopole source is to find the sound pressure, p, at a distance, r, away from the spherical source of radius r_0. The surface velocity when radiating a harmonic wave, for example, is $u_s = u_0 e^{-i\omega t}$, where u_0 is the local particle velocity. This gives a volume velocity of $4\pi r_0^2 u_0$, which is also called the source strength, S_ω (Morse and Ingard 1968). To find the local sound pressure, the surface velocity of the sphere is equated to the radial particle velocity of the air, where the latter is given by,

$$u = \frac{1}{\rho_0 c}\left(1 + \frac{i}{kr}\right)p\,, \tag{2.5}$$

at $r = r_0$ gives,

$$p_{r_0} = -\rho_0 c u_0 e^{-i\omega t}\left(\frac{ikr_0}{1 - ikr_0}\right). \tag{2.6}$$

For a spherically-diverging wave, the pressure varies with distance and time as (Kinsler et al. 2000)

$$p = \frac{A}{r}e^{i(kr-\omega t)}\,. \tag{2.7}$$

Therefore equating Equation (2.6) with Equation (2.7) and solving for the amplitude of the spherical wave, A, gives,

$$A = -\rho_0 c r_0 u_0 \left(\frac{ikr_0}{1 - ikr_0}\right)e^{-ikr_0}\,. \tag{2.8}$$

Finally inserting this back into Equation (2.7) gives,

$$p = -\frac{i\rho_0 c k S_\omega}{4\pi r}\left(\frac{e^{-ikr_0}}{1 - ikr_0}\right)e^{i(kr-\omega t)}\,. \tag{2.9}$$

The above equation gives the sound pressure from a finite-sized monopole source radiating harmonic spherical waves.

2.4.2 Dipole radiation

It is also of interest to define the sound pressure from a dipole sound source. This time, consider two point sources vibrating out of phase with each other and separated by a small displacement (Morse and Ingard 1968). One source has strength S_ω at the point $1/2\,\boldsymbol{d}$ and the other has strength $-S_\omega$ and is at the point $-1/2\,\boldsymbol{d}$, where $\boldsymbol{d}$ is the displacement vector between the sources. A dipole strength vector can then be defined, $\boldsymbol{D_\omega} = S_\omega \boldsymbol{d}$, and broken down into three components along the x, y and z axes. If $\boldsymbol{d}$ is small compared with the wavelength, the pressure in spherical coordinates are (Richardson 2001)

$$p_{dx} = -\frac{\rho_0 c k^2 D_x}{4\pi r}\sin\theta\cos\varphi\left(1+\frac{i}{kr}\right)e^{i(kr-\omega t)}\ , \tag{2.10}$$

$$p_{dy} = -\frac{\rho_0 c k^2 D_y}{4\pi r}\sin\theta\sin\varphi\left(1+\frac{i}{kr}\right)e^{i(kr-\omega t)}\ , \tag{2.11}$$

$$p_{dz} = -\frac{\rho_0 c k^2 D_z}{4\pi r}\cos\theta\left(1+\frac{i}{kr}\right)e^{i(kr-\omega t)}\ . \tag{2.12}$$

The angle θ is the vertical angle and φ is the lateral angle as shown in Figure 2.4.

For the equivalent finite-size sources rather than point sources the change (Hill et al. 2004)

$$D_\omega \rightarrow D_\omega \frac{2e^{-ikr_0}}{2-2ikr_0-k^2r_0^2} \tag{2.13}$$

is required.

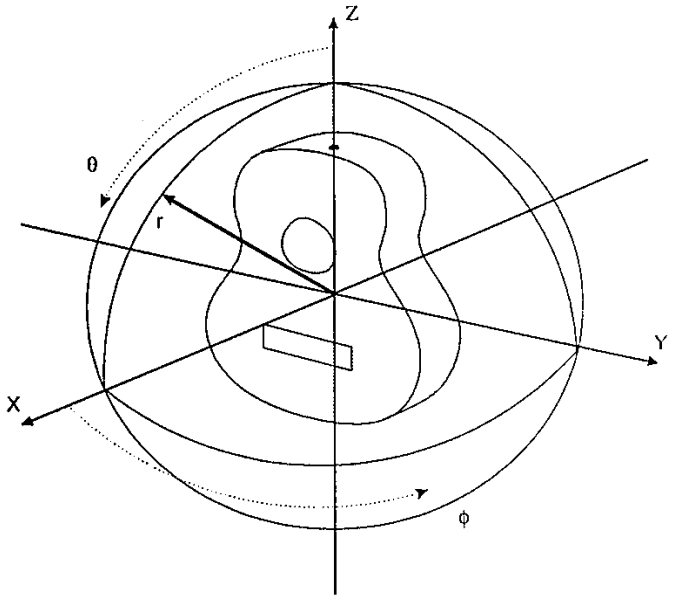

Figure 2.4: Coordinate system used to define the source strengths of dipoles aligned along the X, Y and Z axes. Adapted from Hill et al. (2004) with permission from the author.

Chapter 3 Experimental Methods

This chapter describes the development of analysis techniques and methods for carrying out the physical (as opposed to psychoacoustical) measurements in this thesis. These measurements can then be used either to model the radiated sound from a classical guitar or compare the vibrational characteristics of the classical guitar, folk guitar and banjo. Firstly, the problem of accurately estimating the initial amplitude of decaying partials is discussed. Then the attention is turned towards measuring the characteristic impedance of strings, mechanical response of instrument bodies and mode shapes on the soundboard of an instrument. Finally a brief section is given on the experimental set up that was used to make sound-field measurements. Data from the latter measurement is vital in modelling the sound pressure response of a classical guitar.

3.1 Extracting parameters of exponentially decaying sinusoids

Many signal-processing techniques have been developed over the past half a century to analyse the spectra of various signals. This has come as a result of the rapid increase in computing power with the hope of satisfying the inadequacies of standard Fourier techniques. Such methods include the Prony method (Kay 1987), Kumaresan-Tufts method (Porat and Friedlander 1987), the matrix-pencil method (Laroche 1993) and the closely related ESPIRIT method (Le Carrou et al. 2009). These

methods are reported to achieve high efficiency and resolution for the characterisation of well-behaved exponentially decaying signals. A comparison of the performance of these methods in analysing the signals under investigation here is beyond the scope of this work. What is important is to obtain a tool that is well-understood so that it can be used with confidence. Also, it is useful to analyse the components of the signal in detail, not just to obtain parameter values for each component, but to study the decay profile of the components individually. Using knowledge of the processes that generate the signals (such as those discussed in the previous chapter) it is then possible to make decisions on how well the proposed model describes the observed signals. For these reasons standard Fourier techniques are used in this thesis.

It has been discussed in Section 2.1 that string partials are modelled well as exponentially decaying sinusoids. This simple model may also be applied to characterise the body components of the sound. In this section, a method of extracting the parameters of these signals using the fast-Fourier transform (FFT) will be discussed.

The aim here is to extract the initial amplitude, frequency and Q value of a decaying signal. Extracting these parameters from the sound radiated by different instruments is the first step in characterising their sound. It is also useful to extract these parameters in order to resynthesize the signal using Equation (2.2). In all cases here the signal is sampled at 44.1 kHz in 16-bit. A rectangular window is used for all FFTs here.

First of all a large FFT with a time window of T_L= 6 s is performed on the waveform to obtain a high-resolution picture of the spectrum (spacing of 0.168 Hz between consecutive points). This window does not capture the whole decay, so the signal is truncated. The frequency of the tallest peaks in the vicinity of harmonic frequencies are extracted, labelled f_L. The inharmonicity caused by the stiffness of the string can be taken into account using Equation (2.1) and a reasonable estimate of the inharmonicity parameter B.

Then a series of short-term FFTs (STFFTs) are carried out with a time window of T_b= 0.09 s. Here the start time of each successive STFFT is separated by intervals of 0.045 s, this interval is called the time step. Plotting each STFFT one after the other on a 3D graph shows how each individual component decays with time, this is called a waterfall plot. The frequency and amplitude of the peaks, f_b and A_b respectively, are then measured in each STFFT. Plotting the amplitude of a single component in dB from successive STFFTs shows the decay of the component with time and a straight line is fitted to the appropriate portion of the decay (see Figure

2.2). The Q value of that component is then measured from the gradient of the best fit line, g, using the equation

$$Q = \frac{-20\pi f_L \log e}{g}, \tag{3.1}$$

where e is the natural logarithm constant. The initial amplitude is equal to the intercept of the best-fit line.

3.2 Error in amplitude measurement of decaying sinusoidal signals

There are two problems with measuring the initial amplitude using the method described above. This problem was first observed here when generating synthesised signals of known amplitudes then measuring the initial amplitude using this method. Further investigation showed that decaying signals are subject to spectral smearing (the term used to describe the spreading of spectral energy) due to two factors. Firstly the decay of the signal causes the spectral energy to spread out around the peak frequency; the heavier the damping the more smearing occurs, see Figure 3.1. Secondly, for a signal that is truncated to be FFTed in such a way that there are not an integer number of cycles in the time window, signal and window being non-commensurate (Higgins 1976), the peak in the FFT will again be smeared, see Figure 3.2.

The latter effect is sometimes called leakage error (Thompson and Tree 1980).The worst case of leakage error occurs when the signal is truncated such that there are $j + 1/2$ number of cycles in the time window, where j is an integer. In this case the amplitude measured in the FFT will be $2A/\pi$, where A is the correct amplitude of the signal. This translates to an error in IA of about 4 dB, which is likely to be perceptually significant (see Section 5.4). Interestingly there is only a small error in the measurement of Q because every amplitude measurement in the STFFTs suffer from the same amount of smearing, assuming a constant damping factor, causing the gradient of the best fit line to be unchanged.

Two methods of rectifying this amplitude error will be discussed next. Their performance is then compared in the context of typical signals measured in this thesis.

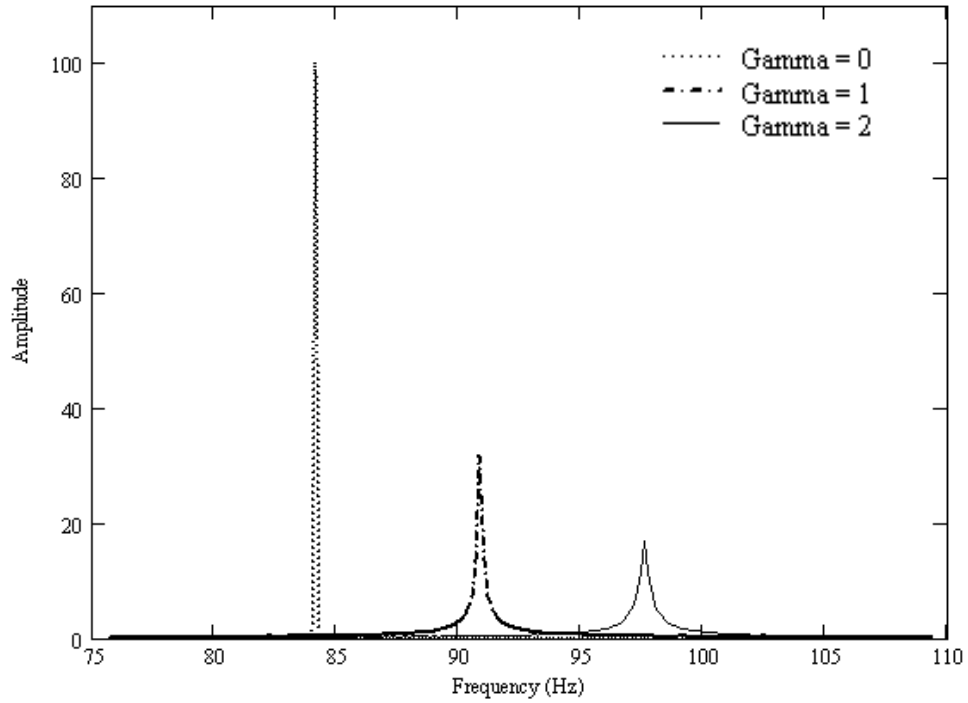

Figure 3.1: FFT of three signals with equal initial amplitude, 200, and different damping factor, gamma. Dotted line is a continuous signal, gamma = 0. Dash-dot line is with a damping factor of 1 and solid line is with a damping factor of 2. The frequency of each signal was chosen such that all three signals have an integer number of wavelengths inside a time window of 6s and are sufficiently far apart to see the three peaks clearly.

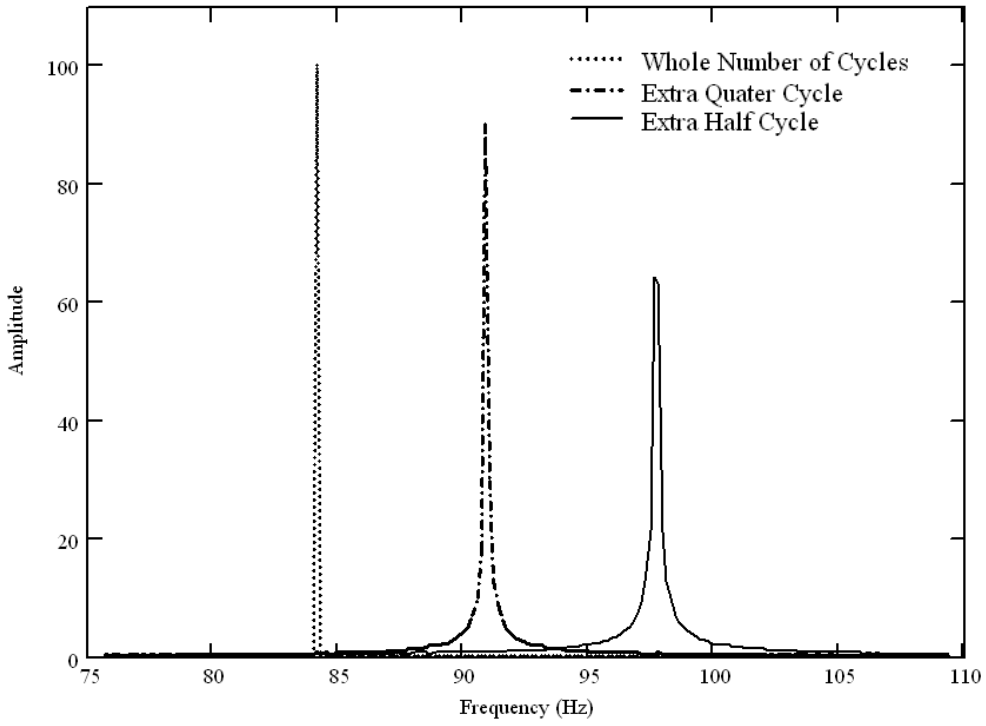

Figure 3.2: FFTs of three signals with equal initial amplitude, 200, time window is 6s. Dotted line has 500 cycles in the time window, dash-dot line has 540.25 cycles and the solid line has 580.5 cycles in the time window. All three signals have no damping.

3.2.1 Parseval's theorem

Equation (3.2) shows a useful equality that links a waveform's time history with its power spectrum. This is called Parseval's theorem (Čížek 1986).

$$\sum_{n=0}^{N-1}|x[n]|^2 = \frac{1}{N}\sum_{k=0}^{N-1}|X[k]|^2 , \tag{3.2}$$

where $x[n]$ is the sampled waveform in the time domain, and $X[k]$ is the power spectrum density in the frequency domain. This relation can be utilised to find the initial amplitude, A, in the following way. First it is assumed that it is possible to sum over a peak in the spectrum using a large FFT without including any other components. This assumption also implies that the decay of this component will be a simple exponential since it will not be interacting with any other component. The right hand side of Parseval's theorem for a single component of the sound signal is then easy to calculate. Now, replacing $x[n]$ on the left hand side with Equation (2.2) and replacing t with n/f_s as for a discrete signal gives

$$\sum_{n=0}^{N-1}\left|A\sin\left(2\pi f\frac{n}{f_s}\right)exp\left(\frac{-\pi f n}{Q f_s}\right)\right|^2 = \frac{1}{N}\sum_{k=0}^{N-1}|X[k]|^2 . \tag{3.3}$$

The frequency is measured using a large FFT, f_L, and the Q value is estimated by fitting a straight line to the decay using the STFFT method presented in the previous section. Now there is sufficient information known about the left hand side of Equation (3.3) to find the initial amplitude in the form

$$A = \frac{\frac{2}{N}\sum_{k=0}^{N-1}|X[k]|^2}{\sum_{n=0}^{N-1}\left|\sin\left(2\pi f_L\frac{n}{f_s}\right)exp\left(\frac{-\pi f_L n}{Q f_s}\right)\right|^2} . \tag{3.4}$$

The factor of 2 in the numerator is included to compensate for discarding the negative frequency components in the FFT algorithm (not always necessary depending on the particular FFT algorithm used). This method solves the problem of spectral smearing due to damping and leakage error at the same time, although the assumptions may not always be valid.

3.2.2 Leakage error

The second method described here is to solve the problem of leakage error and ignore the small amount of spectral smearing due to damping of the signal, this is justified by choosing a small time window for the STFFTs. This method rectifies the amplitude of the signal by considering the process of convolution in the frequency

domain between the signal and time window. An alternative way of avoiding leakage error is to choose a time window such that the signal dies away to nothing by the end of the window. This is incorporated in the method outlined in Section 3.2.1. Another way of minimising leakage error is to apply a weighting function to the window before it is FFTed. This modifies the spectrum by improving some details with the expense of others but we are none closer to an accurate estimate of the amplitude.

The following method for correcting the amplitude of a signal in an FFT was formulated using the text by Lynn (1977) and journal paper by Thompson and Tree (1980).

If one assumes that the time window of the STFFTs is sufficiently short that the smearing due to damping can be ignored then the Fourier transform of the signal can be approximated as a pair of delta functions; one of positive and one negative frequency each with amplitude equal to $A/2$, where A is the original amplitude of the signal. The signal is multiplied by the time window when FFTed, here the time window is of basic rectangular shape and so its Fourier transform is a $sinc$ function. The delta function in the negative frequency space is ignored so that the FFT, indexed k, is a convolution of a single delta function with the $sinc$ function, both indexed n. This convolution is expressed as

$$X_k = \sum_{n=0}^{N-1} \delta_n sinc[\pi(k-n)]\,. \tag{3.5}$$

The delta function is defined as

$$\delta_n = \begin{cases} A/2, & n = fT \\ 0\ , & n \neq fT \end{cases} \tag{3.6}$$

where f and T are the frequency of the signal and length of time window respectively. Using the fact that δ is 0 for all n except at $n = fT$, the summation in Equation (3.5) can be ignored. Then replace n with fT, and δ with $A/2$ to get

$$X_k = \frac{A}{2}\, sinc[\pi(k-fT)]. \tag{3.7}$$

Now a single value for k is chosen corresponding to the tallest point of the peak in the STFFT. Its measured amplitude and frequency are labelled A_b and f_b respectively. These are substituted into the above equation to get

$$A_b = \frac{A}{2}\, sinc[\pi(f_b T_b - fT_b)]\,, \tag{3.8}$$

where T_b is the time window of the STFFTs. Next, the frequency of the signal, f, is approximated by the frequency of the component measured in the large FFT, f_L, then the above equation can be arranged for A.

$$A = \frac{2A_b}{sinc[\pi T_b(f_b - f_L)]}. \tag{3.9}$$

3.2.3 Comparison of methods

The aim here is to analyse and compare the two initial amplitude correction methods described above with the previously used basic method that has no amplitude correction. These will be referred to as the Parseval correction (PC) method, leakage correction (LC) method and basic method (BM). The advantages and disadvantages of the two new methods are then compared with careful consideration for the types of signals that are expected to be analysed.

A synthesised signal was generated and the initial amplitude measured using all three methods for a range of frequencies, these are shown in Figure 3.3. The blue line is the initial amplitude of the synthesised signal and the green line is the measured initial amplitude using the BM. The range of frequencies here were chosen such that there are 10 full cycles in the time window on the left of the graph and 11 full cycles at the right of the graph with 60 increments in between. It is clear that the BM depends strongly on the fraction of cycles included in the time window. As mentioned previously the worst case is at half of this range corresponding to truncating at half a wavelength, IA = 75.9 dB. Note that the amplitude never reaches the generated value of 80dB; this is because of the spectral smearing due to the damping of the signal (Q = 500 here).

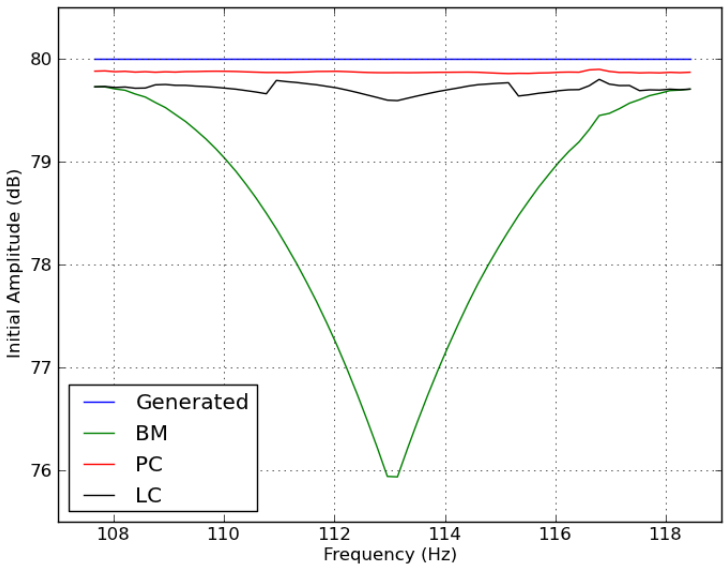

Figure 3.3: Comparison between the three initial amplitude measurement methods and the generated value of 80 dB. The left side of the graph corresponds to a signal of 10 full cycles and the right side 11 full cycles in the time window. The signal had a Q value of 500.

The black curve was generated using the LC method. Note that using a window capturing a full number of cycles yields the same result as the basic method. The LC method was fairly consistent for a simple exponentially decaying signal (average and standard deviation of 79.71 dB and 0.05 respectively). The fluctuations are due to the error in the measurement of f_L and depend on the relative sizes of the large FFT and the STFFTs.

The red curve was calculated using the PC method, which was closer to the generated value and more consistent (average and standard deviation of 79.870 dB and 0.007 respectively).

Although this shows that the PC method gives more accurate results, the precision of both these measurements are likely to be well within the boundaries of perceptual changes to the initial amplitude of a single component. An example from the literature is the smallest perceivable difference in amplitude of the fundamental of a voice sound, the result was 3.2 dB (Kreiman and Gerratt 2010). The overwhelming advantage of the LC method is that one can look at the decay of the signal and decide whether a straight line should be fitted, as well as choosing which portion of the decay to apply the straight line. The PC method relies more heavily on the assumption that the signal follows our simple model. As demonstrated in Figure 2.2 this is not always the case. For more predictable signals the PC method is more effective, but because it is within our interest to investigate each fitted component individually the LC method will be implemented.

3.3 Characteristic impedance of a string

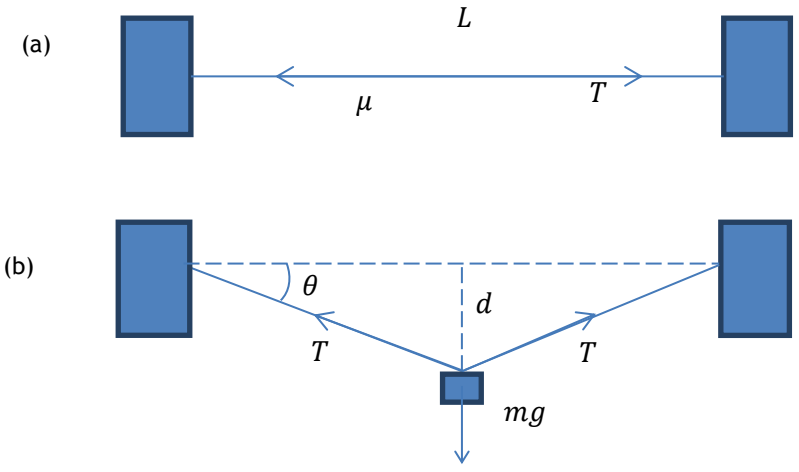

Figure 3.4: String under two conditions; (a) at rest and (b) with mass attached to its centre point. Note g is the acceleration due to gravity.

As previously mentioned, the coupling between the string and the body is important when considering the acoustical signature of a plucked-string instrument. This coupling is analogous to impedance matching in electrical circuits (Schelleng 1962), and so as well as finding the admittance (the reciprocal of impedance) of the body, it is important to measure the impedance of the string. The characteristic impedance of the string is measured here using the following simple method.

Consider a string of length, L, clamped at both ends under the two conditions shown in Figure 3.4. In the first instance, Figure 3.4a, the string has tension and mass per unit length T and μ respectively. The characteristic impedance of the string is then,

$$Z_0 = \sqrt{T\mu}\,, \tag{3.10}$$

and the frequency of the fundamental is,

$$f = \frac{1}{2L}\sqrt{\frac{T}{\mu}}. \tag{3.11}$$

Re-arranging Equation (3.11) for μ and substituting into Equation (3.10) gives,

$$Z_0 = \frac{T}{2fL}. \tag{3.12}$$

The trick is now to find T without measuring it directly. This is done by suspending a known mass, m, half-way along the string and measuring the deflection of the string, d. Note that an assumption is made that the small increase in tension can be ignored.

Resolving forces in the vertical direction in Figure 3.4b gives, $2T\sin\theta = mg$, and solving for T gives,

$$T = \frac{mgL}{4d}. \tag{3.13}$$

Finally substituting this equation into Equation (3.12) gives the characteristic impedance of the string in the form,

$$Z_0 = \frac{mg}{8df}. \tag{3.14}$$

To implement the above equation the following method was used. The string of interest was tuned to standard tuning and all other strings were muted using a cloth. The total playing length was measured and the midpoint of the string marked with a marker. The instrument was then turned upside down and placed between two stools; one at each ends of the instrument such that the strings were free to vibrate. A microphone was used to record the radiated sound from a pluck of the string.

Before adding the mass, the distance between the fret board and the string was measured at its midway point using a ruler accurate to half a millimetre, called d_0.

A 250 g mass was then placed at the centre of the string. The distance from the fret board to the centre of the string was measured again, d_1, such that $d = d_1 - d_0$. The fundamental frequency of the string, f, was measured by applying Equation (2.1) to the first 50 partials of the FFT of the pluck. The errors involved in these measurements are dealt with in the next chapter.

3.4 Mechanical response

The mechanical response of an instrument holds a great deal of information about the vibration of the body. As mentioned in Chapter 2, the form of mechanical response measured here is the input admittance, which we recall is the velocity divided by force. Woodhouse and Langley (2012) state that the most useful single measure of the acoustical performance of an instrument might be the input admittance of the body at the position on the bridge where a string makes contact.

In the next chapter, experiments are carried out to see how the admittance curve changes by changing the measurement position along the bridge of a classical guitar and by adding mass to the anti-nodal area of a body mode. Admittance measurements on different instruments are also compared. It is useful sometimes to characterise some modes using the modal parameters; resonance frequency, Q value and effective mass. One can then track changes in the mechanical response by tracking changes in the modal parameters as the conditions of the experiment are changed.

The modal parameters can be estimated in a number of ways, some methods are mentioned in Section 3.2. For more information about specialised modal extraction routines for admittance data from the guitar or violin the reader should refer to the work of Woodhouse and Langley (2012). Two methods of parameter extraction were initially explored here; a simple peak-picking method and the circle-fit method. These methods tend to give good results for well-defined modes but their performance deteriorates once the modes get close enough to influence the response of each other. The peak-picking method is simple to implement whereas the circle-fit method is more complex and perhaps not as flexible. Although the latter method is more accurate for a single isolated mode, its superiority diminishes when the influence of nearby modes are taken into account. Therefore the simpler method was used as it is more straightforward to implement.

3.4.1 Measuring input admittance

The force is supplied and measured using a small impact hammer that delivers an impulse and measures the force at a wide range of frequencies. A small metal disk was stuck onto the instrument at the striking position; this stops the hammer tip from damaging the instrument and gives a flatter force response. The metal disk weighs only 80 mg, which is small enough to be neglected. The velocity is measured using an accelerometer attached to the instrument as close as possible to the striking position, the acceleration signal is then simply divided by $i\omega$ to yield the velocity. This system was calibrated by fellow PhD student, Ian Perry.

The velocity was also measured using a 3D laser vibrometer system. Using the vibrometer to measure the velocity is more time consuming and more difficult to implement successfully, but it does have the obvious advantage of measuring the velocity in three directions. Using the accelerometer is a simple and robust method, and the extra mass of the accelerometer added to the instrument has been shown to be negligible (Perry 2014). Only results using the accelerometer are shown here.

In all cases the instrument was suspended by rubber bands attached to a solid frame. The strings were damped by wrapping a piece of cloth around the strings. This means that some of the energy delivered by the impact hammer to the bridge will be lost to the cloth through the strings. Woodhouse and Langley (2012) show a simple calculation in order to attempt to correct this added damping to the instrument's vibration. No attempt was made to correct the input admittance in this work because it is only a small correction and bears no real consequences on the results presented here. Each input admittance curve that is shown in this thesis is the average of five measurements.

3.4.2 Simple peak picking

This simple peak-picking method involves an initial estimate of the three parameters, fitting the model to the measurement, and then making small adjustments by trial and error until a reasonable fit is achieved.

The peaks are fitted one by one from low to high frequency. Once a peak is chosen, the frequency is estimated where the imaginary part of the response crosses through zero on the y-axis. For closely spaced modes the imaginary part might not cross through zero, at which point the frequency is estimated by locating the peak in the magnitude of the admittance. The Q value is then estimated either using the full-width at half-maximum points if no other peak is within around 50 Hz (Ewins 1985) or using the technique discussed in Section 3.1 using STFFTs for peaks spaced by 10-50

Hz (Woodhouse and Langley 2012). Accurate parameter estimation is difficult for modal spacing of less than 10 Hz, but an estimate giving a reasonable fit can be found with a little practice. The third parameter, M_{eff}, is adjusted to give the correct amplitude to the peak in the magnitude of the admittance. At this point it is useful to look at the phase of the complex admittance as well as the magnitude, as this can help with small adjustments to the parameters to fit the data. Once the modes of interest are fitted it is useful to go back to the start and make some small adjustments because the shape of the curve is influenced by adding the latter modes.

Some parts of this process were automated but a fully automated parameter extraction process was not sought for as it would not give the desired flexibility.

3.5 Studying mode shapes

Just like the complex vibration of the string, the vibration of the soundboard can be divided into many simpler vibrations; these are the modes of the soundboard. Studying the shapes of these modes aids in understanding the interaction between the strings and the body of the instrument and also the way the instrument communicates with its surrounding air.

A 3D scanning laser vibrometer system was used to study the mode shapes of various plucked-string instruments. In reality it is the operating deflection shapes (ODS) that were measured here rather than the shape of individual modes. However, the ODS of well-separated peaks are a good approximation of the mode shapes. The force was supplied and measured using an impact hammer exciting the instrument near the strings' termination points. The resulting vibration from a single hit was measured using three lasers aimed at a single point. This process was then repeated in an automated way at several points on the soundboard of an instrument to map out the vibrational modes, this is called a scan. The lasers use interferometry to measure the vibration, which can be displayed in many forms; displacement, velocity, acceleration or it can be divided by the excitation force to show compliance, admittance or accelerance. The chosen form here is admittance.

Before a scan can be made the lasers must be aligned firstly with the target, this is called 2D alignment, and then relative to each other, called 3D alignment. The alignment process is not an easy task as 2D alignment is laborious and time-consuming and high accuracy is difficult in 3D alignment. 3D alignment needs to be done once for a particular arrangement of the three lasers relative to each other,

but 2D alignment must be repeated each time there is a new target or the target has moved slightly. The advantage of using three lasers rather than one is that the results show the admittance of the soundboard in three directions. Once the laser alignment is complete the lasers are programmed to measure the vibration at many points on a grid defined by the user using the impact hammer signal as a trigger.

For each scan, the instrument was suspended from rubber bands. A piece of string was tied around the neck as an extra support and the lower end of the instrument rested on some foam, these restraints were put in place to reduce pendulum-like motion.

The swing of the hammer was controlled by a stepper motor that enabled consistent and regular hits on the instrument. This was put together by fellow PhD student, Ian Perry, and further details of this part of the apparatus are given in the next section. For each measurement in a scan, the force and velocity were recorded for 2^{16} samples at a sampling rate of 44.1 kHz. The FFT of the velocity was then divided by the FFT of the force to give the admittance as a function of frequency for all points on the grid. The data was then stitched together by the Polytech software to show the vibration as a function of position and phase.

Scans were carried out on an array of instruments. In the next chapter some simple examples are given of selected ODS of well-separated peaks for five instruments. These instruments include two classical guitars, two steel-string guitars and one banjo.

3.6 Sound-field measurement

Although the sound-field data used in this work was taken by fellow PhD student Ian Perry as part of his doctoral work, it is still informative for the reader to know how a sound-field measurement of a guitar is made. The reader is referred to Perry (2014) for further details of this measurement.

Figure 3.5 shows a block diagram of the set up used in the anechoic chamber to make the sound-field measurement. The guitar was suspended using elastic bands around the tuning pegs from a rotating column at the centre of the anechoic chamber. The instrument was also held lightly in place by a chain of elastic bands across its neck and some foam supported the lower part of the instrument to minimise pendulum motion when the guitar was struck by the impact hammer. The strings of the instrument were damped using a cloth as described previously.

A small metal disk was stuck onto the bridge as a target for the impact hammer so that the hammer would not damage the instrument. A PCB impact hammer (model 086E80) was used to supply and measure the force applied to the bridge, this signal was sent through a PCB charge conditioner and then to the sound card. The hammer was mounted in a specially constructed structure that had a built-in stepper motor so that repeatable strikes would be made in an automated manner.

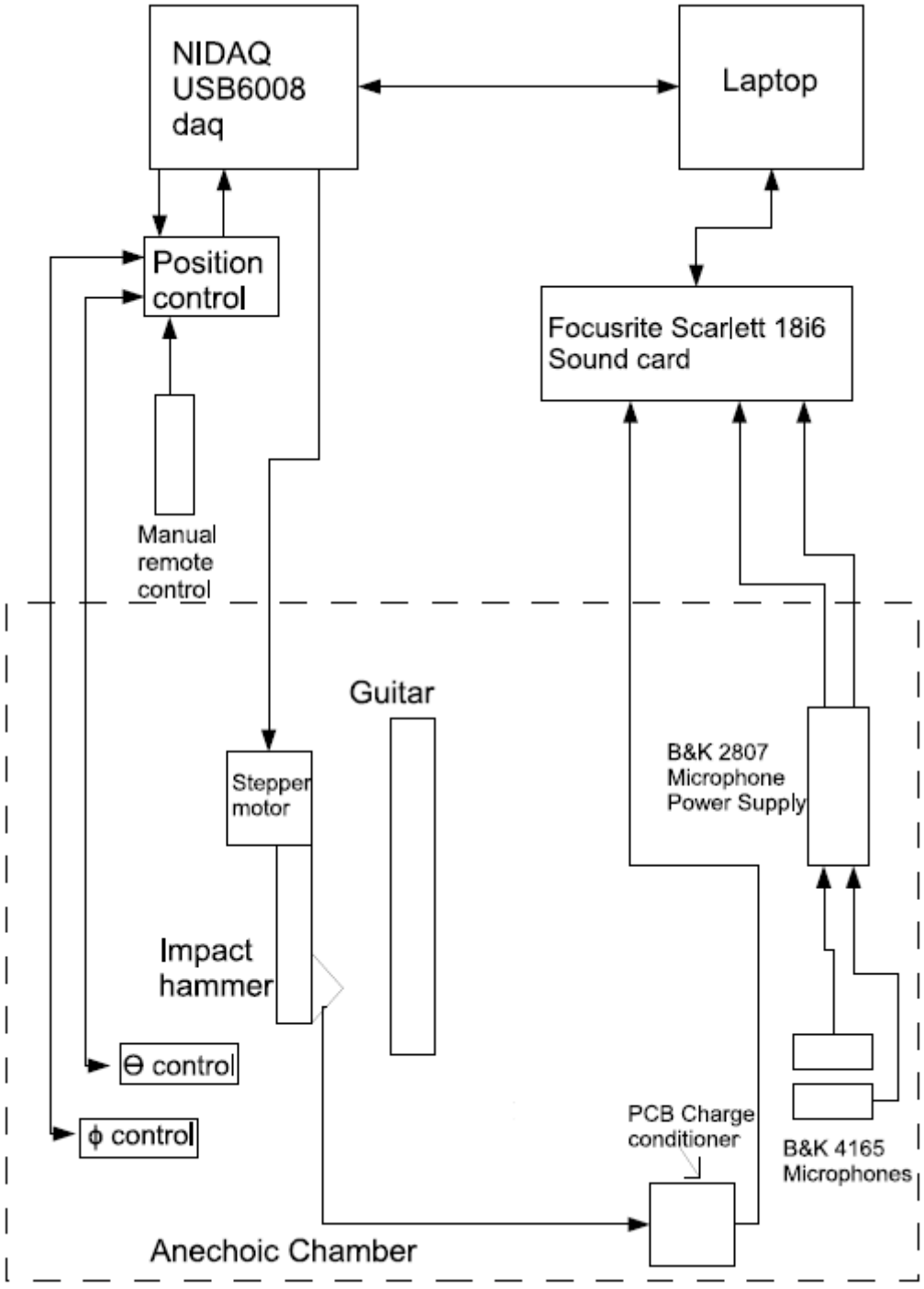

Figure 3.5: Block diagram of the experimental set up used to make a sound-field measurement. Figure was adapted from Perry (2014) with the permission of the author.

The stepper motor producing the swing of the impact hammer was controlled using a data acquisition interface (NI-DAQ USB6008). The same DAQ interface controlled the angle of each sound pressure measurement. The θ (vertical) angle was controlled by changing the angle of an arm that held the two microphones. The φ (lateral) angle was changed by rotating the central column to which the guitar was attached (see Figure 2.4 for the definition of these angles).

The sound pressure was measured using two B&K 4165/2619 microphones at distances of 0.45 m and 0.71 m from the centre of the guitar. The signal from the microphones went through a B&K 2807 microphone power supply and into the sound card.

A laptop was used to control the whole system. The signal from the hammer was used as a trigger to record the sound pressure from the microphones. After two seconds the laptop then sent a signal to the DAQ interface to change the angle of the measurement, and then another measurement was made and so on. The system measured 9 vertical angles and 36 lateral ones to make a total of 324 measurements of the sound pressure from the instrument in order to get good resolution of the guitar's sound-field. A complete sound-field measurement took around two hours.

Chapter 4 Physical Measurements

The methods discussed in the previous chapter were implemented in experiments that are presented in this chapter. The physical origins which possibly generate the perceived differences between the tone qualities of a classical guitar, a folk guitar and a banjo were highlighted by measuring the frequency, initial amplitude and Q value of the string components in the radiated sound from these instruments. Then the characteristic impedances of the strings of each instrument were measured. As well as comparing the input admittance of each instrument, admittance measurements were carried out on classical guitars to track the changes in mechanical response whilst changing measurement position along the bridge and changes due to adding mass to the anti-nodal region of a mode. These two extra investigations will prove to be useful in the context of modelling a classical guitar and influencing the vibrational behaviour of a guitar body. A short section is then given on comparing the global coupling level of a classical guitar, folk guitar and banjo. No new measurements are presented in this section but it is a convenient place to discuss the global coupling level. Finally results are given for the mode shapes of soundboards of various instruments.

4.1 Radiated sound

In this section the analysis method outlined in Section 3.1 was used firstly to compare waterfall plots of the same notes played on the classical guitar, folk guitar

and banjo. Then the parameters of the string partials, consisting of initial amplitudes, frequencies and Q values, were extracted from each open string on the three instruments for a more detailed comparison of their radiated sound.

All recordings were made in a small music studio (reverberation time of about 0.2 s) with the instrument standing vertically on some foam and some cotton string tied around the top of the instrument near the tuning machines to hold it firmly in place. The strings were excited by looping a thin piece of metal wire around the string of interest and pulled away from the instrument. The breaking tension of the wire gave a reasonably consistent force to pluck a guitar or banjo string. This method of plucking a string is called a wire-break. The strings were excited at one-tenth of their total length from the nut of the instrument. It is assumed that there is no significant difference to the string partials whether the string is plucked near the nut or bridge, although perhaps the 'thud' of the body might not be as prominent by plucking near the nut. A half-inch B&K microphone was placed 20 cm in front of the sound-hole of the guitars or centre of the head for the banjo. Due to the various gains added on to the signal before it was recorded onto a PC, the amplitudes of these measurements cannot be compared directly so they are normalised. Each wire-break was recorded in 16 bit with a sampling frequency of 44.1 kHz for six seconds.

4.1.1 Waterfall plots

Figure 4.1 shows waterfall plots for the note D_3 played on classical guitar BR2, a steel-string Simon and Patrick folk guitar and a five-string Fender banjo. The amplitude in each graph has been normalised and the time and frequency scales are linear and go up to 4.5 s and 3 kHz respectively. It is clear that the string partials dominate the radiated sound from these instruments and the body components are difficult to pick out. For example there is one body mode just below the tall peak of the third partial of the D_3 note played on the banjo.

From inspection of these graphs it seems that the balance of vibrational energy between low-order partials (say lowest five) and higher-order partials (above the fifth) is most even for the folk guitar and most uneven for the banjo. The decays of the partials of the folk guitar are the longest and the banjo's partials die out fastest. As mentioned in Section 2.1.1, the higher-order partials die out faster than low-order partials due to internal damping affecting higher-order partials to a greater extent than lower-order ones. The classical guitar has a very strong second partial whereas the other two instruments have three or four low-order partials with similar amplitude.

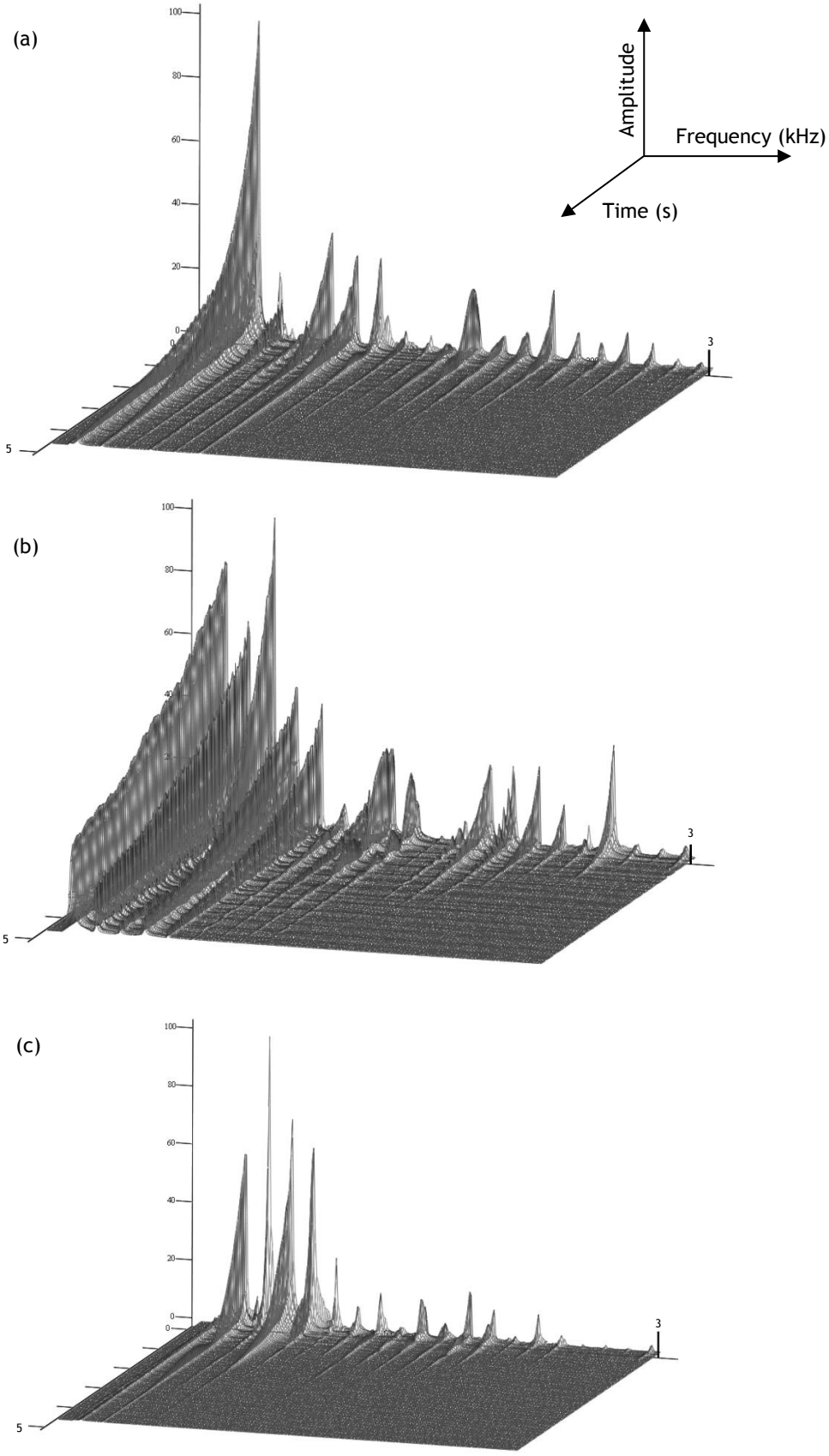

Figure 4.1: Radiated sound of the note D_3 played on the (a) classical guitar (b) folk guitar and (c) banjo. The amplitudes have been normalised and are on a linear scale, the time and frequency scales are linear and are the same in each graph going up to 4.5 s and 3 kHz respectively.

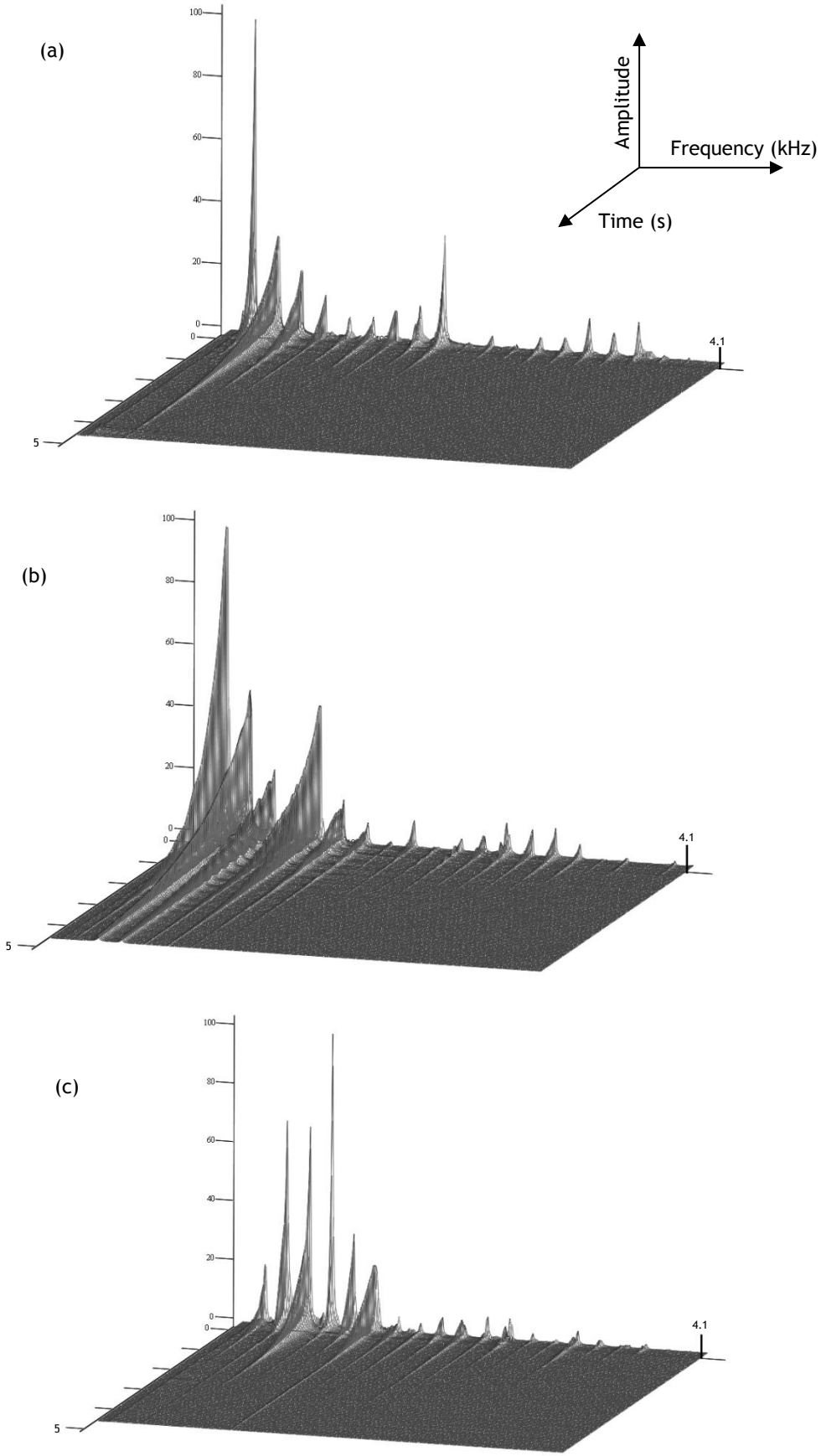

Figure 4.2: Radiated sound of the note G_3 played on the (a) classical guitar (b) folk guitar and (c) banjo. The amplitudes have been normalised and are on a linear scale, the time and frequency scales are linear and are the same in each graph going up to 4.5 s and 4.1 kHz respectively.

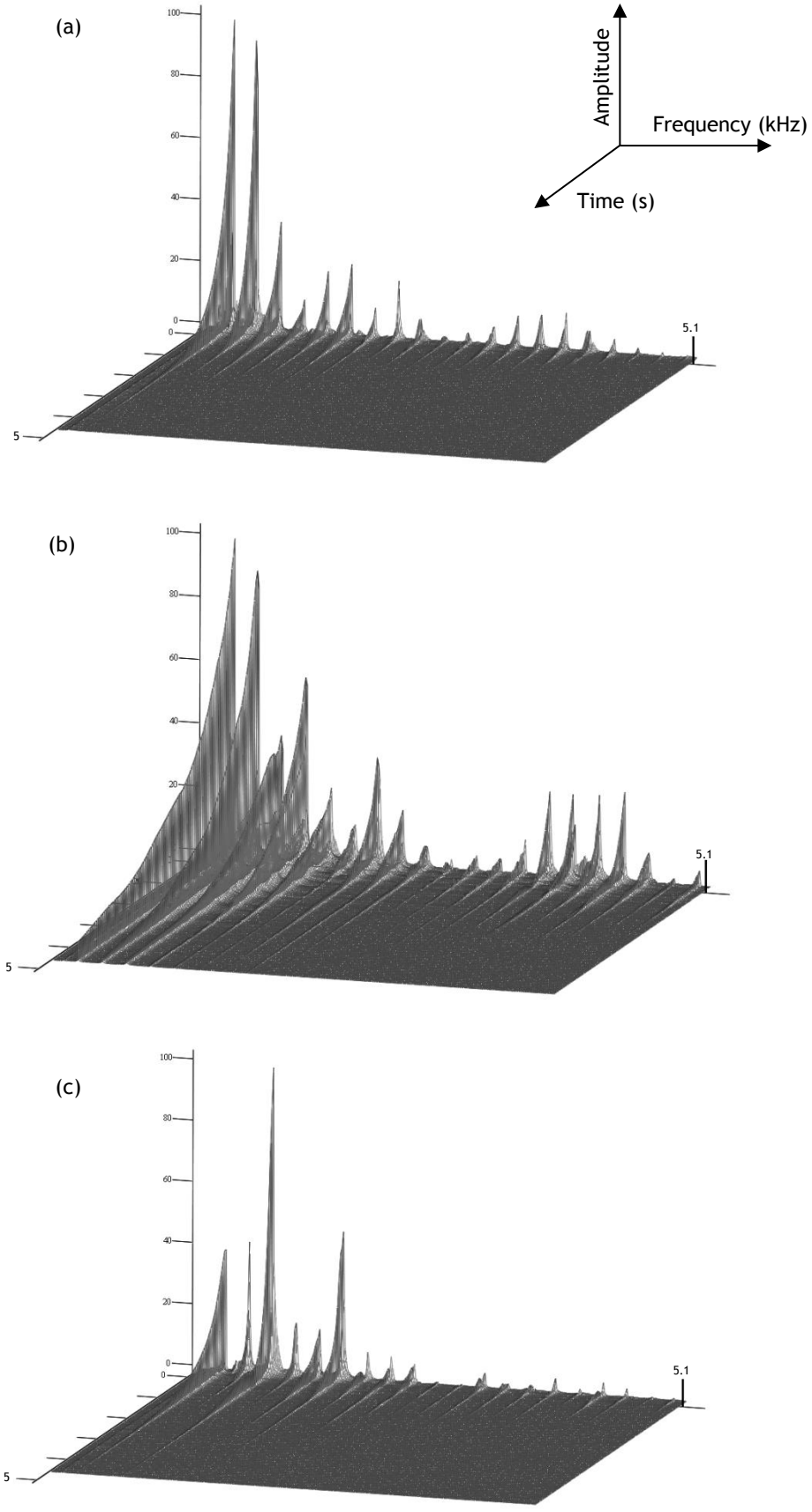

Figure 4.3: Radiated sound of the note B_3 played on the (a) classical guitar (b) folk guitar and (c) banjo. The amplitudes have been normalised and are on a linear scale, the time and frequency scales are linear and are the same in each graph going up to 4.5 s and 5.1 kHz respectively.

Figure 4.2 is similar to Figure 4.1 but for the note G_3. The time scale is the same as before but the frequency scale is now up to 4.1 kHz in order to fit 20 partials into each graph. In all three cases it seems that this note decays faster than the note D_3.The fundamental of the note from the classical guitar resembles one of the low-order partials of the banjo with large initial amplitude and a fast decay. The partials of the folk guitar again have the longest decay and this time the decays of the partials of the classical guitar and banjo look similar.

Figure 4.3 is similar to the previous two figures but this time for the note B_3. The frequency scale has been adjusted up to 5.1 kHz in order to fit 20 partials into the graphs. Once again the partials of the folk guitar have the longest decay and the decays of the partials of the classical guitar and banjo look very similar.

Note that there are only a few strongly beating components in the graphs shown in this section. This suggests that including two string polarisations in the modelling of these instruments is not likely to yield any significant improvements to a model including just one string polarisation.

From a basic inspection of these graphs it seems that the folk guitar and banjo are the most dissimilar instruments, with the classical guitar in between.

4.1.2 String parameters

The initial amplitudes, Q values and frequencies of the first 32 partials on each string were extracted from the radiated sound of the classical guitar, folk guitar and banjo studied here. This amounts to a large amount of data and not all of it is readily comparable. Therefore only some of the data is shown in order to demonstrate the main differences in tonal qualities between the sounds of the three instruments due to their string partials.

Figure 4.4 shows the mean initial amplitudes and Q values for the three similar open strings on the three instruments of interest. The initial amplitudes have been normalised to the strongest partial before converting them into dB. Every tenth partial has been omitted from these graphs because their low amplitude resulted in noisy data with large errors.

The banjo seems to have a consistently weak fundamental, about 15 dB lower than the second partial, which is quite odd. This could be due to the fundamental sharing much of its vibrational energy with a mode of the head because of strong coupling. This will become clearer with further investigation of the instrument's mechanical response later. In the case of the banjo, the three notes chosen here have five strong components, partials two to six, followed by a large drop of about

15-20 dB. The higher-frequency content of these notes is clearly weaker in the banjo than the two guitars. The two guitars are fairly well balanced at low-order partials but the folk guitar has a stronger presence towards higher partial numbers.

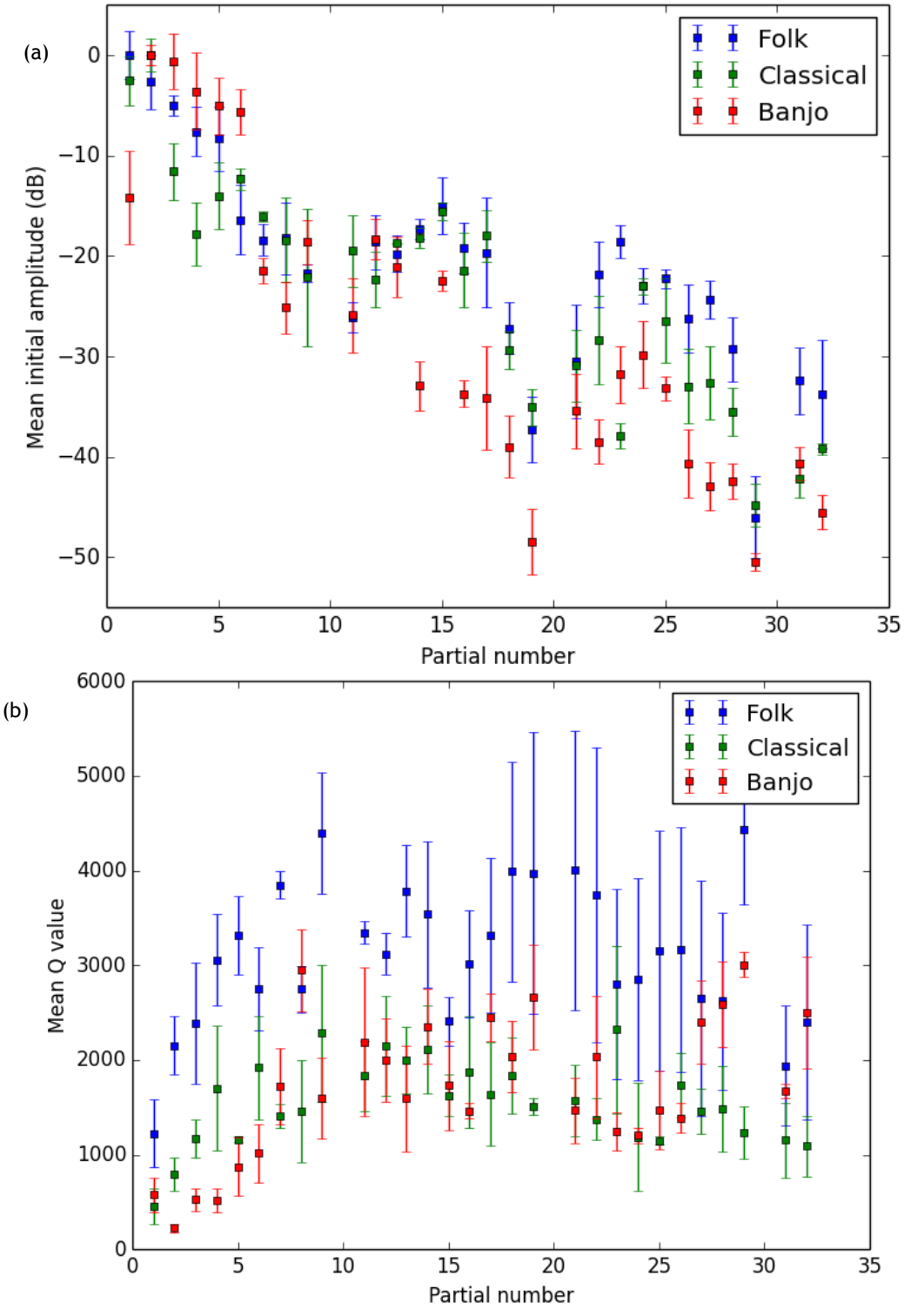

Figure 4.4: Mean (a) initial amplitudes and (b) Q values of notes D_3, G_3, and B_3 plotted against partial number. Error bars show the mean of the standard deviations from three plucks of each note.

Comparing mean Q values of the three notes on these instruments in Figure 4.4b, we see that the folk guitar has consistently higher Q values than the other two

instruments. Below the tenth partial the banjo generally has the lowest Q values. Between the tenth and 26th partials the classical guitar and banjo have similar Q values, and above the 26th partial the banjo has higher Q values than the classical guitar. This cross over is because at lower frequencies the banjo string is so strongly coupled to the head that energy is transferred quickly to the head resulting in a low Q value, whereas towards higher frequencies the steel banjo string acts more like the steel string of the folk guitar.

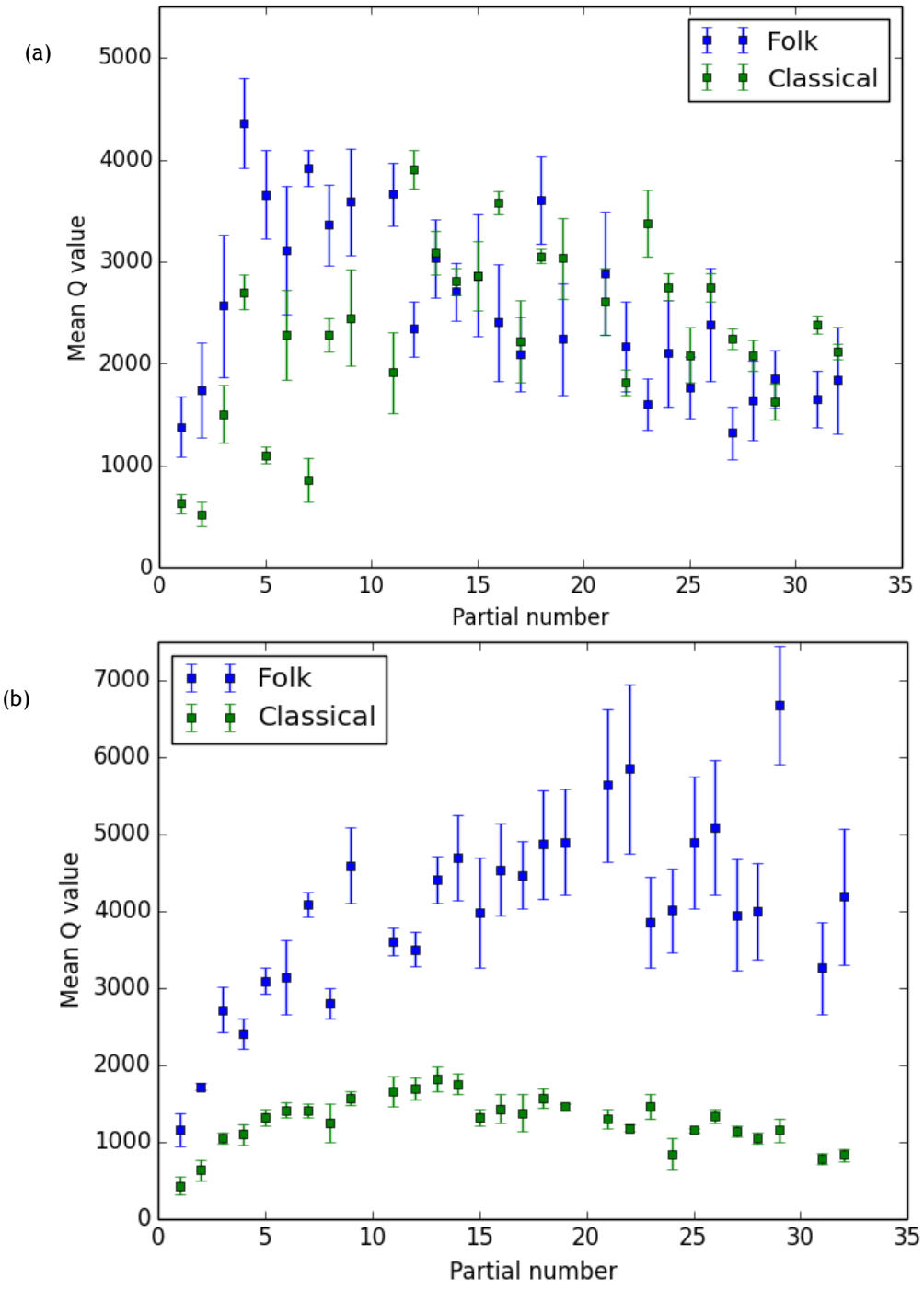

Figure 4.5: Mean Q values for (a) wound and (b) plain strings on classical guitar BR2 and the Simon and Patrick steel-string folk guitar.

The averaging process between the notes D_3, G_3, and B_3 above was repeated for all strings on the two guitars to compare these two instruments further. The mean initial amplitudes and Q values for all six open strings showed similar results as the previous figure, therefore not particularly interesting. However, when the data was split into groups of wound strings and plain strings a clear difference was observed in the Q values of the string partials. This is demonstrated in Figure 4.5.

For wound strings (low-frequency strings), the Q values of the classical guitar below the tenth partial are consistently lower than that of the folk guitar suggesting a higher coupling level on the classical guitar at low-frequencies. Above the tenth partial, the Q values of partials on wound strings are similar on both instruments. In the case of the plain strings the Q values are four to five times larger for steel monofilament strings than nylon monofilament strings. There was not a significant difference in the corresponding initial amplitude graphs.

The above results are summarised as follows. Comparing mean initial amplitudes of string partials between these instruments showed that the sound of the folk guitar might be perceived as relatively 'bright' because of the higher level of higher-order partials, the sound of the banjo may be perceived as relatively 'dark' or 'dull' because of a lower level of higher-order partials. The notes of the folk guitar have the longest sustain, especially when it comes to comparing plain strings. On the other hand, the banjo and three plain strings of the classical guitar have a relatively short decay.

The third parameter to compare between instruments is the frequencies of the partials; these are shown as inharmonicity in cents. That is, the amount by which a certain partial deviates from being harmonic in units of cents, where there are 100 cents in one semi-tone. Equation (2.1) was converted into cents in order to fit the frequencies of the partials as a function of partial number. The function 'curve_fit' from the 'scipy.optimize' module in Python was used to fit the curve given by

$$F_n = 1200 \log_2 \left[f_0 n (1 + B n^2)^{1/2} \right], \tag{4.1}$$

to the equation $1200 \log_2 (f_n / n)$, where f_n is the measured frequency of partial n, and f_0 and B are the frequency of the fundamental and inharmonicity coefficient respectively. The latter two parameters were estimated using a non-linear least-squares fitting method by scipy's curve_fit function. The fitted curve and data were then divided by the estimated fundamental, in cents, to give the curves shown in Figure 4.6.

This simple model for the inharmonicity, on the whole, fits the data well. The model takes into account the inharmonicity due to the stiffness of the string but does not take into account the frequency perturbations due to strong coupling between

the string and the body of the instrument. Thus, decent fits are achieved for the two guitars, but the effect of strong string-body coupling is much more pronounced in the case of the banjo. This is a perfect example of the consequence of using a membrane instead of a plate as the primary sound radiating component of the instrument. There are cases where strong coupling has caused the first few partials of the guitars to deviate from the model. This is because lower-order body modes are more strongly coupled to the strings. From the data shown here, the fundamental of the note G_3 played on the banjo is the partial that deviates the most from the model, at around 20 cents below where it should be. In general a slightly better fit was achieved for the classical guitar than the two instruments with steel-strings.

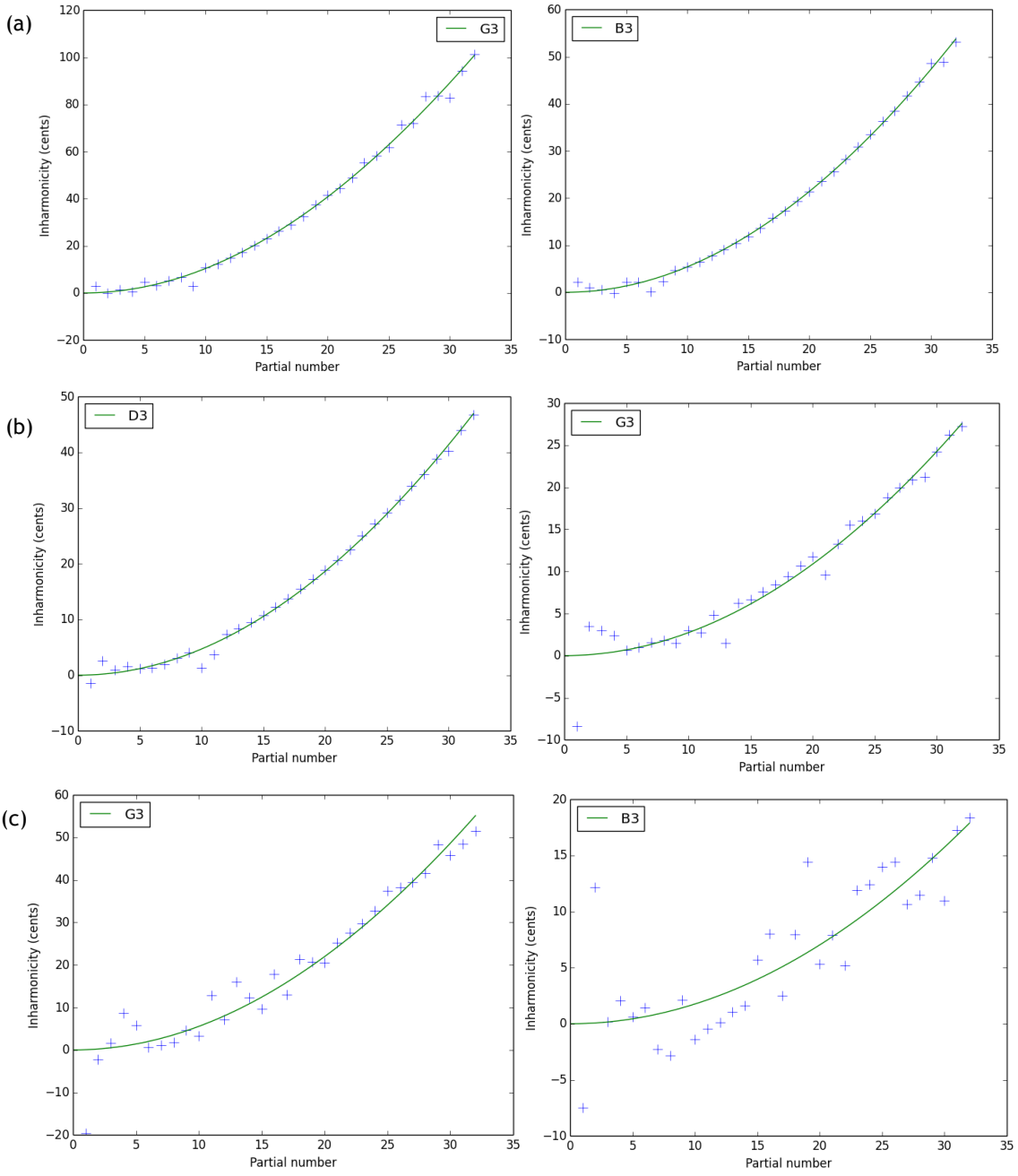

Figure 4.6: Examples of inharmonicity fits for strings on (a) classical guitar, (b) folk guitar and (c) banjo.

This analysis was carried out on all strings on the three instruments, the estimated fundamental frequency and inharmonicity coefficient are shown in Table 4.1. These results for the inharmonicity coefficient of nylon and steel strings agree well with results reported by Woodhouse et. al. (2012). The one result that sticks out the most here is the inharmonicity of the string G_3 on the classical guitar. It is well known by musicians that this string is sometimes difficult to tune properly due to its large inharmonicity. String manufacturers have attempted to solve this problem by producing a nylon-wound nylon string, but this type of strings has not gained widespread acceptance in the musical world.

String number	Classical guitar			Folk guitar			Banjo		
	Note	f_0 (Hz)	B x10^{-6}	Note	f_0 (Hz)	B x10^{-6}	Note	f_0 (Hz)	B x10^{-6}
1	E_4	329.4	38.8	E_4	329.2	16.7	D_4	294.5	17.4
2	B_3	247.0	62.5	B_3	246.2	68.8	B_3	247.6	20.4
3	G_3	196.3	121	G_3	196.1	31.6	G_3	195.3	64.2
4	D_3	146.6	18.4	D_3	146.1	54.4	D_3	146.4	31.4
5	A_2	110.0	11.0	A_2	109.9	72.2	G_4	392.1	26.8
6	E_2	82.4	16.9	E_2	82.6	106			

Table 4.1: Estimated fundamental frequencies and inharmonicity coefficient for all strings of classical guitar BR2, Simon and Patrick folk guitar and a Fender banjo.

Järveläinen and Karjalainen (2006) showed that the inharmonicity coefficient increases with fret number for a given string, and measured B to be 520 x 10^{-6} at the 12^{th} fret of the third string of a classical guitar. By carrying out listening tests they went on to find that the threshold for perceiving inharmonicity also increases with frequency. They concluded that the inharmonicity measured in nylon strings is above the perceivable threshold level but the inharmonicity in steel strings is more obvious because of their higher level in the three lower-frequency strings (see Table 4.1).

To summarise the results in this section the main differences in tonal quality between these instruments are highlighted below.

The differences between the two guitars studied here can be separated into two groups, one for wound strings and one for plain strings. In the former group the tones of the folk guitar have a 'brighter' sound due to a higher level of high-frequency partials, a longer sustain in low-order partials and larger inharmonicity than the classical guitar. For plain strings, the folk guitar again has a brighter sound, there is no significant difference in inharmonicity (apart from the third string of the classical guitar of course) and the folk guitar has a much longer sustain.

The banjo has a 'duller' sound due to a lower level of higher-order partials, its notes have a relatively short sustain and the inharmonicity due to stiffness of the

string is, on average, smaller than the steel-string guitar. However, the simple model used here for the inharmonicity of the partials is not detailed enough to represent the measured inharmonicity of the banjo. Therefore there must be another source of inharmonicity that is more prominent in the banjo than the other two instruments. This is likely to be strong string-body coupling that perturbs the frequency of many string partials and could be significant to the instrument's acoustical signature.

4.2 Characteristic impedance results

The method described in Section 3.3 was applied to all of the strings of two classical guitars, two steel-string guitars and two banjos. The results are shown in Table 4.2. The deflections of the strings were typically around 6 mm for the classical guitars, around 3 mm for the steel-string guitars and around 5 mm for the two banjos. The error in measuring the string deflection was +/- 0.5 mm. The error in calculating the fundamental frequency of the string f was estimated to be +/- 0.5 Hz. These errors were then used in a standard formula to give the error in characteristic impedance, which was typically around 0.01 kg/s and a maximum of 0.04 kg/s.

The results in Table 4.2 demonstrate that on a given instrument the characteristic impedance tends to increase towards the lower frequency strings, which of course are the heavier strings. In general, the strings of the steel-string guitars have the largest characteristic impedance, then the banjo strings and finally the nylon strings of the classical guitars.

It is also worth noting the variation in characteristic impedance of the strings on one instrument. In the case of the steel-string guitars it increases four-fold from string one to six. The characteristic impedance of the banjo strings increase about two-fold from highest to lowest frequency strings, and for the nylon strings Z_0 increases three-fold from string one to six.

These results will be revisited later in this chapter when discussing the global coupling between the strings and the bodies of these instruments.

Instrument		String 1		String 2		String 3		String 4		String 5		String 6	
		f_0	z_0	f_0	z_0	f_0	z_0	f_0	z_0	f_0	z_0	f_0	z_0
Classical guitars	BR1	329.6	0.21	246.9	0.21	196.0	0.26	146.8	0.35	110.0	0.46	82.4	0.62
	BR2	329.6	0.17	246.9	0.17	196.0	0.21	146.8	0.35	110.0	0.43	82.4	0.58
Steel-string guitars	S&P	329.6	0.23	246.9	0.35	196.0	0.62	146.8	0.83	110.0	0.80	82.4	1.05
	X10	329.6	0.26	246.9	0.31	196.0	0.63	146.8	0.70	110.0	0.80	82.4	1.06
Banjos	Gretsch	293.7	0.21	246.9	0.24	196.0	0.35	146.8	0.42	392.0	0.22	-	-
	Fender	293.7	0.21	246.9	0.16	196.0	0.20	146.8	0.36	392.0	0.19	-	-

Table 4.2: Results for characteristic impedance of individual strings of various instruments.

4.3 Input admittance

4.3.1 Comparing the response at different positions along the bridge of a classical guitar

A brief experiment was carried out to compare the admittance at different string termination points on two classical guitars, BR1 and BR2. The reason for doing this is to see how much various peaks in the admittance curve change as a function of position along the bridge. This experiment has been done before (Richardson 2001), but it is useful to re-visit the experiment to form a discussion that is relevant to other work presented in this thesis.

For each measurement the accelerometer was placed one side of the string on the tie block and the hammer used to excite the body at the other side of the string. The principle of reciprocity ensures that, for a linear system, placing the hammer on the left side of the string and accelerometer to the right of the string would yield the same result as if the hammer and accelerometer were to interchange positions (Kinsler et al. 2000). The results for guitar BR1 are shown in Figure 4.7 and are labelled according to their string number.

Figure 4.7 shows that some peaks stay at a consistent height and similar shape regardless of the position of the measurement along the bridge. Other modes change quite dramatically; the reason for these discrepancies is due to the shape of the modes. A vibrational mode is easiest to excite at its antinode(s), i.e. for a given force, the largest amplitude of vibration will result from excitation at its antinode. As mentioned previously, the effective mass will in this case be of the order of the actual mass of the vibrating system. The opposite is also true; theoretically it is impossible to excite a mode at a nodal point or line, here the effective mass increases towards infinity. The first two modes shown in Figure 4.7 are T(1,1) modes, their shape is similar (although not identical) and is shown on the left-hand side of Figure 4.19. These modes have a consistently high peak in the admittance curve because the anti-nodal region of this mode is spread over the bridge of the instrument. The third peak is called a T(2,1) mode, its shape is shown in at the centre of Figure 4.19. This time the outer strings terminate near anti-nodal regions but the middle strings terminate near a nodal line. This results in a large change in the mode's effective mass and hence changes the shape of the admittance curve from one position to another. This is shown clearer in Figure 4.8, which is zoomed in on the $T(1,1)_2$ and T(2,1) modes.

Note that if the soundboard was completely symmetrical along the vertical axis running through the centre of the bridge, then one would expect the admittance at string one to be the same as string six. The same would be true for strings two and five, and for strings three and four. The fact that they are not the same suggests that the anti-nodal region of the T(2,1) mode on the left-hand side of the instrument, near string six, is larger than the anti-nodal region on the right-hand side. This data also suggests that the $T(1,1)_2$ mode is slightly off-centre towards the higher-frequency strings.

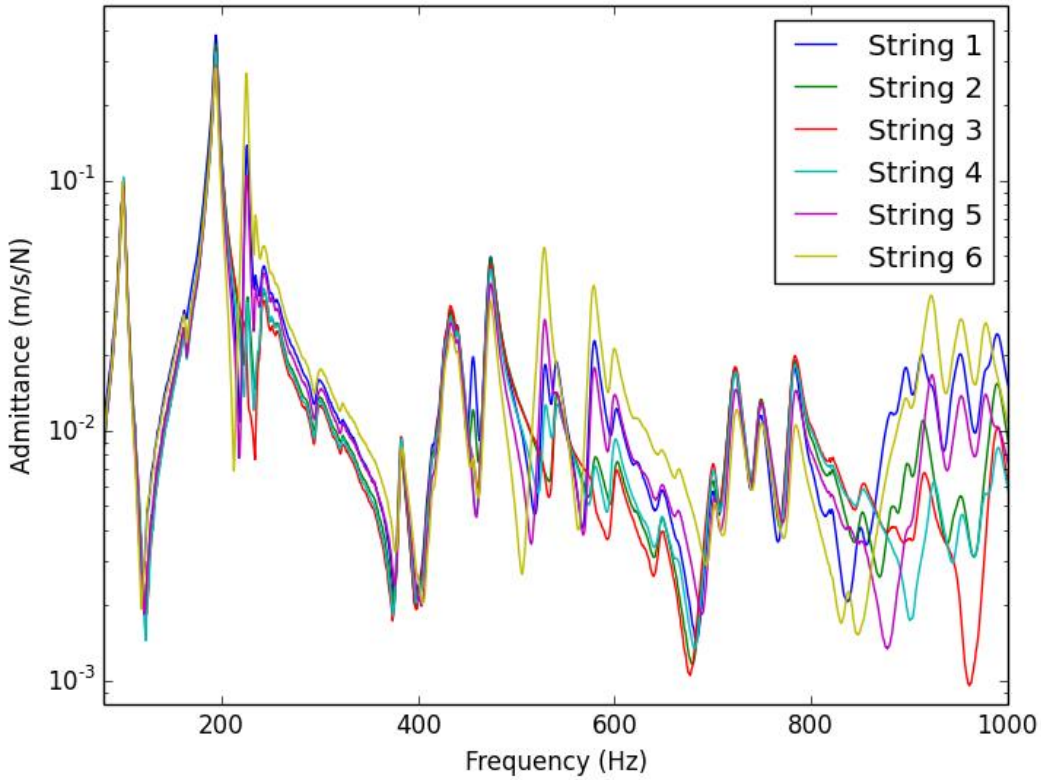

Figure 4.7: Input admittance at the six string positions along the bridge of guitar BR1. The lowest-frequency mode is the $T(1,1)_1$ mode. A zoomed in image of this graph between 150-280 Hz is given in Figure 4.8.

Two important points can be taken from these results that are useful for later discussions. Firstly, there are regions where the admittance changes quite dramatically from one string position to another. Therefore when modelling the mechanical response at the bridge it is best to measure the admittance at string two or five in order to model the instrument. This is because these represent a sort of 'mean' admittance from all string positions. Some might argue that string position 1 is the most important to model because this string is responsible for most of the melody lines played on the instrument. As only one string position will be modelled here and used to represent all string positions it was decided the string position with the 'mean' admittance was the most sensible choice to model. The second point is

that when looking for possible wolf notes on the instrument it is important to take into consideration the frequency of the fundamental of a note and also the string number at which the note is played. Using admittance data taken from the termination point of string six along with a note that is played on string three is likely to yield very misleading results.

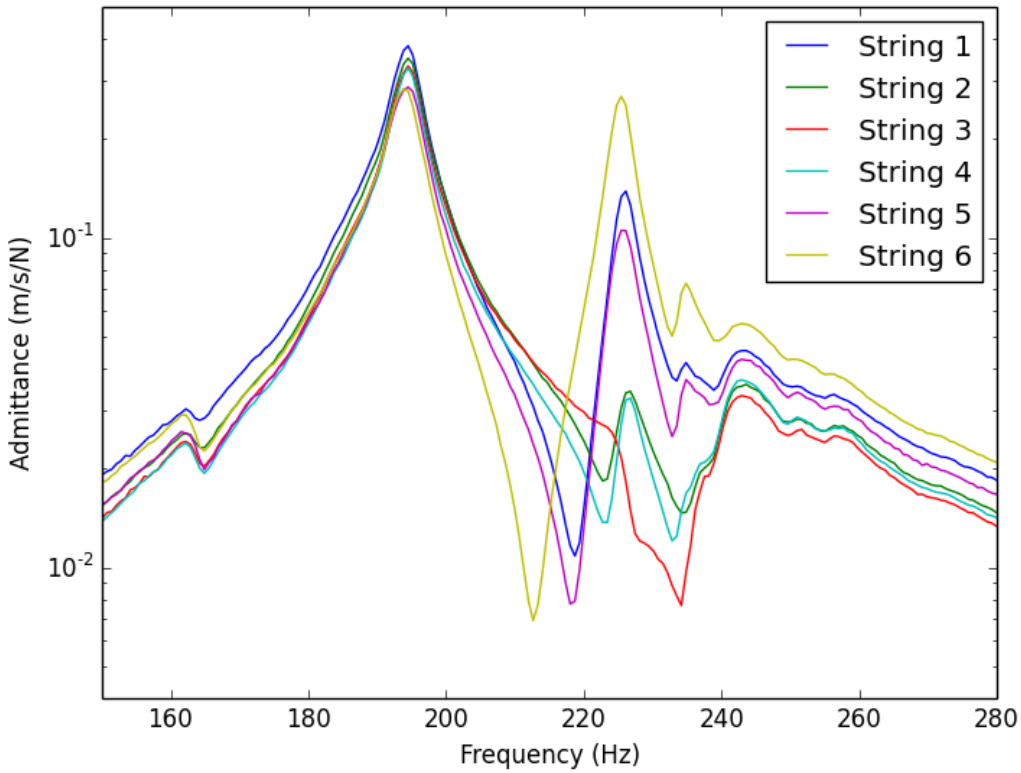

Figure 4.8: A zoomed in version of Figure 4.7 showing the input admittance at the six different string positions of guitar BR1. The peak at 190 Hz is the $T(1,1)_2$ mode and the peak at 225 Hz is the T(2,1) mode.

Similar graphs to Figure 4.7 and Figure 4.8 were obtained for guitar BR2, these are shown in Figure 4.9 and Figure 4.10 respectively. From inspection of these latter two graphs there is similar variation between string positions in the wide frequency range, with again, string positions two and five representing a sort of 'mean' admittance along the bridge. From inspection of Figure 4.10, it seems that the T(2,1) mode is more symmetrical along the vertical axis running through the bridge than for guitar BR1. This is because the T(2,1) mode has a similar height at the corresponding string position on opposite sides of the central vertical line.

Although one can infer the shapes of the modes from admittance measurements, much more information is readily available by mapping out the mode shapes properly using a laser vibrometer system. Results from such measurements are shown later in this chapter.

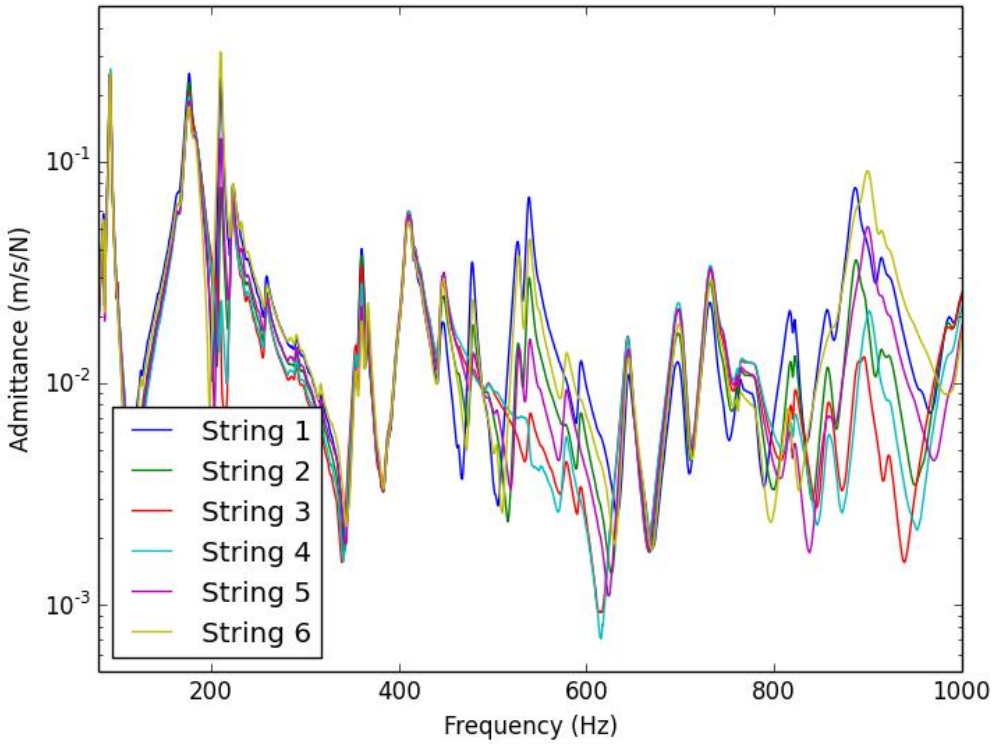

Figure 4.9: Input admittance at the six string positions along the bridge of guitar BR2. The lowest-frequency mode is the $T(1,1)_1$ mode.

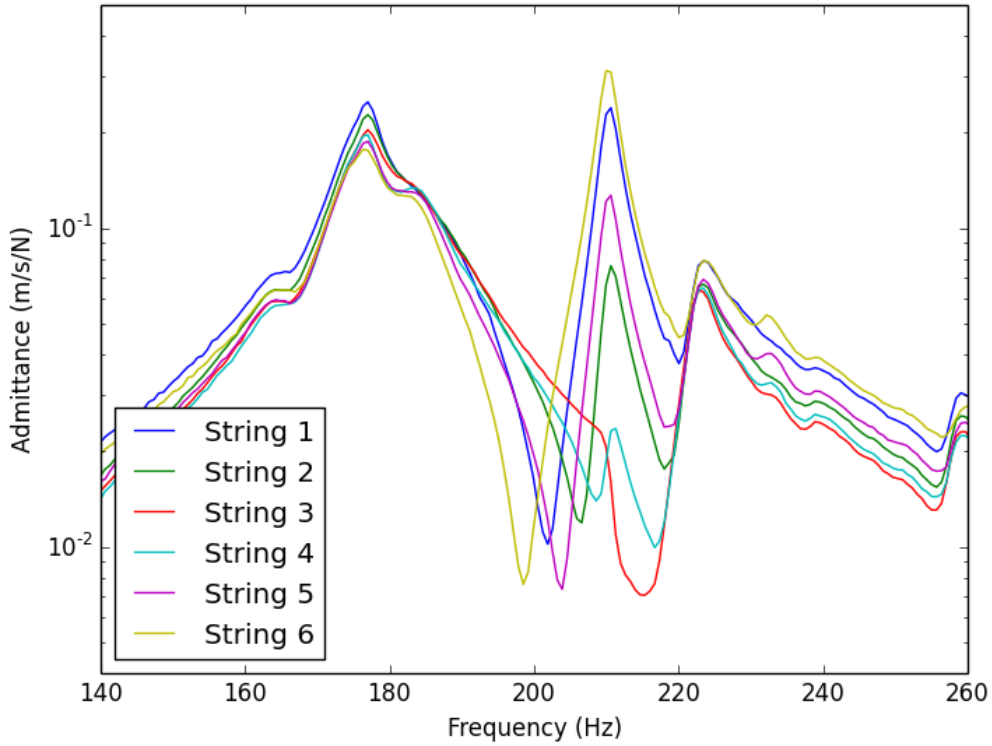

Figure 4.10: A zoomed in version of Figure 4.9 showing the input admittance at the six different string positions of guitar BR2. The peak at 175 Hz is the $T(1,1)_2$ mode and the peak at 210 Hz is the T(2,1) mode.

4.3.2 Adding mass to the anti-nodal region of a mode

An experiment was carried out to try and influence a single peak in the admittance curve with minimal disruption to others. Small amounts of mass were added to the anti-nodal region of a mode to try and reduce the height of that mode in the admittance curve. The location of the anti-nodal region was determined by looking at the mode shapes of the instrument from the scanning vibrometer measurements (see Figure 4.20). The mass used in this experiment was in the form of blue-tack. This meant it was easy to apply small amounts of mass to the soundboard whilst the instrument stayed hanging on the rack, suspended by elastic bands.

The experiment was first carried out on guitars BR1 and BR2 but the results were poor showing many split peaks and what seemed like noisy data. Therefore the results shown here are for guitar MAL. The $T(1,1)_2$ mode was chosen as the focus of the experiment as this mode is an important mode that is strongly coupled to the strings making it the prime suspect for wolf notes on the classical guitar. The masses were added firstly in steps of 0.5 g and increased to steps of 1.0 g up to a total of 5.5 g. The results showed a trend in peak movement with increasing mass loading, therefore only four admittance curves are shown in Figure 4.11.

Figure 4.11 shows that there is virtually no change in the peaks at 92 Hz and 340 Hz. All other modes below 1 kHz are subject to some form of change. Changes to the Q values and effective masses of these modes are unlikely to be perceivable (see Section 8.2), but the small shift in frequency of these modes could well be audible (Woodhouse et al. 2012).

By zooming in on the $T(1,1)_2$ and T(2,1) modes, shown in Figure 4.12, we see that the latter is subject to a small change in frequency, about 2.2 Hz, although this is not likely to be perceivable by most listeners (Woodhouse et al. 2012). The change in frequency of the $T(1,1)_2$ mode is about 4.6 Hz, which according to Woodhouse et al., could well be a perceivable change.

Although the change in frequency is a predictable change to the peaks in the admittance, the most interesting change lies in the effective mass of the $T(1,1)_2$ mode. It is therefore useful to extract modal parameters from these admittance curves to evaluate the effect of adding mass to the anti-nodal region of a mode. The first four peaks were fitted and modal parameters extracted to track the changes to these parameters as more mass was added. The results for the effective mass and frequency of the $T(1,1)_2$ are shown in Figure 4.13a and Figure 4.13b respectively. A straight line was fitted to the data to obtain an estimate of how much these two parameters changed by adding mass to the soundboard. The frequency decreased (0.76 +/- 0.03) Hz per one gram of mass loading and the effective mass increased by

(60 +/- 3) g per one gram of mass loading. One would not expect a linear dependence for very large masses, but in the range 0-5.5 g, this relation seems applicable.

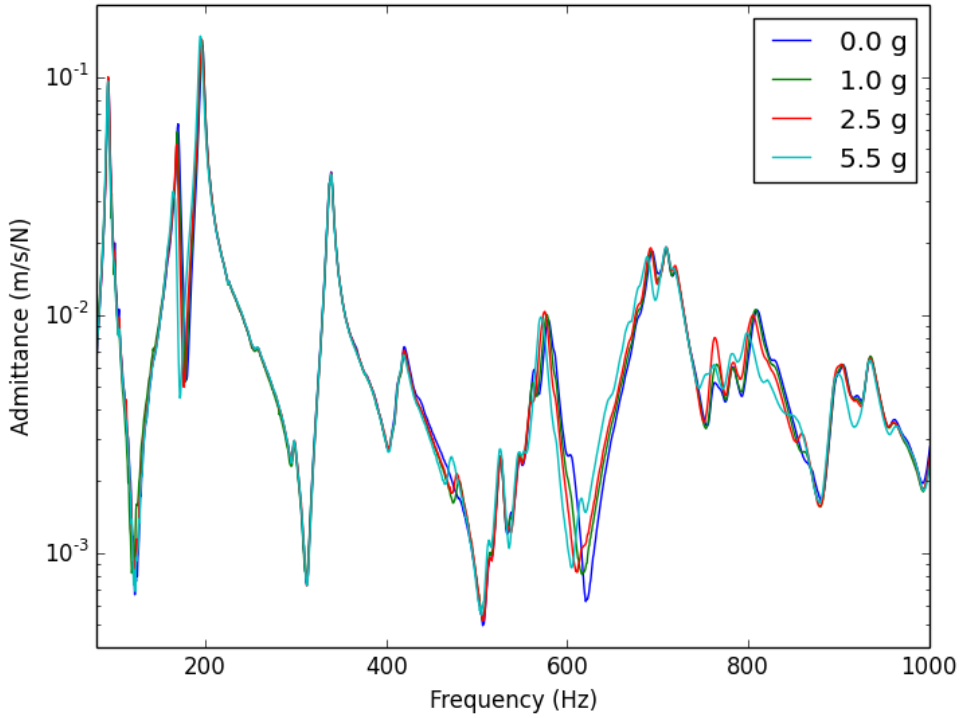

Figure 4.11: Admittance curves taken at the termination point of string four at the bridge of guitar MAL, with increasing mass loading at the centre of the anti-nodal region of the $T(1,1)_2$ mode. This mode is at 170 Hz on this instrument.

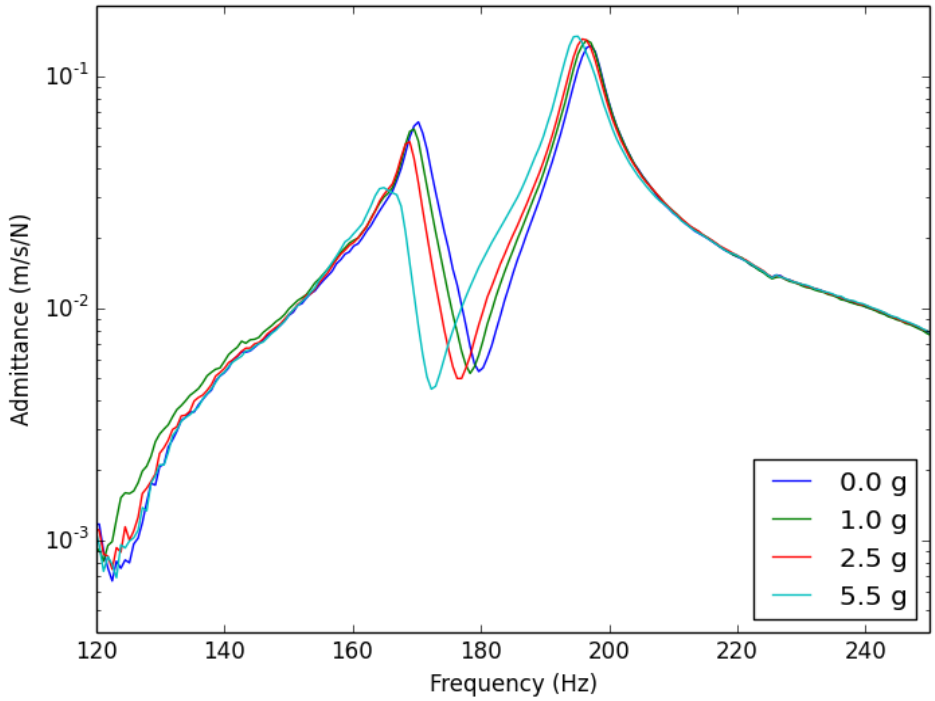

Figure 4.12: A zoomed in version of Figure 4.11 showing how the peaks of the $T(1,1)_2$ and T(2,1) modes change by adding mass to the soundboard of guitar MAL.

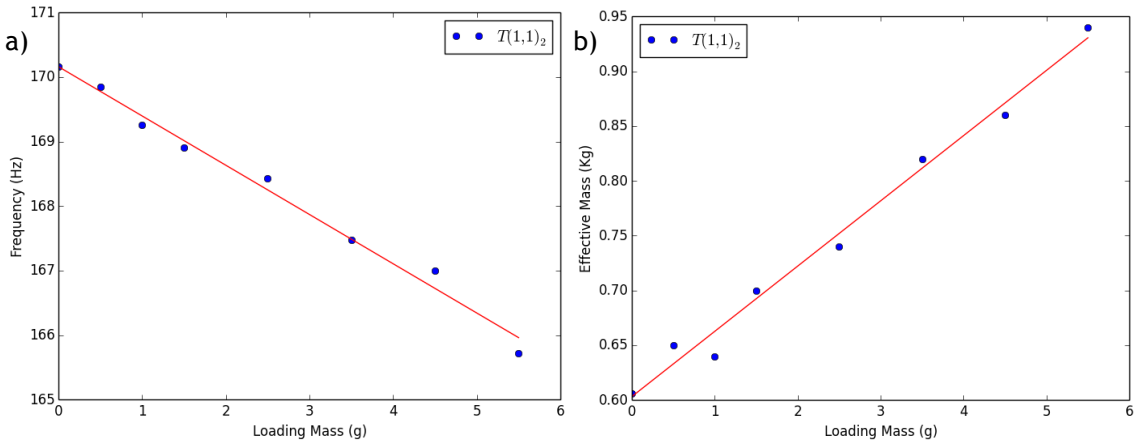

Figure 4.13: (a) Frequency and (b) effective mass of the $T(1,1)_2$ mode on guitar MAL as a function of mass loading on to the anti-nodal region of this mode on the soundboard.

These results may also be linked to perceivable differences from the psychoacoustical experiments carried out in Chapter 8.

4.3.3 Input admittance of a banjo

The general characteristics of the input admittance of classical guitars and steel-string guitars are well established in the literature (Richardson 1994; Woodhouse and Langley 2012). However, it seems that there has been a discrepancy about the admittance of banjos according to Stephey and Moore (Stephey and Moore 2008). Stephey and Moore show the input impedance of a banjo without its back showing quite an unfamiliar trend, which they admit 'differs considerably' from that presented in a conference paper by Rae and Rossing (2004) (note that the author was unable to access this conference paper and therefore cannot comment on the mechanical response of the banjo presented in this paper). One possible reason is that during the measurement by Stephey and Moore, the strings of the instrument were not damped. Nonetheless, there is no other published work showing the input admittance of a banjo.

The admittance of two banjos are shown in Figure 4.14. The strings were damped between the nut and bridge for these measurements but not damped between the bridge and tailpiece. One banjo is a mid-high priced Gretsch broadkaster supreme banjo, and the other is a medium-priced Fender banjo. In both cases the back of the instrument was removed and the accelerometer attached to the inside of the head where the bridge foot made contact with the head, the back was then re-attached to the instrument. A steel disk was stuck on as a target for the hammer, located on the opposite side of the head to the accelerometer at the top of the bridge near the 5th string. The only consequence of having the accelerometer on

the other side of the head to the hammer is that the phase of the complex admittance will look upside-down compared with normal measurements.

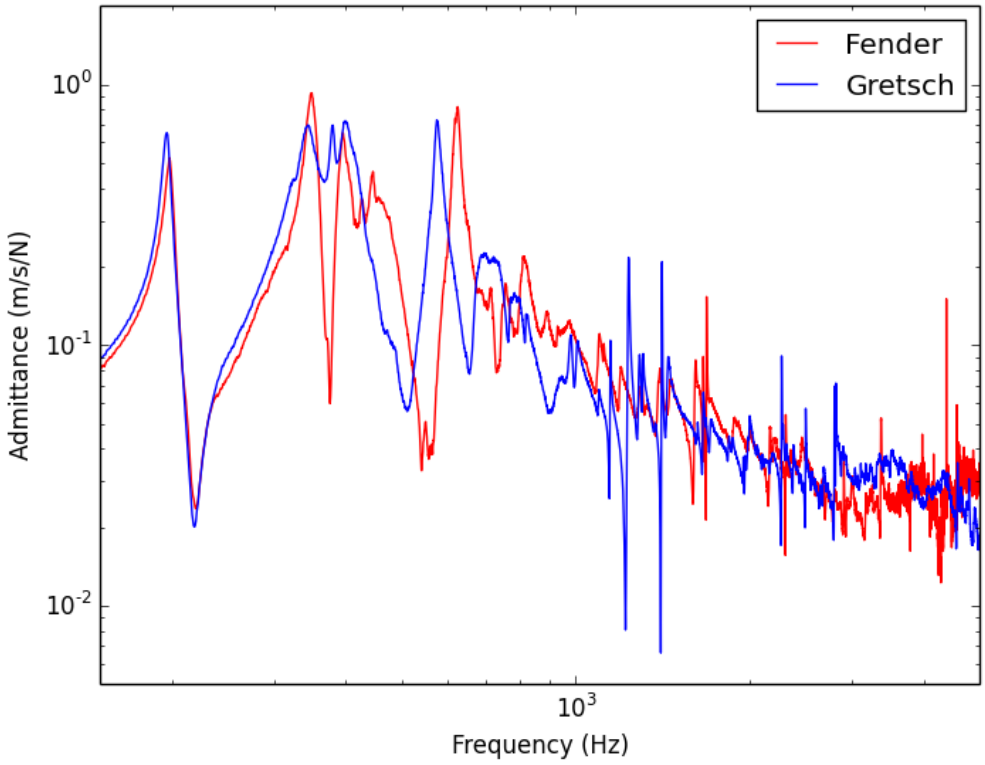

Figure 4.14: Input admittance of two banjos. Note that both axes are on a log scale.

It is interesting to note that although the head tension is an easily adjusted parameter on the banjo, the head of these two instruments, which were set up by two different players, have been tuned to a similar 'pitch'. It seems that both players wanted their instrument set up such that the fundamental head mode (second peak in both admittance curves in Figure 4.14) is at about 350 Hz, which coincides with the fundamental of the note F_4. Following the discussion in Section 2.3.1 on the effects of coincident tuning between string and body modes, it seems strange that musicians should deliberately tune their instrument in such a way. It is possible that such perturbation effects are so prominent in the banjo that they are not considered as much of a problem as in the case of the guitar, and so there is no objection to coincident tuning of string and body modes. Note that this particular frequency for tuning the fundamental head mode is around 30 Hz less than that stated by Dickey (2003) as the 'standard value'.

No effort was made to measure precisely the volume of the internal cavities or the area of the holes around the flange on these two instruments. However, along with the fact that the fundamental head mode on both banjos are at a similar frequency, it is no surprise that the lowest mode of the two instruments appear at

nearly the same frequency, around 197 Hz. This is 1 Hz above the fundamental of the note G_4. If the heads of these banjos were tightened up to the frequency suggested by Dickey, it is likely that the bass response of these instruments would be weaker due to the increase in frequency of the Helmholtz mode and weaker coupling between the first two modes. Perhaps this is preferred by some musicians as it would also result in a 'brighter tone' and 'higher Q values' of the head modes according to Dickey.

Another important observation is the sharpness of some modes above 1 kHz. This suggests that the banjo-head has modes with a large Q value in this range, although the reader should be reminded that the strings were not damping between the bridge and the tailpiece. The section of string that was not damped is roughly six times smaller than the section that was damped, assuming equal tension and mass per unit length in a given string, this corresponds to fundamental frequencies of 0.9-1.8 kHz. This explains the sharp peaks towards higher frequencies in the banjo's mechanical response.

4.3.4 Comparing input admittances of different instruments

It is convenient to compare the general characteristics of the mechanical response of the three instruments studied in this thesis. The input admittance of classical guitar BR2, which is a hand-made instrument, a Simon and Patrick 'Songsmith' steel-string guitar and a Gretsch 'Broadkaster Supreme' banjo are shown in Figure 4.15. For the two guitars the admittance was measured at the termination point of the 5th string on the bridge, as this has been shown to give a sort of average admittance of the instrument along the bridge. The accelerometer and steel disk were attached to the banjo in the same way as described in the previous section.

Before discussing the difference in heights of these curves, a quick note should be made on the presence of what is usually referred to as neck-bending modes in the admittance of the two guitars, and the lack of a neck-bending mode in the case of the banjo. The wooden body of a guitar is more flexible than the predominantly metal body of the banjo. Due to the shape of the guitar, there is a low-frequency bar-like mode of vibration with the waist at a node dividing the upper bout and neck from the lower bout. This results in a peak at around 70-75 Hz in their admittance curves and is called the neck-bending mode. Although this peak is clearly seen in the admittance, this mode contributes very little to the sound radiation from the instrument. There is no such analogy for the banjo because of the large impedance

change from the head to the rest of its body and it has a solid metal bar running from one end of the instrument to the other, called the coordinator bar.

The most significant difference between the admittance curves of these three instruments is the height of the curves. The tallest peak of the banjo is 7 dB higher than that of the classical guitar, and 15 dB higher than the tallest peak in the admittance of the folk guitar. The mean admittance level of the banjo is 18 dB higher than that of the classical guitar between 80 Hz and 5 kHz, and there is a further 9 dB between the average levels of the classical and folk guitars in this range.

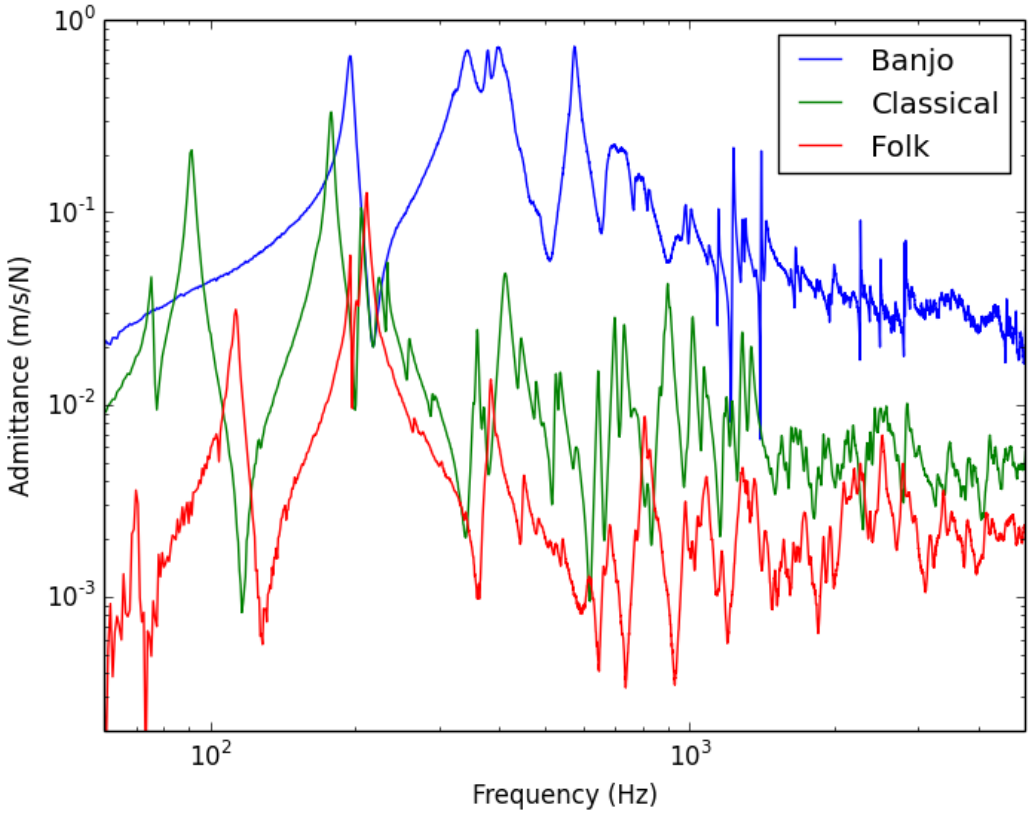

Figure 4.15: Input admittance of three different plucked-string instruments.

The large difference between the mean level for the banjo and the two guitars could well have been predicted by considering the differences in design and materials used for the construction on these instruments. The banjo-head is much more flexible than the heavier and stiffer wooden soundboards of the guitars. Also, the soundboard of the folk guitar is thicker and has much heavier bracing than that of the classical guitar. The reason for this is that the folk guitar needs to withstand the larger tensions of its steel strings, there is also an element of 'built to last' rather than 'built to sing' to most factory-made instruments.

The next point to make is on the frequency of the lowest-frequency modes. The instrument with the lowest frequency mode is the classical guitar at 91 Hz, then the

folk guitar at 113 Hz, and the lowest frequency mode on the banjo is at 196 Hz. It is worth reminding the reader that the fundamentals of the lowest notes to be played on the guitars and banjo are (usually) 82.4 Hz and 146.8 Hz respectively. This means that the fundamentals of the lowest notes on all three instruments are likely to be weak, but more so in the case of the banjo (see Figure 4.1c) and folk guitar.

Some comments should also be made on the general shape of each curve. For the two guitars there are three tall peaks below 300 Hz, corresponding to the $T(1,1)_1$, $T(1,1)_2$ and T(2,1) modes. Then, as the modes get closer together, the peaks are not so well-defined and their amplitude decreases, reaching a point of modal-overlap around 1 kHz. Above 1.5 kHz the modes tend to settle onto a base level of around 4 mm/s/N for the classical guitar and 2 mm/s/N for the folk guitar, although there is a slight incline in the base line of the folk guitar with increasing frequency. In the case of the banjo there are about five tall peaks below 600 Hz, then a brief band of well-defined peaks before reaching modal-overlap somewhere between 1-1.5 kHz. Above 1 kHz it is more suitable to characterise the base level as decreasing about 4.8 dB per octave. The reason for this decline in admittance is because the higher-order modes cannot sustain the high admittance level; this is proven later when modelling the admittance of the instrument.

It is also worth noting how the admittance curves affect the radiated sound of the string partials. To do this each admittance curve was split into six one-octave bands; 80-160, 160-320, 320-640, 640-1280, 1280-2560 and 2560-5120 Hz. The mean admittance in each band was then converted into dB using the mean admittance over the range 80-5120 Hz as the reference. This enables the balance of admittance to be compared in octave bands between the three instruments. A bar plot of this data is shown in Figure 4.16.

The first band is not very important in the case of the banjo because the lowest note on this instrument, D_3, is at 146.8 Hz, though this does explain why the fundamental of this note is so weak as pointed out earlier. The low admittance level of the folk guitar in the third band means that the note E_4 (f_0= 329.6 Hz) has a weak fundamental, using STFFT analysis it was measured to be 10 dB lower than the strongest partial of this note. The instrument with the highest relative admittance level in the last two bands here is the folk guitar, and the lowest relative admittance belongs to the banjo. This is consistent with the results from Section 4.1.2, where the higher level of higher-order partials was found in the folk guitar and lowest level in notes on the banjo.

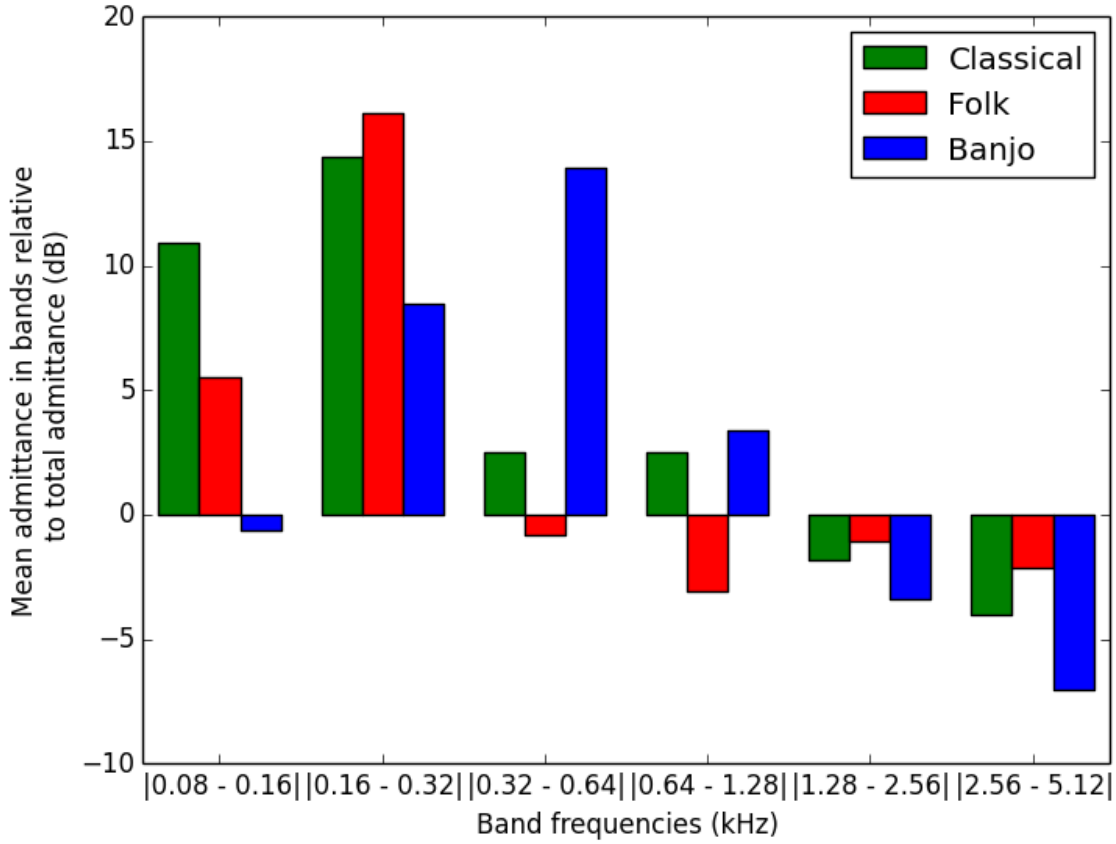

Figure 4.16: Mean admittance in octave bands plotted in dB relative to the mean of the admittance between 80-5120 Hz.

4.3.5 Modal parameters of plucked-string instruments

The modal parameters for the lowest eight modes were extracted from the admittance curves shown in Figure 4.15, the results are shown in Table 4.3. The mean modal spacing of the first eight modes on this classical guitar, folk guitar and banjo are 46, 53 and 83 Hz respectively. Calculating the mean modal spacing in cents rather than Hz paints a rather different picture, giving 372, 359 and 340 cents for the classical guitar, folk guitar and banjo respectively. The latter set of values is more useful because of the spacing of notes on these instruments. Therefore there are on average between 3.4-3.7 notes per mode in the low-frequency range of these instruments. These differences are small and insignificant, but mean modal spacing will become more interesting when it is considered across a wider range of frequencies later in this thesis.

The average Q values of low-order modes of the classical guitar, folk guitar and banjo are 42, 40 and 26 respectively. The modal Q values of the two guitars are therefore very similar and the difference is not perceptually significant. The modes of the banjo on the other hand have Q values that are about 1.6 times smaller than

the guitars studied here. Richardson et. al. (2008) found that halving the Q values of body modes in a physical model of a classical guitar did not lead to large differences in the sound of the instrument. Woodhouse et. al. (2012) measured the JND in Q values of all body modes of a guitar to be a scale factor of about 1.2, which is not a great deal smaller than the measured change in average Q value between the guitars and banjo here.

Classical guitar			Folk guitar			Banjo		
f_0 (Hz)	Q	M_{eff}(kg)	f_0 (Hz)	Q	M_{eff}(kg)	f_0 (Hz)	Q	M_{eff}(kg)
91.4	45	0.292	113.2	33	1.473	196.1	32	0.040
178.6	46	0.102	196.0	103	1.925	347.3	14	0.009
206.5	56	0.423	202.1	30	1.226	378.8	32	0.028
224.1	31	0.645	221.0	45	0.263	397.3	24	0.017
257.7	29	1.120	265.0	20	2.883	574.7	33	0.013
288.9	23	2.705	384.2	39	1.202	681.7	20	0.026
359.2	58	1.016	449.6	30	3.266	718.6	20	0.037
411.3	45	0.319	483.5	17	3.233	775.6	32	0.059

Table 4.3: Modal parameters for the lowest eight modes of classical guitar BR2, Simon and Patrick folk guitar and Gretsch broadkaster supreme banjo.

The average effective mass of the classical guitar, folk guitar and banjo are 0.828, 1.934 and 0.029 kg respectively. There is about a factor of two between the two guitars and nearly two orders of magnitude between the banjo and the two guitars. The largest change in modal parameters between the instruments studied here is therefore the change in effective mass. According to previous work at Cardiff (Wright 1996; Richardson et. al. 2008) these changes are likely to lead to large perceptual differences between all three instruments.

In the light of these results it would be interesting to carry out psychoacoustical work to find the most significant changes between instruments. There is no known work in the literature that attempts to do this. The first step would be to develop a physical model for the banjo that not only reproduces an accurate representation of its radiated sound, but also is compatible with current models for the guitar. At this point the above measurements along with previously published work mentioned above is enough to be convinced that the changes in effective masses between these instruments are the main cues in helping us to distinguish between the sound of the folk guitar and banjo. Such comparisons between the two steel-string instruments and the classical guitar are not applicable due to the strings being quite different.

4.4 Global coupling level

It is now a convenient time to discuss the global coupling level between the strings and bodies of the three instruments under investigation. Having measured the characteristic impedance of strings in Section 4.2 and input admittance in Section 4.3.4, the global coupling level can be calculated by multiplying the mean of the former with the latter. This can also be thought of as the input admittance of the body normalised by the mean string admittance.

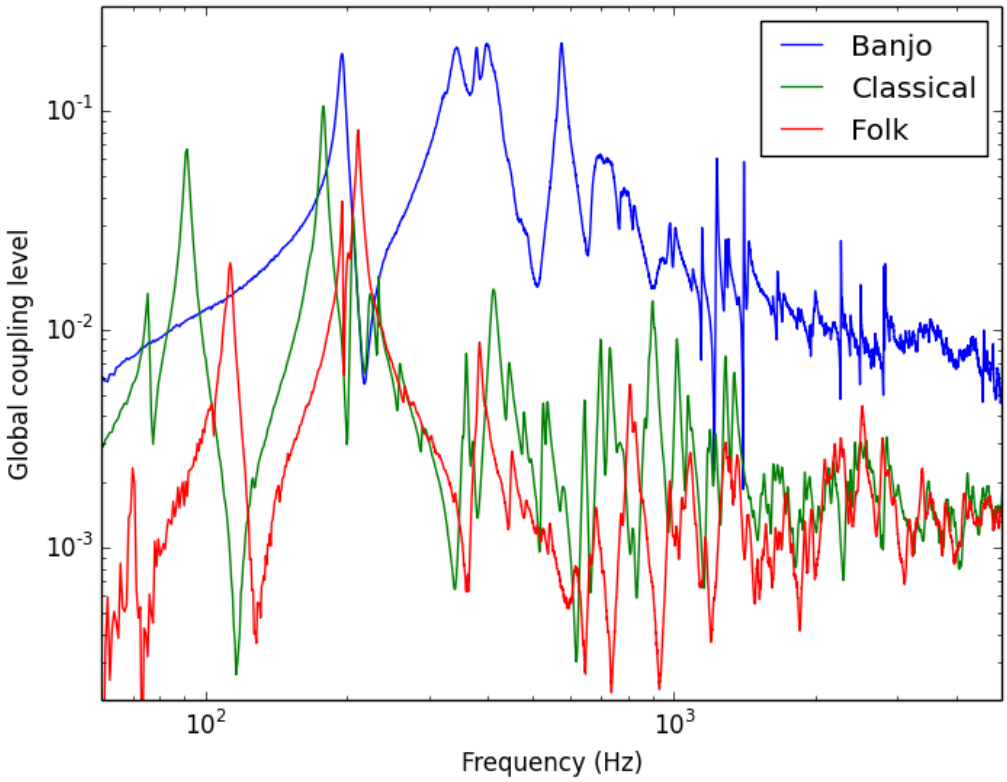

Figure 4.17: Mean impedance of the strings multiplied by the admittance to give the global coupling level for a banjo, classical guitar and a folk guitar.

Figure 4.17 shows the global coupling level of a banjo, classical guitar and folk guitar. The frequency scale is the same as Figure 4.15 making these two graphs easy to compare. There is 17.4 dB between the mean coupling level of the banjo and that of the classical guitar, and there is a further 2.5 dB between the classical and folk guitars. These values stated above were calculated in the frequency range from the fundamental frequency of the lowest note played on the instrument up to 5 kHz. It is not a surprising result that the banjo is so much higher than the two guitars considering the large difference in stiffness of the materials used for the soundboards of these instruments. On the other hand, it is a surprising result that the two guitars are so close to each other. From this picture it is much more difficult to differentiate between the classical guitar and the folk guitar.

Another way to show this coupling level is to plot the input admittances of the instrument bodies and the inverse of the characteristic impedances of the strings on the same graph; this is done in Figure 4.18. This graph helps to better understand Figure 4.17 because the coupling level is shown here as the gap between the admittance curve of the body and the corresponding admittance points of the strings. A large difference shows a low coupling level and a small difference shows a high coupling level. Thus, the difference between the body and string admittances of the folk guitar is very similar to that of the classical guitar.

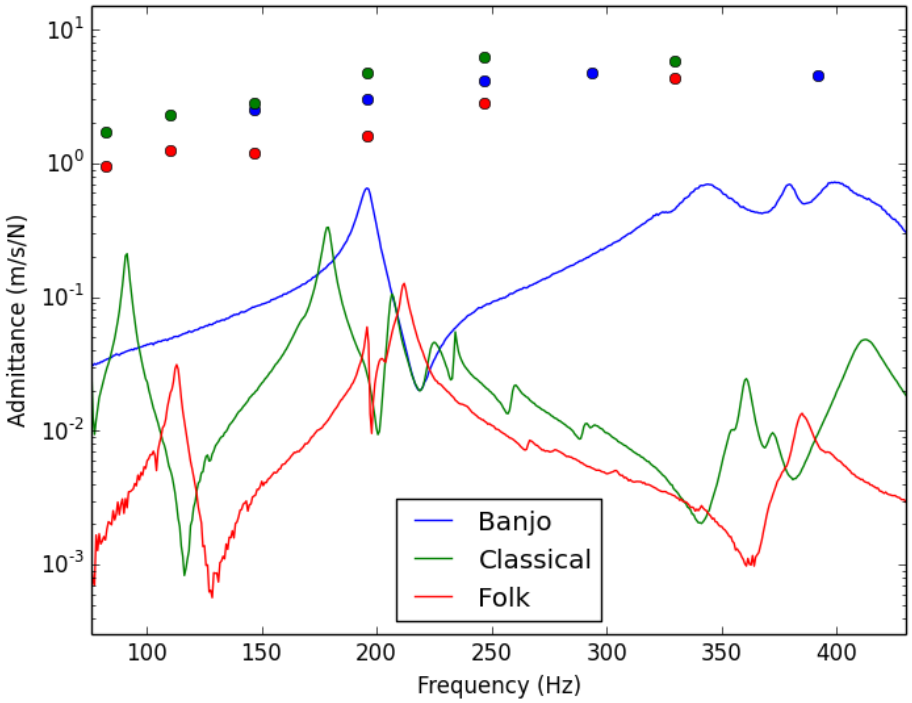

Figure 4.18: Input admittances of a banjo, classical guitar and folk guitar. Also plotted are the inverses of the characteristic impedances of the strings on each instrument against their fundamental frequency.

4.5 Mode shapes

Simple examples of mode shapes are shown in this section along with a basic discussion for each instrument investigated. Strictly speaking, the mode shapes shown here are in fact operating deflection shapes, or ODS. However, the resonances chosen to show here are well separated between neighbouring peaks in the frequency response of the instrument. It is therefore assumed that the influence of neighbouring resonances is very small and the ODSs are referred to as mode shapes. The measurements were made using a Polytech 3D laser vibrometer system as described in Section 3.5. The mode shapes are linked to the bracing pattern of the

instrument, the effect of mode shape on coupling to the strings and efficient sound radiation is also discussed.

4.5.1 Classical guitars

Figure 4.19 shows three low-order modes of guitar BR2, which is a traditional hand-made Torres style guitar with fan bracing (see Figure 1.1 as an example of fan bracing). The different colours represent the velocity normalised to force. Note that there is a section missing from the fret board to the bridge, this is because it was not possible to obtain data for this area due to the strings obstructing the laser beam's path. The frequency and scale for each of the modes shown are given in Table 4.4. Note it is likely that the scale would change if the striking position of the hammer would change, or if it were possible to obtain data for the centre of the anti-nodal regions of the $T(1,1)_2$ and T(1,2) modes.

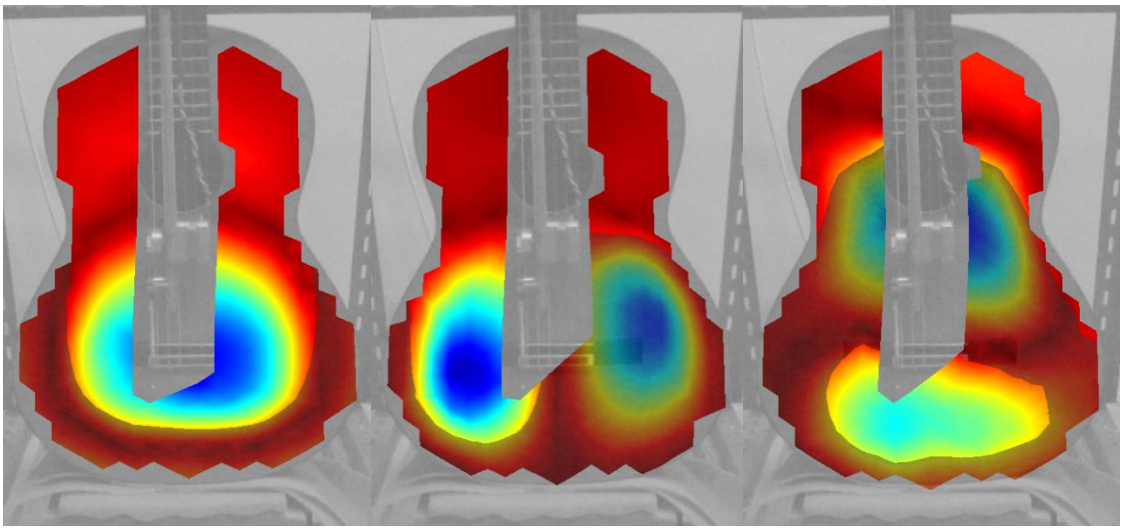

Figure 4.19: Three low-order modes of classical guitar BR2. From left to right; $T(1,1)_2$, T(2,1) and T(1,2).

Mode	Frequency (Hz)	Scale (mm/s/N)
$T(1,1)_2$	191.3	0-200
T(2,1)	232.5	0-700
T(1,2)	375.0	0-80

Table 4.4: Data for BR2 body modes shown in Figure 4.19

These modes are nearly symmetric about the vertical axis down the middle of the guitar. This means that the T(1,1) modes are strongly coupled to the strings and make the most out of the larger area of the lower bout to move a large volume of

air. On the other hand, it also means that the T(2,1) mode has nearly-equally sized anti-nodal areas that move in opposite phase, making this mode inefficient at radiating sound in front of the instrument due to phase cancellation.

Figure 4.20 shows three low-order modes of the guitar MAL, which is an over-constructed factory-made instrument made from plywood. The bracing pattern of this instrument is also shown in the figure. The frequencies and scales of these modes are given in Table 4.5.

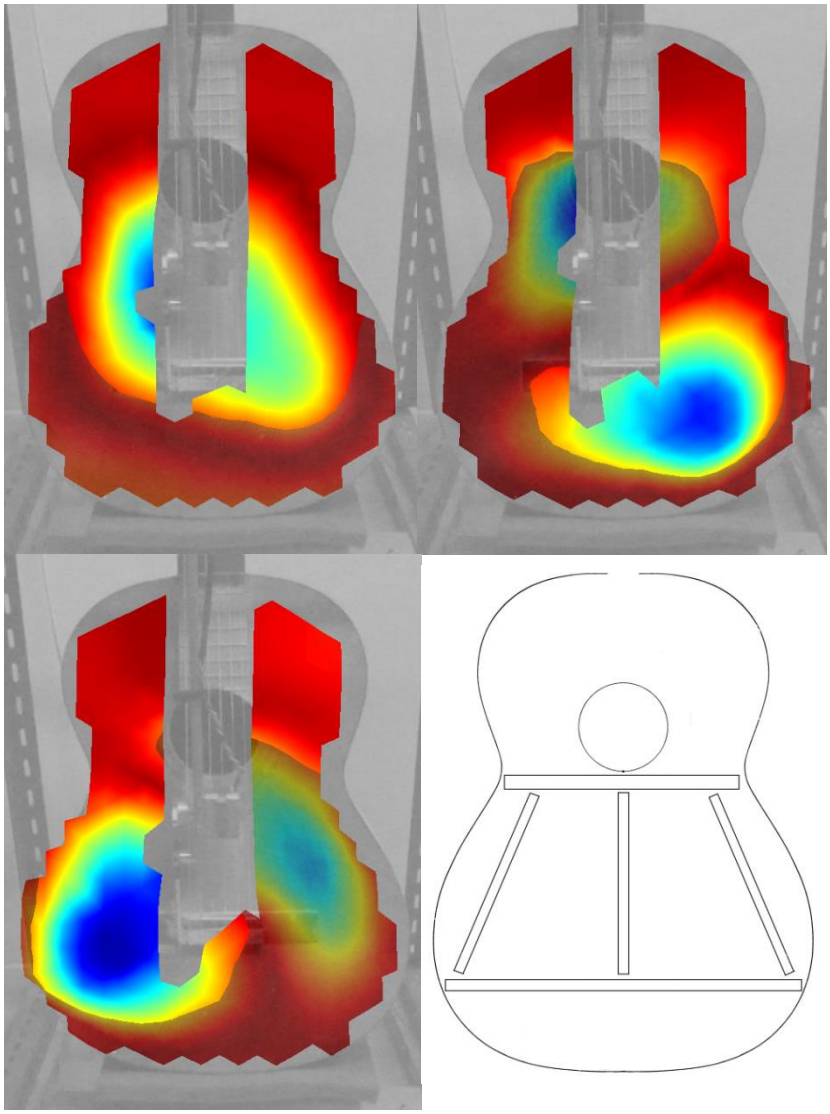

Figure 4.20: Some low-order modes on guitar MAL. Top-left is the $T(1,1)_2$, top-right is a T(1,2), bottom-left is a T(2,1) mode and bottom-right shows the bracing pattern on the soundboard of this instrument.

Mode	Frequency (Hz)	Scale (mm/s/N)
$T(1,1)_2$	171.9	0-70
T(1,2)	200.6	0-180
T(2,1)	340.0	0-180

Table 4.5: Data for MAL body modes shown in Figure 4.20

The anti-nodal region of the $T(1,1)_2$ is located closer to the waist than the centre of the lower bout meaning it is not as strongly coupled to the strings and does not make the most of the large radiating area of the lower bout. The fact that the T(1,2) appears at a lower frequency than the T(2,1) on this instrument suggests that the top-plate is overly stiff across the grain. This could be due to the bracing pattern, but is more likely to be because the plywood has a cross-band or cross-ply, meaning that the grain of at least one layer of the ply runs in a perpendicular direction to the primary grain direction. These modes are less symmetric than those of the previous guitar meaning that the T(2,1) might be a more efficient radiator in front of the instrument. However, this also depends on the peak admittance of the mode, which is nearly four times smaller than the same mode on guitar BR2.

4.5.2 Steel-string guitars

Figure 4.21 shows three low-order modes of a Simon and Patrick steel-string folk guitar along with the bracing pattern of the top plate. The large X made by the two longest struts is a typical feature of bracing patterns on steel-string guitars, the rest of the bracing varies from one manufacturer to another and between models.

The $T(1,1)_2$ mode has a more triangular shape than that of guitar BR2. This is most likely due to the large X on the top plate and the small blocks of wood shown as shaded parts of Figure 4.21 that help to restrict the mode to this area. The T(2,1) is not quite symmetric due the asymmetry of the bracing, which again should result in a more efficient production of sound from this mode in front of the instrument.

The mode with the highest peak above the T(2,1) mode for this guitar is the other mode shown in Figure 4.21. This has been labelled a T(3,1) mode although it is not exactly the same as a T(3,1) mode on a classical guitar (see Figure 2.3c) and could be labelled as a T(2,2) mode that has been rotated by 45 degrees. In the case of the classical guitar the middle section of this mode has an anti-nodal area near to the bridge. This mode has been shown to be an efficient radiator on the classical guitar (Perry 2014) and therefore an important mode for an instrument with fan bracing. However, for a guitar with an X-bracing the bridge seems to be near a nodal point as the nodal lines follow the large X shape. This means that the coupling between the strings and this mode is likely to be smaller. Also the anti-nodal areas of opposite phase are of a similar size making this mode less efficient at radiating sound in front of the instrument. This shows that the same modes are not necessarily important on every type of guitar, and that the bracing pattern can heavily influence which modes are the ones that radiate strongly.

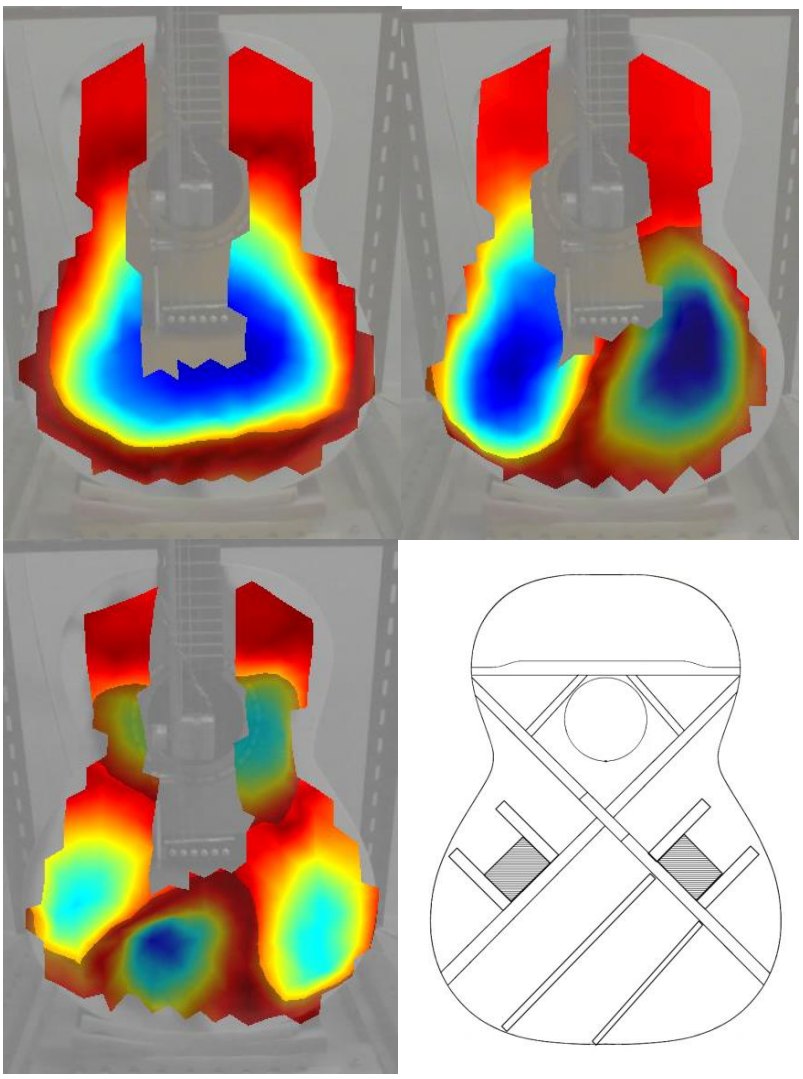

Figure 4.21: Low order modes of a steel-string Simon and Patrick folk guitar. Top-left is the $T(1,1)_2$ mode, top-right is the T(2,1), bottom-left is a T(3,1) mode and bottom-right shows the bracing pattern on the soundboard of the instrument.

Mode	Frequency (Hz)	Scale (mm/s/N)
$T(1,1)_2$	208.1	0-100
T(2,1)	383.8	0-100
T(3,1)	659.4	0-250

Table 4.6: Data for S&P body modes shown in Figure 4.21

Figure 4.22 shows three low-order modes of a carbon-fibre guitar X10. The bracing pattern has not been shown because it has no bracing. Note that this guitar has a cut-away body meaning it is easier for the player to reach notes high up on the fret board. The top and back plates are arched like those of a violin.

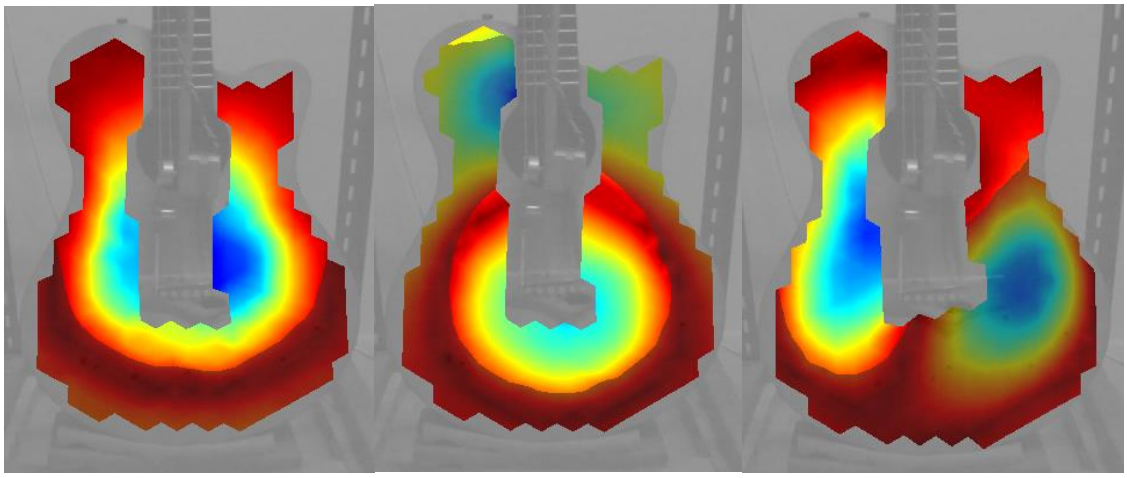

Figure 4.22: Low-order modes of carbon fibre guitar X10. Left to right: $T(1,1)_2$, T(1,2) and T(2,1)

Mode	Frequency (Hz)	Scale (mm/s/N)
$T(1,1)_2$	218.8	0-60
T(1,2)	273.8	0-60
T(2,1)	380.6	0-120

Table 4.7: Data for X10 body modes shown in Figure 4.22

The $T(1,1)_2$ mode, as for guitar MAL, is positioned a little high and this mode would communicate better with the strings if there were a cross strut below the sound hole to restrict this mode to the lower bout. This would perhaps raise the frequency of the mode slightly but overall it would probably improve the bass response of the instrument. Again, as is the case for guitar MAL, the T(1,2) is at a lower frequency than the T(2,1). The carbon-fibre of this guitar was constructed in layers perpendicular to each other resulting in a material with similar stiffness in both vertical and horizontal directions. For a homogeneous rectangular plate, as the resonance frequency increases, modes with nodal lines that are perpendicular to the longest dimension of the plate appear before modes with nodal lines that are parallel to the longest dimension (Fletcher and Rossing 1998). This simply means that one would expect the T(1,2) mode to occur at a lower frequency than the T(2,1) on this instrument, as was the case for guitar MAL.

Having the cutaway on the right-hand side of the soundboard results in the left anti-nodal area of the T(2,1) mode being larger than the one on the right, which helps increase the efficiency of this mode. Again, the strings would communicate better with the T(2,1) mode if the left anti-nodal area was situated a little lower.

4.5.3 Banjo

Figure 4.23 shows three of the lowest-frequency modes of a banjo without a back. Removing the back made it easier to take measurements because the impact hammer could excite the head from behind the instrument. As a result of taking measurements without its back, this instrument has only one T(1,1) mode because it has no interval cavity like a normal banjo or guitar. Therefore the first mode in Figure 4.23 is just called the T(1,1) mode.

The most significant difference to point out is the difference in admittance level between the banjo and the other instruments, there is a difference of about one order of magnitude. The frequencies of the modes are also higher than the other instruments. These points have already been discussed in Section 4.3.4 in comparing the admittances of these instruments.

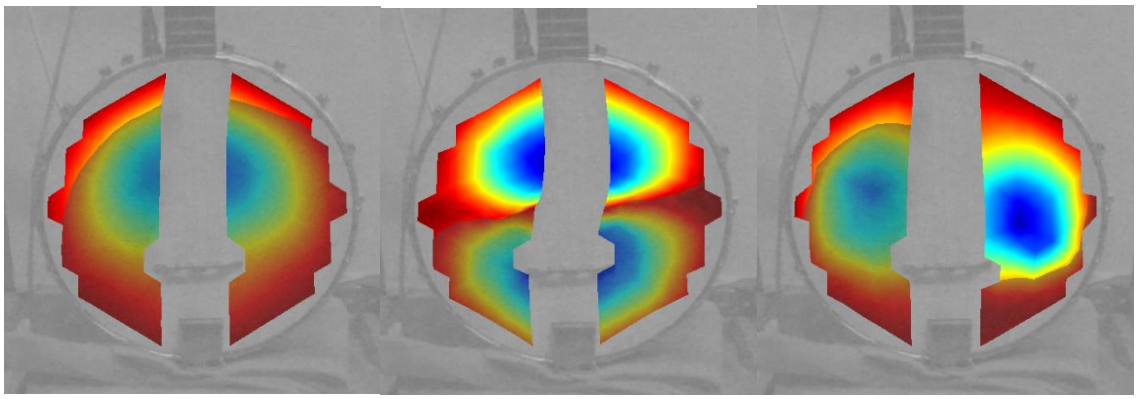

Figure 4.23: Three low-order modes of a banjo. From left to right: T(1,1), T(1,2) and T(2,1).

Mode	Frequency (Hz)	Scale (m/s/N)
T(1,1)	198.8	0-0.7
T(1,2)	300.0	0-1.2
T(2,1)	350.0	0-4.0

Table 4.8: Data for banjo-head modes shown in Figure 4.23

The T(1,1) is not quite at the centre of the head due to the influence of the bridge pressing down on it. In principle the other two modes shown in Figure 4.23 could be orientated in any number of angles due to the head being circular, but they appear as they do because of the location and orientation of the bridge pressing against the head. The high level of symmetry of these two higher-frequency modes is likely to result in relatively poor efficiency in radiating sound in front of the instrument.

4.5.4 Discussion

The difference in shapes between the modes of the two classical guitars is quite obvious here. The anti-nodal areas of the modes on guitar BR2 are situated in the lower bout, where the strings drive these modes. They also have a much higher level of admittance and therefore BR2 is likely to produce a much louder sound for a given force applied to the strings.

The shapes of the two lowest-order modes of the S&P guitar differ to those of BR2 only by a small amount considering their radically different bracing patterns. The low-order modes are not too dissimilar probably because the overall shape of the body is very similar and there are struts on both instruments that restrict the low-order modes to the lower bout. It seems that the detail of the bracing has a larger influence on modes above 500 Hz.

It is suggested from previous psychoacoustical work (Wright 1996; Meyer 1983a) that the modal parameters of modes above 500 Hz are less important than modes below 500 Hz. Therefore the detail of the bracing pattern is not likely to be significantly influential to the perceived tone quality. What is important is the presence of primary struts to restrict low-order modes to the lower bout and some light bracing to increase stiffness without adding too much mass.

The banjo is of course quite a different instrument from the guitar, both in its construction and its perceived sound. Its basic functionality on the other hand is the same and, as shown in this section, its soundboard has modes that vibrate the air surrounding the instrument just like the guitar. This bodes well for using similar modelling techniques for the banjo and the guitar.

Chapter 5 Psychoacoustics

In this chapter some basic knowledge of psychoacoustics will be presented that highlight some of the difficulties that arise in signal detection measurements. The procedure of the listening test implemented in this thesis is then described and related to the theory discussed in the former section. A brief section is then given on masking signals and critical bands of the auditory system. Finally, some basic listening tests are carried out to gauge the amount of change in the sound from a plucked-string instrument that is needed in order to be perceivable.

There is a tendency here to use alien terminology to the physicist, an effort has been made to avoid jargon and define only the absolutely necessary terminology to understand the theory.

5.1 Signal detection theory

In an ideal world, the definition for a threshold would be the intensity above which a stimulus is detected and below which it is not. Although this definition is logically sound, it does not reflect the processes of the human auditory system (Moore 1997).

Imagine a test measuring the threshold of a signal masked by noise. As the signal level is increased relative to the noise the listener has a choice of two answers: ‘yes, the signal is present’ or ‘no signal present’. A single subject repeating the test several times would produce different results depending on any biases in the

test. One such bias could be either increasing the stimulus level from zero, which is likely to yield a relatively high threshold, or decreasing the stimulus level from a clearly audible level, likely to yield a relatively low threshold. There are also physiological effects that affect the result such as spontaneous neuron firing. These can build up and cause the listener to claim that the stimulus was present when in fact it was not. Therefore there is a range of values at which the stimulus will sometimes be audible and sometimes not.

The exact value of a perceived threshold is thus difficult to measure and it is more suitable to define a range of values where the threshold may be found. This range of values is described by the 'probability density function' and is assumed to be in the shape of a Gaussian or normal distribution, as much for mathematical ease as modelling real physiological processes (Moore 1997). From this definition, the probability of the threshold lying in a certain interval can be found by integrating the probability density function between the limits of that interval. Note that the total area under the probability density function is 100%.

A subject's response to the above mentioned experiment can also be shown in the form of a psychometric function. This curve is determined by plotting the percentage of 'positive responses' (correctly identifying the stimulus) against the intensity of the stimulus (Levitt 1971). In this simple example the shape of the psychometric function is the cumulative sum of the probability density function. An example is given in Figure 5.1.

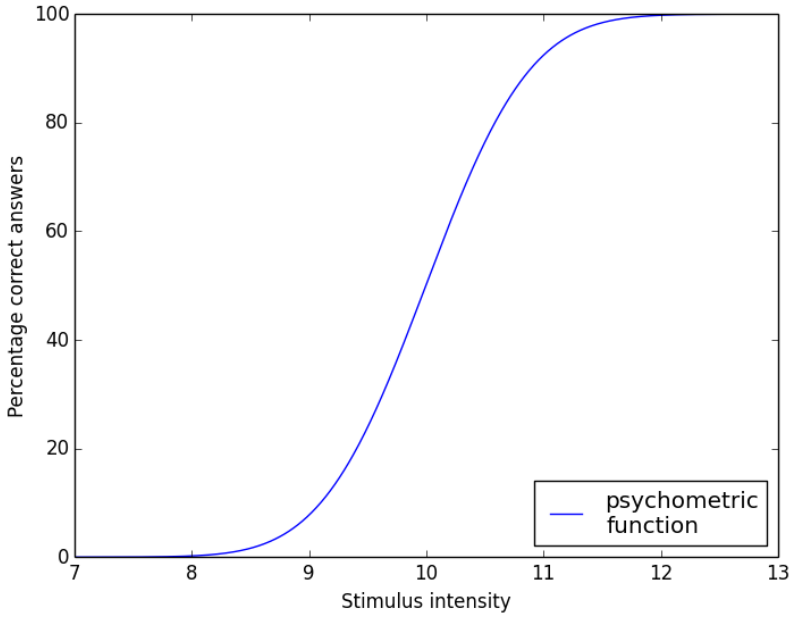

Figure 5.1: Psychometric function showing percentage positive responses as a function of stimulus level. Note that the psychometric function does not always start at 0 on the y-axis. This is because of possible spontaneous neuron firing causing the subject to claim that the stimulus is present where in fact it is not.

To describe this function in detail two values need to be defined, like defining the mean and standard deviation of a Gaussian distribution. However, the type of listening test chosen in this thesis is a forced-choice test, where it is of interest to find only one point on the psychometric function. The details of this test are given in the following section.

There is one assumption in signal detection theory that can restrict the applicability of the psychometric function. The assumption is that the probability of a positive response increases monotonically with stimulus level. This is assumed to be true in all listening tests in this thesis.

5.2 Adaptive listening tests

5.2.1 Test procedure

The most popular tests in psychoacoustics are forced-choice adaptive procedures, because they are consistent with signal detection theory. A graphical representation of an example of an adaptive test is given in Figure 5.2.

In a forced-choice adaptive test the listener is presented with a series of trials consisting of usually three individual stimuli (usually the case in musical acoustics). In this case, two stimuli are the same, called the reference tone, and one is different, called the modified tone. The task of the listener is to identify the 'odd-one-out', i.e. the modified tone. If the listener cannot tell the difference they must guess the correct answer, this is what is meant by 'forced-choice'. A test where each trial consists of three stimuli is a three-alternative forced-choice (3AFC) test. The amount by which the modified tone is different from the reference tone is called the modification. Hence, an adaptive procedure is defined as one where the modification in a given trial is determined by the preceding stimuli and listener responses (Levitt 1971).

The 'up-down' method is a form of testing that involves a decrease in modification following a *positive response sequence* and an increase in modification following a *negative response sequence*, the amount of increase or decrease is called the step size. The simplest up-down procedure is a one-up one-down procedure in which one positive response decreases the modification and one negative response increases the modification. Another example is the two-down one-up procedure where the down sequence is now two consecutive positive responses and the up sequence is again one negative response. Similarly the three-down one-up test has a

down sequence of three consecutive correct answers and an up sequence of one incorrect answer.

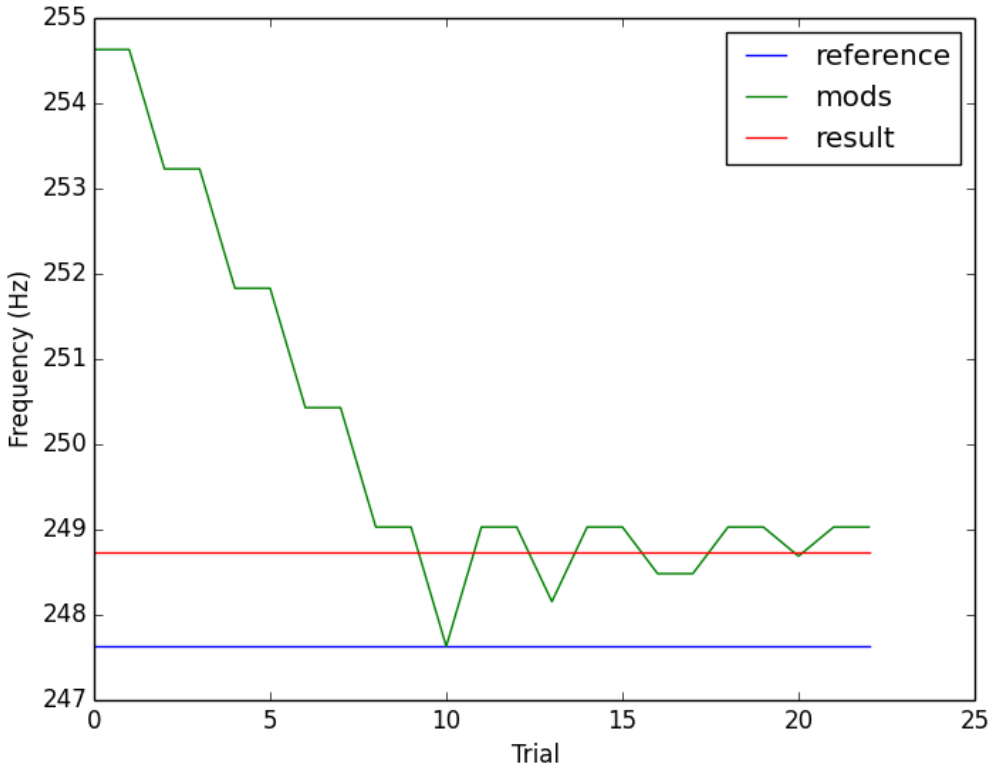

Figure 5.2: Example of a 3AFC listening test using a two-down one-up procedure. This test measured the JND in fundamental frequency of the note B_3. The reference f_0 is 247.6 Hz (blue line) and the modified f_0 starts at 254.6 Hz (green line). After two correct answers the modification is decreased, after one incorrect answer the modification is increased. There are a total of eight turning points, the result (red line) is the average of the last five mid-runs, which are the midway points between two turning points.

An example of a test using the two-down one-up procedure is shown in Figure 5.2. The ordinate axis can be thought of as stimulus level and the trial number is on the abscissa. The blue line is the reference level, which stays the same throughout the test. The green line is the modified level and tends towards the reference level after two consecutive correct answers and away from the reference after one incorrect answer. This particular test measured the JND in fundamental frequency of the note B_3.

A positive response sequence followed by a negative response sequence, and vice versa, is defined as a turning point. The test lasts for a total of eight turning points where the step size is decreased slightly every-other turning point, resulting in a more rapid convergence to the result. The half-way point between two adjacent turning points is called a mid-run. The result of the tests in this thesis is defined as the mean of the last five mid-runs, shown as the red line in Figure 5.2, the error of the measurement is the standard deviation of the last five mid-runs.

Before all of the tests carried out in this work the listeners were given a brief practice to familiarise themselves with the type of stimulus in the test and to get used to identifying the modified tone from the reference tone. The practice consisted of three sets of examples; in each set the reference tone was played twice followed by the modified tone. If the subject could not hear a difference between the reference and modified tones, the initial modification was increased. Levitt (1971) warns that the reduction in efficiency is large if the initial step is too small, but only a small reduction in efficiency results from an initial step that is larger than the 'optimal' value.

5.2.2 Relating test result to psychometric function

Each of the different up-down methods produces its own 'transformed response curve' that relates the result of the test with a different position on the listener's psychometric function.

Up-down adaptive tests tend to converge on the stimulus level at which point there is equal probability of the next sequence being an up or down sequence, i.e. 0.5. Thus, from a theoretical viewpoint, the 50% point on the transformed response curve is mapped onto the psychometric curve to find the point of the psychometric function that is measured in that test. An example is given in Figure 5.3 for the two-down one-up procedure.

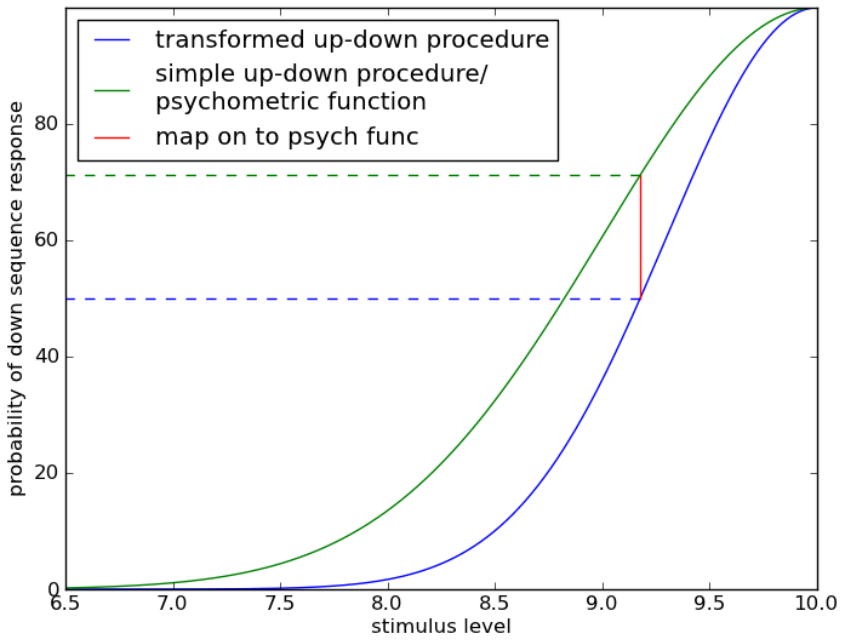

Figure 5.3: Mapping the transformed response curve for the two-down one-up procedure onto the psychometric function, showing the point on the psychometric function that is being measured by this test.

The blue dotted line shows the 50% point on the transformed response curve for a two-down one-up procedure, this is then mapped onto the subject's psychometric function to show the position on the subject's psychometric function that was measured in the test, the 71% point.

In practice, this point is found using a simple numerical calculation. A two-down sequence means a sequence of two consecutive positive responses. If the probability of a positive response at stimulus level X is P(X), then the probability of getting a positive response sequence is simply $[P(X)]^2$. As mentioned earlier, the test converges on a stimulus level where the probability of getting a positive response sequence is 0.5. Therefore, $[P(X)]^2=0.5$ so $P(X)=0.71$ (see y-intercept of green dotted line in Figure 5.3). In the case of the three-down one-up procedure $[P(X)]^3=0.5$ and so $P(X)=0.79$. Therefore using a two-down one-up procedure measures the 71% point of the subject's psychometric function, and the three-down one-up procedure measures the 79% point on the subject's psychometric function.

5.2.3 Choice between two-down and three-down tests

During the course of the test there will be a point where the listener can no longer hear a difference between the reference and modified tone and so the listener must guess the correct answer. The two-down one-up procedure is more liable to what is sometimes called false positives than the three-down one-up procedure. This is demonstrated by looking at the probability of the listener guessing the correct answer two and three times consecutively. The probability of the listener guessing the correct answer once is 1/3; the probability of guessing the correct answer in two trials is $(1/3)^2=1/9$; and guessing the correct answer in three consecutive trials is $(1/3)^3=1/27$. Hence there are obvious reasons why a three-down procedure is better than a two-down procedure from a statistical point of view. However, the three-down procedure is more time consuming and fatigue is likely to affect the subject's performance.

Considering the choice between three-down and two-down tests, one must choose whether to avoid fatigue or likelihood of getting 'false positives', then simply state to which point of the psychometric function that the test converges. By consistently choosing one method over the other one can compare results from different listeners, and compare the mean results from different tests.

5.3 Masking and critical bands

In order to explain certain results from some listening tests in later discussions it is important for the reader to be familiar with the concepts of masking and critical bands. For a more comprehensive discussion on these topics and further examples from the literature, the reader is advised to see Moore (1997).

The psychological phenomenon known as masking is closely related to measuring the frequency selectivity of the auditory system. Masking was defined by the American Standards Association in the 1960s as 'the process by which the threshold of audibility for one sound is raised by the presence of another (masking) sound'. Hence it is more difficult to detect, for instance, a sinusoidal signal in the presence of noise. It is increasingly difficult to detect the signal if the frequency band of the noise surrounds the signal. Thus, masking is related to frequency selectivity because in a complex sound, such as a guitar pluck, some components of the sound can mask other components.

Experiments exploring different types of masking have led to the theory of critical bands in the auditory system. As an example imagine a sinusoidal signal surrounded by a small bandwidth of noise where the signal is just about detectable. Increasing the bandwidth of the noise by a small amount at a constant intensity will make the signal undetectable. Next the intensity of the signal is increased so that it is, again, just about detectable. Then the process is repeated; increase the bandwidth of noise then increase the intensity of the signal so that it is just about detectable. In this experiment there will be a point where it makes no difference how much the bandwidth of noise is increased, the signal will remain just about detectable. The width of the band of noise at which point this occurs is called a critical band.

The idea is that the ear works in such a way that signals of different frequency fall into different critical bands. If there is more than one signal in a single band then it is more difficult to discriminate between the signals because they stimulate similar nerves in the auditory system. The ear-brain system therefore works a little bit like a Fourier transform, where a sound is separated into bins and components that are close to each other tend to be obscured somewhat.

The sides of the critical bands are known to be sloped; in fact the exact shape depends on intensity of the masker as well as central frequency (frequency of the signal). Nevertheless, it is useful to define an equivalent rectangular band (ERB) in order to try and characterise the change in bandwidth with central frequency. Moore (1997) collected data from several sources to find the dependence of the ERB on

central frequency. He found that the following equation seems to match results from five different experiments,

$$ERB = 24.7(4.37F + 1)\,, \tag{5.1}$$

where F is the central frequency in kHz and ERB is assumed to be the width of the critical band in Hz.

Thus this gives us a way of estimating whether certain components of guitar plucks will be strongly masked by other components by finding whether they lie within the same critical band.

5.4 Basic JND tests

This section introduces some basic listening tests that can be used as a reference for later discussions in this thesis. Initially this investigation was intended to find the just noticeable differences (JNDs) in parameters of the fundamental string component of a low-register guitar pluck on the classical guitar, consisting of three tests; JND in frequency, Q value and initial amplitude of the fundamental. These tests were taken by a group of five amateur musicians, named group A.

It was then decided to extend the investigation and carry out the same tests on a mid-range note for comparison, now including six tests. Also, it was thought to be useful to compare these results with the same six tests but including all string partials as opposed to just the fundamental, making a total of 12 listening tests. Persuading the same musicians to take all 12 tests seemed unfair considering there was no gain on their behalf because it was not possible to pay them. Therefore the 12 listening tests were taken by myself, and were repeated another nine times to get a reasonable average for each test. Two different tests were taken in one sitting and a maximum of eight tests were taken in one day. The results from these tests are labelled group B.

The point of these tests is not to get accurate thresholds for specific changes in the vibrational behaviour of an instrument; rather, they are an indication of how much a parameter of a string component in the radiated sound must change for us to perceive a difference. This should put further findings and discussions in a clearer context.

5.4.1 JNDs in parameters of the fundamental of note A_2

The radiated sound of a plucked note A_2 on classical guitar BR2 was recorded. The parameters of the fundamental were extracted, and then the fundamental was filtered out of the tone using a basic Fourier filter. A new fundamental was then added using additive synthesis with the desired parameters. Using the same parameters as the original fundamental produced a tone that was indistinguishable from the original tone; this was the 'reference tone'. The same method was used for creating the 'modified tones', i.e. the same filtered tone but with an added fundamental with slightly different frequency, initial amplitude or Q value, depending on the listening test. The tones were 1 s long, making them long enough to be perceived as decaying guitar tones but short enough to make some use of echoic memory.

The reference values, initial modifications, mean results of the five amateur musicians (group A) and mean results of the author (group B) are shown in Table 5.1. The quoted error is the standard error of the mean.

Parameter	Reference	Initial Modification	Mean group A (of 5)	Mean group B (of 10)
Frequency (Hz)	110.02	117.02	1.8+/-0.2	1.17+/-0.08
Initial amplitude (dB)	64.7	71.7	4.0+/-0.8	1.3+/-0.2
Q value	510	255	260+/-30	140+/-10

Table 5.1: Results for JNDs in parameters of the fundamental of note A_2 on a classical guitar.

Comparing the latter two columns in Table 5.1 underlines an interesting point. It is clear that the results for group B are consistently lower than that of group A. This suggests that the author can hear smaller differences to the parameters of the fundamental of a guitar tone than the mean of the other five musicians. However, it is not clear how much my performance was improved by the amount of practice I had whilst designing the test and repeating results. In my opinion, if the other five musicians were as familiar as I am with the task of identifying the fundamental in a guitar tone, I think they could achieve lower thresholds.

An important question to address arises from these results, that is which set of results should be taken as the just noticeable differences? Should the just noticeable difference be the smallest difference possible to hear, therefore allowing subjects to practice listening tests? If so, how much practice is enough? These questions are not answered clearly in the literature, as some work involve a small number of experienced listeners to take tests (Moore et al. 1985), other authors have larger sample groups assumed not to have extensive practice before carrying out a listening

test (Fritz et al. 2007), and other authors choose the results of the four best listeners from a larger sample group (Woodhouse et al. 2012).

We will proceed with caution and state the types of groups of people who would hear certain changes to the sounds tested in this thesis.

5.4.2 Extending investigation

The same method described in the last section was used to synthesise tones for the listening tests measuring the JND in frequency, initial amplitude and Q value of the fundamental of the note B_3 on the classical guitar. This time the tests were only taken by the author (group B), and repeated nine times to get a reasonable mean. The results are presented in Table 5.2. These will be discussed in the next section.

Parameter	Reference	Initial Modification	Mean group B (of 10)
Frequency (Hz)	247.63	254.63	1.2+/-0.2
Initial amplitude (dB)	67.5	74.5	1.1+/-0.1
Q value	331	165	68+/-9

Table 5.2: Results for the fundamental string parameters of the note B_3 on a classical guitar.

Finally, listening tests were carried out to measure the JND in frequency, initial amplitude and Q value of *all string components* of a low note, A_2, and a mid-range note, B_3, to compare with the previous six tests. The same synthesis method used previously could not be used here because all string partials had to be altered for the modified tone rather than just the fundamental. This time the parameters of all string partials up to 5 kHz were extracted as well as seven strong low-order body components and used to construct the test tones using additive synthesis. There were 44 string components for the note A_2 and 20 for the note B_3. This time the reference tone was clearly different from the original guitar tone. It is not essential that the synthesised tone is identical to the original guitar tone here, what is important is that these two tones have similar characteristics as seen by the human auditory system i.e. the presence of string partials and some body components to stimulate the ear-brain in a similar manner to the real guitar tone.

All of the string components were modified by a certain percentage in the frequency and Q value tests; this means that the modified tone in the JND in frequency test had a different pitch to the reference tone but had the same amount of inharmonicity as the reference. A percentage change in dB has no real meaning,

therefore the results for initial amplitudes are stated in dB. A broadband change of 1 dB is defined here as a 1 dB increase to all string components.

5.4.3 Results and discussion

In order to compare all of the results presented in this section the results from the first set of tests were converted into a percentage of the corresponding reference parameter, apart from initial amplitude results which remain in dB. This comparison is shown in Figure 5.4. Only results from group B were used in this graph because the results from group A for the fundamental of note A_2 are not readily comparable. The numbers on the graph are the results as percentages or dB and the error bars show the standard error of the mean.

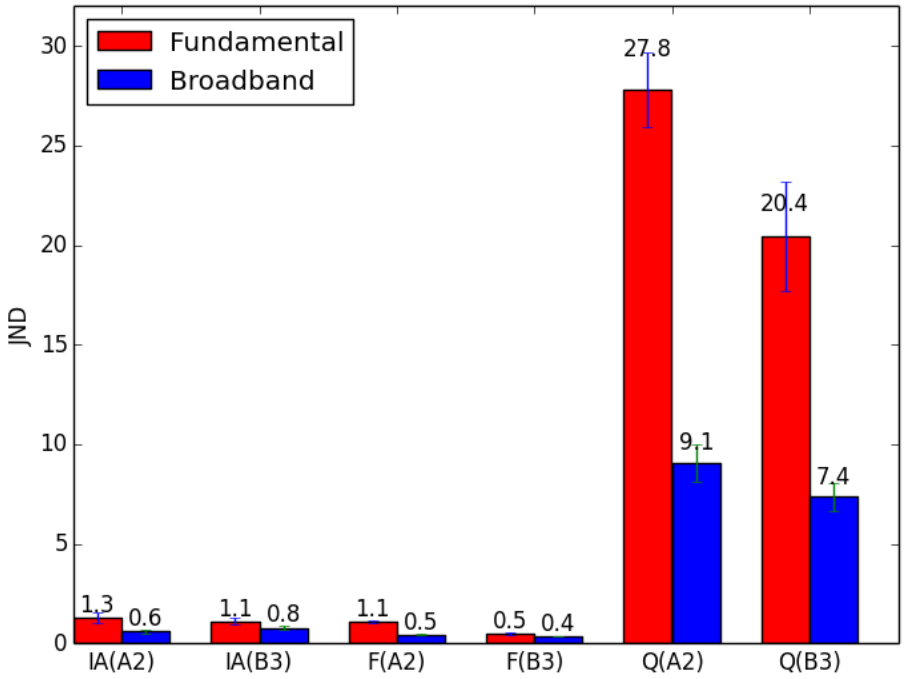

Figure 5.4: JNDs of various parameters of; the fundamental (in red) and all string partials (in blue) of the notes A_2 and B_3. IA stands for initial amplitude, F is frequency and Q is Q value.

As mentioned earlier, the purpose of these tests was to get a general feel for perceivable differences in the string partials of guitar tones. The results shown in Figure 5.4 can be summarised like so:

- The ear is more sensitive to changes to all string partials than solely the fundamental.
- The ear is most sensitive to percentage changes in frequency and least sensitive to percentage changes in Q value. The measured changes in initial amplitudes are not so easily compared.

- The ear is more sensitive to changes to mid-range notes than lower-range notes.

The first point above is trivial, that is, one would expect a change to all components to be more obvious than the same change to a single component.

The second point is interesting if one compares changes in frequency and initial amplitude to changes in Q value. These results show that we can hear rather subtle changes in frequency or loudness to a complex tone, but a much more substantial change must be made to the decay of a tone for us to hear a difference. This is consistent with the findings of Richardson et. al. (2008). Perhaps this reflects our ability to perceive similar changes in the voice; changes in pitch or loudness in a conversation can convey an obvious emotion, whereas accurate analysis of the decay of sounds is not as useful to us in order to communicate.

An exception to the third point can be seen in the initial amplitude of all string components. The JND for the lower-pitch note is smaller than for the higher-pitch note. This is most likely due to the fact that there were 44 string partials in the note A_2 and 20 partials in the note B_3. Therefore one would expect a 1 dB increase to 44 components to be a more obvious change than a 1 dB increase to 20 partials. It is unclear whether the same result would be found if all string partials up to 10 kHz would be used in the listening tests.

The third point above is consistent with the literature for changes in frequency of the fundamental (Moore et al. 1985). Moore et al. found inharmonicity thresholds of 5% and about 2.5% to the fundamental of complex tones with a 100 Hz and 200 Hz fundamental respectively. Moore's results are about five times greater than what was measured here, but this discrepancy is explained by the fact that the tones used by Moore et al. used components of equal loudness, whereas here the fundamental is louder than the other components (e.g. see Figure 4.3a) making changes to the fundamental easier to detect.

There is no work in the literature that could be found to do with JND of decay rates of complex tones, perhaps because such measurements are not deemed as important as loudness or frequency experiments. One thing that became obvious when taking the tests is that it was easier to detect a change in the Q value if the decay of the tone was relatively short compared with the length of the test tone (each test tone was chosen to be 1 s in these experiments). This is reflected in the results because the average decay rates of all string components below 5 kHz for A_2 and B_3 are 6.9 s^{-1} and 11.0 s^{-1} respectively, where a larger decay rate corresponds to a shorter sustain.

Chapter 6 Wolf notes on the classical guitar

In Section 2.3.1 a model by Gough (1981) describing perturbations to frequencies and Q values of coupled string-body modes was discussed. Here the model is introduced in more detail and then developed further. The more detailed model is validated by comparing results from the model with real measurements. Psychoacoustical measurements are then incorporated into the model so that the perceptibility of these perturbation effects can be established.

6.1 Modelling coupled string-body modes

6.1.1 Previous model

The solutions to the coupled equations by Gough that yield the frequency and Q value of the coupled modes are (Gough 1981)

$$\Omega_{\pm}^2 = \frac{\omega_B^2 + \omega_S^2}{2} + \frac{i}{2}\left(\frac{\omega_B^2}{Q_B} + \frac{\omega_S^2}{Q_S}\right) \pm \left\{\left[\frac{\omega_B^2 - \omega_S^2}{2} + \frac{i}{2}\left(\frac{\omega_B^2}{Q_B} - \frac{\omega_S^2}{Q_S}\right)\right]^2 + \alpha^2\right\}^{\frac{1}{2}}, \tag{6.1}$$

where ω_B and ω_S are the frequencies of the uncoupled body and string modes respectively, Q_B and Q_S are the Q values of the uncoupled body and string modes respectively and α is the coupling strength, given by

$$\alpha = \frac{{\omega_S}^2}{n\pi}\left(\frac{2m_s}{M_{eff}}\right)^{\frac{1}{2}}. \tag{6.2}$$

The frequencies of the coupled modes are given by the real part of Equation (6.1), $Re(\Omega_{\pm})$, and the imaginary part is related to the Q values of the coupled modes, ${\omega_S}^2/Im(\Omega_{\pm})$.

As a simple investigation of the dynamics of the system, Gough considered the situation where the unperturbed string and body modal frequencies coincide, $\omega_s = \omega_B$. Equation (6.1) then becomes

$$\Omega_{\pm}^2 = \omega_B^2 + \frac{i}{2}\left(\frac{\omega_B^2}{Q_B} + \frac{\omega_B^2}{Q_S}\right) \pm \left\{\alpha^2 - \left[\frac{1}{2}\left(\frac{\omega_B^2}{Q_B} - \frac{\omega_B^2}{Q_S}\right)\right]^2\right\}^{\frac{1}{2}}. \tag{6.3}$$

The origin of the parameter K now becomes clear (see Equation (2.4)). When the term inside the square-root of Equation (6.3) is greater than zero there will be a frequency perturbation. Therefore setting this term equal to zero and re-arranging everything to one side results in the definition of K, where $Q_S \gg Q_B$. The usefulness in applying this simplified version of the model to real instruments is limited. Note that Equation (6.3) describes the dynamics of the system specifically when a string mode and body mode are tuned to exactly the same frequency, which is a nearly impossible occurrence on a real instrument. In reality the amount of perturbation in frequency and Q value depend on both coupling strength, indicated by the ratio m_S/M_{eff}, and difference in frequency of the uncoupled modes, $|\omega_B - \omega_S|$. Gough effectively fixed the latter by equating it to zero and characterised the system using only the coupling strength.

6.1.2 Developing the model

A more detailed model is needed to describe the dynamics of a real instrument accurately. Here we will effectively take a step back from Gough's simplification and look to describe the system for string modes 'in the vicinity' of a body mode. We proceed by expanding the square-root in Equation (6.1) and collecting real and imaginary terms, p and q respectively.

$$p = \left(\frac{\omega_B^2 - \omega_S^2}{2}\right)^2 - \frac{1}{4}\left(\frac{\omega_B^2}{Q_B} - \frac{\omega_S^2}{Q_S}\right)^2 + \alpha^2\,, \tag{6.4}$$

and

$$q = \left(\frac{\omega_B^2 - \omega_S^2}{2}\right)\left(\frac{\omega_B^2}{Q_B} + \frac{\omega_S^2}{Q_S}\right). \tag{6.5}$$

The square-root of a complex number $(p+iq)^{1/2}$ can be written as $(\beta+i\varepsilon)$ where (Mostowski and Stark 1964)

$$\beta=\frac{1}{\sqrt{2}}\left(\sqrt{p^2+q^2}+p\right)^{1/2}\quad,\qquad \varepsilon=\frac{\operatorname{sgn}(q)}{\sqrt{2}}\left(\sqrt{p^2+q^2}-p\right)^{1/2}\ . \tag{6.6}$$

Note that $\operatorname{sgn}(q)$ means "the sign of q", i.e. if q is negative then replace with -1. This simplifies Equation (6.1) into the following form,

$$\Omega_{\pm}^2=\frac{\omega_B^2+\omega_S^2}{2}+\frac{i}{2}\left(\frac{\omega_B^2}{Q_B}+\frac{\omega_S^2}{Q_S}\right)\pm(\beta+i\varepsilon)\ . \tag{6.7}$$

As mentioned previously, the frequencies of the coupled modes are given by the real part, $\omega_{\pm}^{*}=Re(\Omega_{\pm})$, and the imaginary part is related to the Q values of the coupled modes, $Q_{\pm}^{*}=\omega_S^2/Im(\Omega_{\pm})$, to yield

$$\omega_{\pm}^{*}=\left(\frac{\omega_B^2+\omega_S^2}{2}\pm\beta\right)^{1/2}\quad, \tag{6.8}$$

and

$$Q_{\pm}^{*}=\frac{\omega_S^2}{\frac{1}{2}\left(\frac{\omega_B^2}{Q_B}+\frac{\omega_S^2}{Q_S}\right)\pm\ \varepsilon}\ . \tag{6.9}$$

The above expressions give the perturbations in frequency and Q value of coupled string-body modes.

6.1.3 Validating the model

In order to use the model it is important first of all to show that it accurately describes the dynamics of a real system. The method used to validate the model is described below.

Firstly the input admittance at a certain string position was measured and modal parameters of the body mode of interest were extracted using the previously-mentioned peak-picking technique. As usual the strings were damped for this measurement. This gives the body mode's uncoupled frequency, uncoupled Q value and effective mass. Then a note with a fundamental frequency near to the body mode was chosen and detuned about 10 Hz below the body mode. An accelerometer was used to measure the acceleration at the bridge from a wire-break excitation of the string. The frequencies and Q values of the two closely spaced peaks in the acceleration signal were extracted using STFFTs, these are the *coupled* frequencies and Q values. The uncoupled frequency of the string mode was estimated from an inharmonicity plot of the first 30 string partials, similar to those shown in Figure 4.6.

Two parameters are now left, which are the uncoupled Q value of the string mode and the mass of the string. The former was estimated using data from previous experiments at Cardiff that measured the vibration of a guitar string attached to a solid bar with a mounted force transducer. The idea is that the measured Q value in this experiment is due to air damping and internal damping only. Incidentally, the exact value of the uncoupled Q value of the string mode has little influence on the model as it is far greater than that of the body mode. The mass of the string was taken from the D'addario website (D'addario 2015), where information on their strings is readily available.

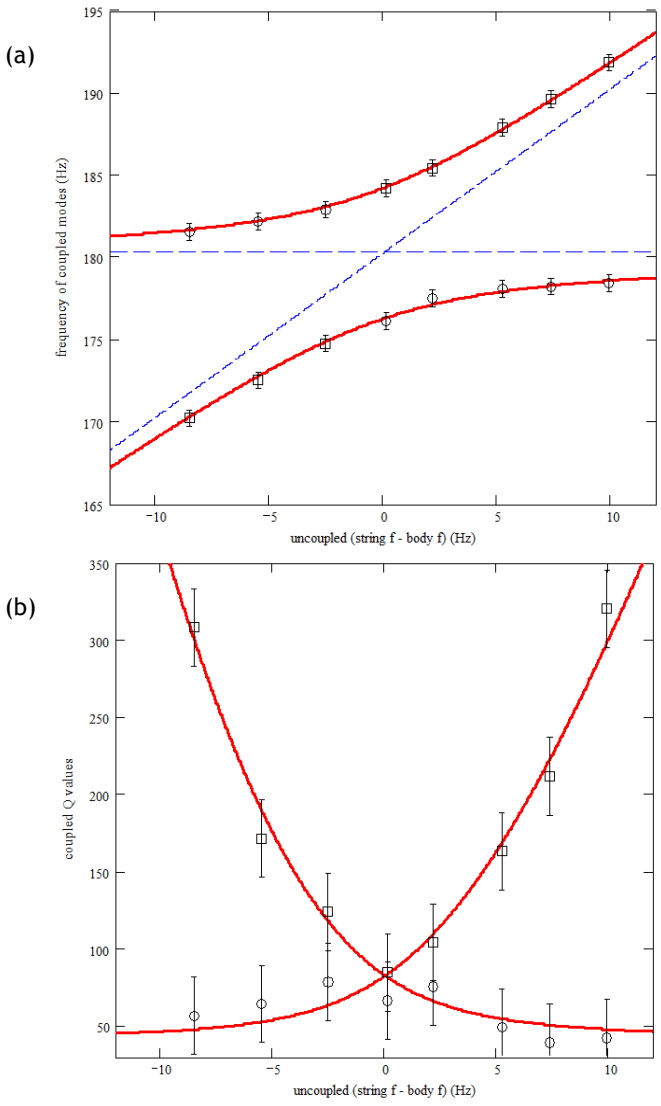

Figure 6.1: Coupled (a) frequencies and (b) Q values plotted against uncoupled values. The largest peak in the FFTs has been plotted as squares and the smallest peak of the two are plotted as circles.

The string was essentially tuned through the frequency of the uncoupled body mode with velocity measurements from wire-break string excitation taken every few Hz. The data was plotted on graphs of frequency and Q value of the coupled modes against uncoupled frequency and the model was put on top to see how well it

describes the system. The mode under consideration here was the $T(1,1)_2$ mode of guitar BR2. The peak-picking process applied to the input admittance at the termination point of string four on the bridge yielded $\omega_B/2\pi = 180.1$ Hz, $Q_B = 44$ and $M_{eff} = 0.11$ kg.

Figure 6.1a shows the measured frequencies of the two close peaks against the calculated uncoupled frequencies of the fundamental. The model is plotted on top as red curves and show good agreement within experimental error. Similarly, Figure 6.1b shows the measured Q values of the two close peaks against their calculated uncoupled frequencies. Note that there is slight disagreement between data and model in this graph. The Q values of the coupled modes should be nearly identical for the points nearest the 0 point on the horizontal axis. The reason for this is thought to be due to the large error in Q value estimation (error of +/- 25 shown here).

These graphs prove the validity of this model within the vicinity of a strong body mode. It was found that as the string was tuned further away from the body mode the model was less useful (roughly greater than 10 Hz), this is because of the influence from other modes, not included in the model, becoming more significant.

6.1.4 Dynamics of coupled string-body modes

It is now useful to explore the results from the model as a function of coupling strength. This is done by defining $\omega = (\omega_B + \omega_S)/2$, and varying the ratio m_S/M_{eff}. Figure 6.2 shows the interaction between the $T(1,1)_2$ mode and its nearest string mode, the fundamental of the note $F\#_3$. The top two graphs in Figure 6.2 were generated with the general formulation developed here and the bottom two show the results using Gough's approximation. The $K = 1$ point is clear from the lower set of graphs, at around $\alpha/\omega^2 = 0.01$, where the dynamics of this system are exactly as described by Gough. Looking at the top left-hand graph one can see that the frequency perturbations occur at a smaller coupling strength than that predicted by Gough. In fact, if one were to zoom in on the left-hand side of the frequency perturbation graph, one would find that the splitting occurs at $\alpha > 0$, this can also be found by manipulation of Equation (6.1). Nevertheless, Gough's approximation gives a reasonable estimate of the frequency and Q value perturbations for a string mode that is very close in frequency to a body mode.

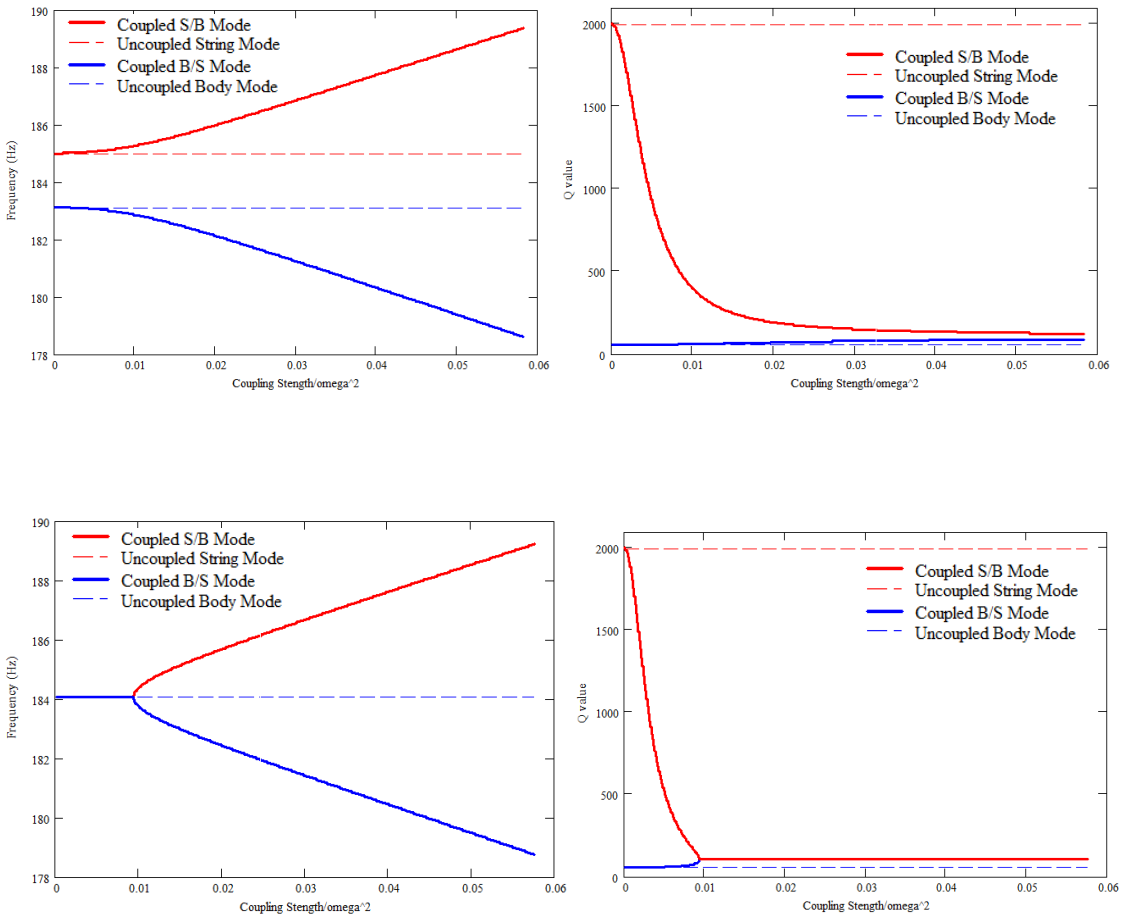

Figure 6.2: Frequencies and Q values of the fundamental of note F#$_3$ and mode T(1,1)$_2$ on guitar BR2. The top two graphs are the result of the general formulation and Gough's approximation was used to generate the bottom two graphs.

As one looks further away than the nearest note the approximation is not satisfactory. Figure 6.3 shows the result for the same body mode coupled to the fundamental of the note G$_3$. Note that the bottom two graphs are similar to the bottom two of Figure 6.2, with the frequency curves shifted up to the new average of the uncoupled mode frequencies.

For the string-body system shown in Figure 6.3, the coupling between the string and body mode was measured to be $\alpha/\omega^2 = 0.05$, and so Gough's formulation predicts a frequency perturbation of 4.2 Hz, whereas Equation (6.9) predicts a perturbation of 1.4 Hz.

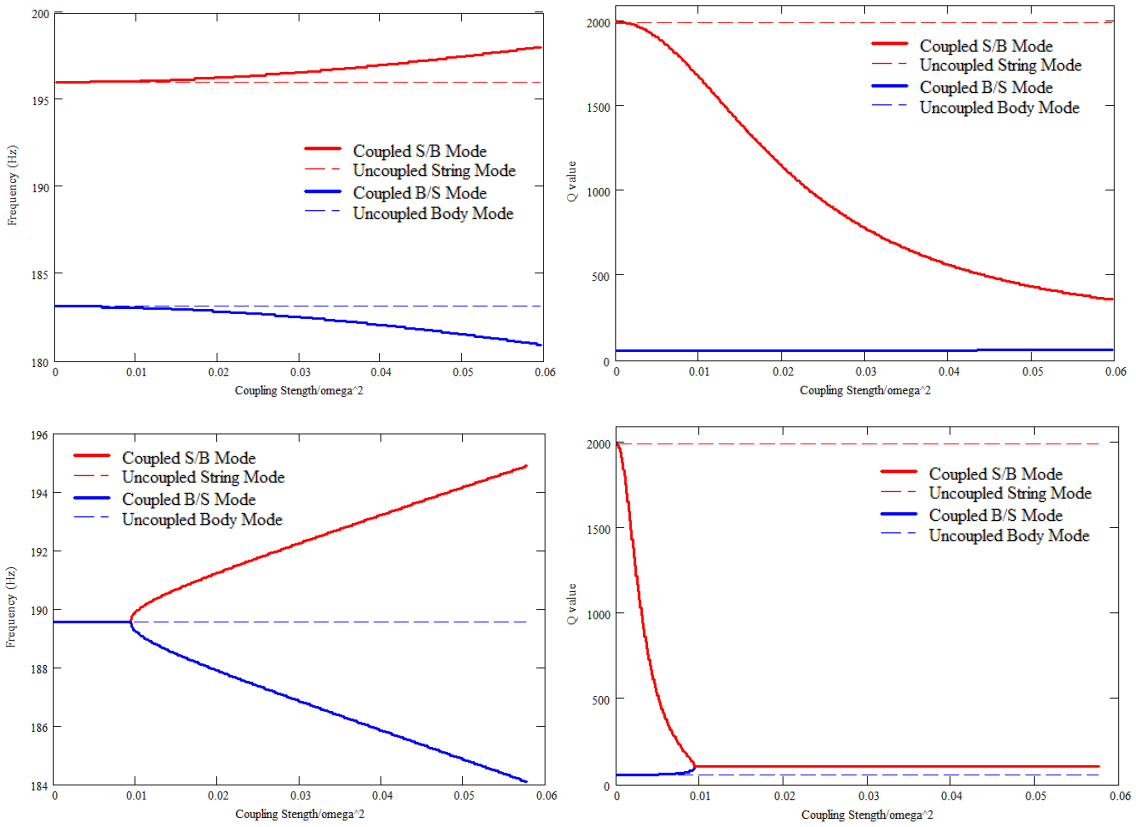

Figure 6.3: Frequencies and Q values of fundamental of note G_3 and $T(1,1)_2$ of guitar BR2. Again, Equations (6.8) and (6.9) were used to get top two graphs, and Gough's approximation was used to get bottom two graphs.

6.2 Combining psychoacoustical measurements with model

In the previous section the model was validated and the dynamics of the system were explored a little. It is now possible to implement the model and incorporate psychoacoustical measurements to find whether these perturbations are perceivable.

6.2.1 Theory

It is well known that the body modes that are coupled most strongly to the strings are the T(1,1) modes (Wright 1996). In particular the $T(1,1)_2$ mode, which typically lies just below 200 Hz, usually has the lowest effective mass. Therefore a good starting point is to look at the coupling between the $T(1,1)_2$ mode and nearby fundamental string modes.

Let the smallest perceivable frequency and Q value perturbations to the fundamental string component be $JND(\omega_0)$ and $JND(Q_0)$ respectively. These two values are measured using individual listening tests. Next the frequency and Q value of the fundamental at which point these effects are perceivable are defined.

Note that the frequency perturbation can sharpen or flatten the fundamental depending on the frequency of the fundamental relative to that of the body mode, giving $\omega_{JND} = \omega_S \pm JND(\omega_0)$. The treatment of the Q value is slightly cruder, because a typical Q_S of an uncoupled string is around 2000, whereas a typical Q value of the fundamental of a low guitar note is around 400. Therefore the average Q value of the fundamentals of notes on a guitar in the vicinity of this body mode is calculated, called Q_{mean}, and used as the reference in the listening tests. Q_{mean} is defined here as the average of the fundamental Q values of the nearest five notes to the body mode. The reason for this definition is that adjacent notes should have relatively similar string parameters for even tonal quality from one note to another. The effect that this coupling has on the string mode is to reduce its Q value, so the smallest perceivable difference is subtracted from this reference value, yielding $Q_{JND} = Q_{mean} - JND(Q_0)$.

Now ω_{JND} and Q_{JND} are substituted into Equations (6.8) and (6.9) for ω^* and Q^* respectively, then the two equations can be re-arranged for the coupling strength, giving

$$\alpha_\omega = \left\{\left(\omega_{JND}^2 - \frac{\omega_B^2 + \omega_S^2}{2}\right)^2 - \frac{q^2}{\left[2\omega_{JND}^2 - (\omega_B^2 + \omega_S^2)\right]^2} - \left(\frac{\omega_B^2 - \omega_S^2}{2}\right)^2 + \frac{1}{4}\left(\frac{\omega_B^2}{Q_B} - \frac{\omega_S^2}{Q_S}\right)^2\right\}^{\frac{1}{2}}, \tag{6.10}$$

and

$$\alpha_Q = \left\{\frac{q^2}{4}\left[\frac{\omega_S^2}{Q_{JND}} - \frac{1}{2}\left(\frac{\omega_B^2}{Q_B} - \frac{\omega_S^2}{Q_S}\right)\right]^{-2} - \left[\frac{\omega_S^2}{Q_{JND}} - \frac{1}{2}\left(\frac{\omega_B^2}{Q_B} - \frac{\omega_S^2}{Q_S}\right)\right]^2 - \left(\frac{\omega_B^2 - \omega_S^2}{2}\right)^2 + \frac{1}{4}\left(\frac{\omega_B^2}{Q_B} - \frac{\omega_S^2}{Q_S}\right)^2\right\}^{\frac{1}{2}}. \tag{6.11}$$

The two equations above give the amount of coupling needed to produce a perceivable frequency perturbation and Q value reduction, hence a perceivable wolf note.

6.2.2 Method

The guitar tones used for the psychoacoustical tests were constructed in the following way. The radiated sound from a wire-break excitation of the note D_3 on guitar BR2 was recorded in a small music studio (reverberation time of about 0.2 s). This note was chosen because the most likely wolf notes on this instrument are on the third and fourth frets of this string. The notes with fundamentals closest to the $T(1,1)_2$ mode could have been used but it was simpler to use an unfretted note. The frequency, Q value and initial amplitude of the fundamental of the note were extracted. The fundamental was then filtered out of the original recording using a basic Fourier filter. This allowed the fundamental to be reconstructed with slight adjustments to its parameters before it was added to the filtered tone using additive synthesis. This is similar to the method described in Section 5.4.1. The frequency of the fundamental of the reference tone was estimated using Equation (4.1), producing a graph similar to those shown in Figure 4.6. The initial amplitude and Q value of the fundamental were the average of these parameters for five notes near the body mode under consideration, ranging from the note $D\#_3$ to G_3 on the fourth string of the instrument.

The body component of the sound, which is generated by the strongly coupled body mode, was not added to the synthesised tone. In order to include the body component an assumption must be made to either keep ω_B constant and change α, or to keep α constant and change ω_B. This makes choices for the parameters of the reference tone in the listening tests very difficult and also heavily restricts the application of the results. Therefore it was decided to ignore the body component in the radiated sound. The downside of doing this is that the synthesis method will not include the beating effect between the string and body component.

3AFC listening tests were used, one to find $JND(\omega_0)$ and the other measuring $JND(Q_0)$. A two-down one-up paradigm was used for two reasons. Firstly it evaluates the result closer than the three-down one-up test to the 50% point of the subject's psychometric function, which is a more intuitive notion of 'threshold of perception'. It also involves fewer trials to reach the result therefore the listener will not suffer as much fatigue.

Seven subjects were asked to take the two tests, all of whom consider themselves to be amateur musicians. The tests were taken in the usual conditions as stated in Section 5.4. Each tone in the tests was 1 s long allowing some use of echoic memory but also making sure the tones were long enough to register the decay.

6.2.3 Results

The average $JND(\omega_0)$ of the note D_3 between the seven subjects was found to be (2.2 ± 0.2) Hz, which is equivalent to about 26 cents. The average $JND(Q_0)$ of the note D_3 between the seven subjects using a reference Q value of Q_{mean} = 389 was found to be (200 ± 22), which is equivalent to about 51%.

The results for $JND(\omega_0)$ and $JND(Q_0)$ were then used to find ω_{JND} and Q_{JND}, which were then inserted into Equations (6.10) and (6.11) respectively. Both of these equations also use the resonant frequency and Q value of the body mode and Q value of the string, which were the same as those used in Section 6.1.3. α_ω and α_Q were then plotted on separate graphs as a function of $\omega/2\pi$ with $\omega_S = \omega$ to show the minimum amount of coupling needed to produce a perceivable perturbation in frequency and Q value of the fundamental of a guitar tone. These curves are shown in Figure 6.4. Also plotted on these graphs are the estimated coupling strengths between nearby fundamentals and the $T(1,1)_2$ mode. The string mass and effective mass of the body mode used to calculate these coupling strengths were the same as were used in Section 6.1.3.

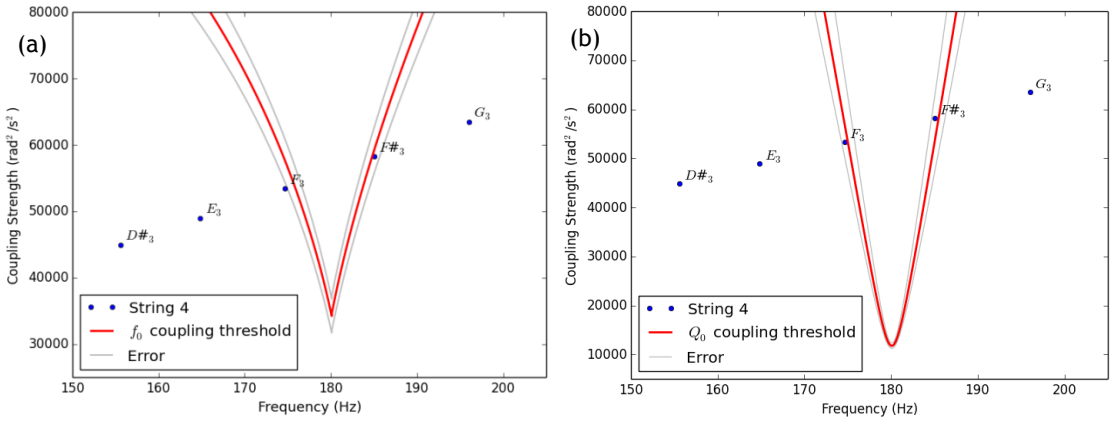

Figure 6.4: Coupling threshold curves for (a) frequency and (b) Q value perturbation of the fundamental of a guitar tone. The points represent the coupling strength of nearby fundamentals. Points that lie within the red curves highlight the perceivable wolf notes on this instrument. The error in the measured $JND(\omega_0)$ and $JND(Q_0)$ are represented by the grey lines.

Thus, points that lie within the confines of the red walls of the coupling threshold curves in Figure 6.4a and b represent the notes that would suffer from perceivable perturbations in frequency and Q value respectively. The error curves represent the error from the listening tests. Using these particular parameters in the model show that frequency perturbation to the fundamental of the note $F\#_3$ might be perceivable by some of the subjects that took the listening tests here, but not by others. A similar result is found for the Q value of the fundamental of this note. If the string under consideration were tuned a little sharp then the points representing

the notes in Figure 6.4 would move up and to the right leaving the note F_3 above the coupling threshold curves and the note $F\#_3$ below the coupling threshold curves. In this example the note F_3 would now be a wolf note and the note $F\#_3$ would not be a wolf note.

6.2.4 Discussion

The frequencies of low-order body modes have been shown to vary from day to day due to humidity changes. Wright (1996) measured the frequency of the $T(1,1)_2$ mode on this guitar (BR2) over several weeks and found a variation of around ± 5%. This amount of movement corresponds to this wolf note moving between the notes F_3 and $F\#_3$. Perhaps a more useful indication of the number of wolf notes here is to measure the width between the red curves at the point of intersection with the line drawn out by the points on the graph. This is named the width of the wolf note and should be stated in cents. The following general rule of thumb can then be used; a width less than 50 cents is unlikely to produce a wolf note, between 50-150 cents is likely to yield one wolf note and greater than 150 cents is likely to yield at least one wolf note. The wolf note width in Figure 6.4a and b are 87 and 102 cents respectively.

By changing various parameters in the model it is possible to evaluate different ways of avoiding wolf notes. Halving the Q value of the body mode leads to a wolf note width of 65 cents to the curve in Figure 6.4a, whereas doubling the Q value increases the width to 91 cents. Halving the effective mass of this body mode increases the width to 226 cents and doubling the effective mass decreases the width to 13 cents. Therefore increasing the Q value has little effect compared with decreasing the effective mass.

In Section 4.3.2 it was found that adding 5 grams of mass (blue-tack) to the anti-nodal region of the $T(1,1)_2$ mode on guitar MAL increased the effective mass of this mode by 50%. If the same were true for guitar BR2, this would decrease the wolf note width due to frequency perturbation to 40 cents. Note that adding mass to the anti-nodal region of the $T(1,1)_2$ mode on guitar MAL is likely to affect the string-body coupling less so than on guitar BR2, because the anti-nodal region of the $T(1,1)_2$ mode on the latter guitar is situated in the same region as the bridge. Therefore this is perhaps not a wise option to eliminate a wolf note on a well-built instrument.

An alternative way to decrease the string-body coupling is to choose a lighter gauge string. The string parameters used here are for a D'addario Pro Arte hard tension composite string, with mass per unit length of 1.95 g/m and tension 71.2 N.

Choosing the lighter string up from this one, having mass per unit length of 1.76 g/m and tension 63.6 N, would reduce the wolf note width to 69 cents. This would of course come at the cost of having a string that is not as responsive to the players touch, but it is a strong option if the wolf note is 'unbearable' to the player's ears and most likely a better option than adding mass to the soundboard.

A quick note should be made on the relative significance on the two results shown in Figure 6.4. The assumptions used to get the coupling threshold curves are far more acceptable in the case of frequency perturbation than Q value perturbation. This is because defining the frequency of the reference tone in the listening tests is much simpler than the definition of the Q value of the reference tone. That is, an ideal fundamental should have a non-perturbed frequency and that frequency is easy to calculate, whereas the same is not true for the Q value of an 'ideal' fundamental. Therefore the definition of the reference Q value here, Q_{mean}, is rather arbitrary and averaging the Q values of four notes would yield a different result to averaging between five or six. Also, it was suggested in Section 5.4.3 that the JND for Q value depends on the decay rate of the string partial under consideration relative to the length of the test tone. For these two reasons the results for the coupling threshold due to frequency perturbation should be treated with greater credibility than the coupling threshold due to Q value perturbation.

Chapter 7 Physical modelling

An important part of the work in this thesis is to make objective judgements of the radiated sound from an instrument using a method that enables control over the mechanical and acoustical properties of the instrument. It is therefore essential to have a physical model of the instrument that can reproduce the sound pressure at a point in space from an excitation of the string to the highest level of accuracy as possible.

Woodhouse (2004a) carried out an investigation on the problem of synthesising the transient of a plucked guitar string. He tried several methods to model the acceleration response from the soundboard of the instrument to a step force applied to the string. This does not simply translate to the pressure response of the instrument as demonstrated by Hill et al. (2004), but is the first stage in modelling the instrument as a whole. Woodhouse found that the two most successful methods were a modal superposition method and a frequency-domain method.

In this chapter two methods of physical modelling will be discussed, firstly a modal superposition model and then a transmission-line model, the latter is a frequency-domain model. The results from the two models are compared with each other and the application of these models in listening experiments is discussed. The problem of coupling the instrument to its surrounding air is then discussed, followed by the modelling procedure. The next section of this chapter is on extending the model. This is an important part of the work as it enables psychoacoustical measurements to be made that have not been carried out before. The final section of this chapter is on applying the same modelling technique for the steel-string guitar

and banjo. By doing this we can learn more about the differences of the vibrational behaviour of these instruments that lead to the differences in perceived tone quality.

7.1 Choosing a model

7.1.1 Modal superposition model

A brief summary of the modal superposition method is given here, for a more detailed description see Woodhouse (2004a). Examples of the theory can be found in engineering texts by Craig (1981) and Newland (1989).

This method enables a set of N simultaneous equations, indexed n, to be uncoupled by changing the coordinate system to the so-called modal coordinate system. The motion of a linear system with multiple degrees of freedom is given by

$$M\ddot{\boldsymbol{q}} + C\dot{\boldsymbol{q}} + K\boldsymbol{q} = 0\,. \tag{7.1}$$

The degrees of freedom involved here, N, can be large so it is sensible to use matrices for the following analysis. Therefore, M, C and K are the mass, damping and stiffness matrices respectively and $\boldsymbol{q}$ is a set of generalised coordinates. The mass and stiffness matrices are obtained from the potential and kinetic energies of the system respectively (Craig 1981). In the case of a stringed musical instrument, these matrices include measured parameters of the string and body of the instrument.

The system is uncoupled by solving an eigenvalue problem, and in order to set up an eigenvalue equation, a double length vector is defined,

$$\boldsymbol{p} = \begin{bmatrix} \boldsymbol{q} \\ \dot{\boldsymbol{q}} \end{bmatrix}, \tag{7.2}$$

and a $2N \times 2N$ matrix,

$$A = \begin{bmatrix} 0 & I \\ -M^{-1}K & -M^{-1}C \end{bmatrix}. \tag{7.3}$$

(Note that this matrix appears differently from Equation (5) in Woodhouse (2004a), but is consistent with Equation (8.2) in Newland (1989)). Now it is possible to rewrite the equations of motion, Equation (7.1), as $\dot{\boldsymbol{p}} = A\boldsymbol{p}$, where a modal solution $\boldsymbol{p}(t) = \boldsymbol{v_n}\exp(\lambda_n t)$ leads to the eigenvalue problem,

$$A\boldsymbol{v}_n = \lambda_n \boldsymbol{v}_n\,. \tag{7.4}$$

Solving this equation yields the complex eigenvalues and eigenvectors of the system that can be summed to give an impulse response function.

This method was applied to the guitar with the coordinates chosen to represent the modal displacements of the string and the body. In this case the result is the velocity response of the body from applying a step force to a point on the string. Results from the model are shown later in this section.

7.1.2 Transmission-line model

The most recent physical model to be developed at Cardiff is a transmission-line model. Electrical-analogues for vibrating strings coupled to a structure have been used effectively for a long time, e.g. by Kock (1937). The development in using transmission-line theory to describe these systems was taken further by Schelleng (1962) and Gough (1981). It was then applied to the classical guitar by Bernard Richardson at Cardiff and has since been expanded and improved accordingly over the years. This model is discussed in more detail than the modal superposition model as there is only a brief derivation available in the literature (Richardson et al. 2008).

The diagram below shows the system under consideration. A string of length L, tension T, and characteristic impedance Z_0, is fixed at $x = 0$ and attached to a load with impedance Z_L at the point $x = L$.

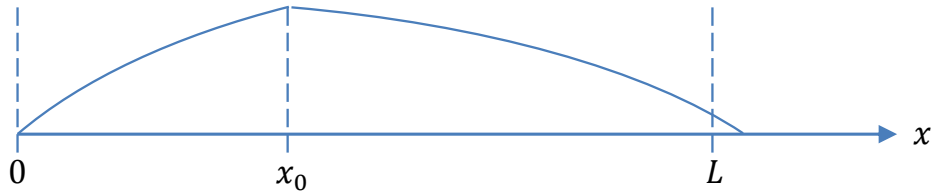

Figure 7.1: Diagram of a string fixed at $x = 0$, connected to a load at $x = L$ and with a discontinuity at $x = x_0$.

Here the load impedance represents the impedance presented to a string by the body of a classical guitar. As previously mentioned, the input admittance of a single body mode is given by

$$Y(\omega) = \frac{i\omega}{M\left(\omega^2 - \omega_0^2 + i\omega_0\frac{\omega}{Q}\right)}, \tag{7.5}$$

where M, ω_0 and Q are the effective mass, resonance frequency and Q value of the body mode respectively. Note that for a system with a single degree of freedom, the terms M, C and K from Equation (7.1) are equivalent to M, $M\omega_0/Q$ and $M\omega_0^2$ in

Equation (7.5). The input admittance is summed over all modes of interest and its reciprocal is taken to give the load impedance,

$$Z_L = \frac{1}{\sum Y}. \tag{7.6}$$

What is of interest here is the input admittance Y at the point $x = x_0$ and the transfer admittance, $Y_T(x)$, between a force applied to the point $x = x_0$ and the velocity at point x, eventually at $x = L$. It is often more convenient to describe dynamical systems in terms of impedances rather than admittances, which are related like so, $Y = 1/Z$ and $Y_T = 1/Z_T$. Therefore an expression for the input impedance will be derived,

$$Z(x_0) = \frac{F(x_0)}{\dot{y}(x_0)}, \tag{7.7}$$

and also the transfer impedance,

$$Z_T(x) = \frac{F(x_0)}{\dot{y}(x)}. \tag{7.8}$$

In the following derivation we adopt the convention that harmonic vibrations are described by $\exp(-i\omega t)$ so that a positive wavenumber, k, denotes a wave travelling from left to right, or positive x direction, in the above diagram.

Transverse waves on the string are described by,

$$y = A_I \exp[i(kx - \omega t)] + A_R \exp[i(-kx - \omega t)], \tag{7.9}$$

where A_I and A_R are the amplitudes of the incident and reflected waves respectively, relative to the point $x = L$. The velocity and restoring force due to a displacement of the string from its equilibrium position are given by,

$$\dot{y}(x,t) = -i\omega \exp(-i\omega t)\,[A_I \exp(ikx) + A_R \exp(-ikx)], \tag{7.10}$$

and

$$F(x,t) = -T\frac{\partial y}{\partial x} = -iTk \exp(-i\omega t)\,[A_I \exp(ikx) - A_R \exp(-ikx)]. \tag{7.11}$$

Therefore the input impedance of the string as a function of position is given by Equation (7.11) divided by Equation (7.10),

$$Z(x) = Z_0 \left[\frac{A_I \exp(ikx) + A_R \exp(-ikx)}{A_I \exp(ikx) - A_R \exp(-ikx)}\right], \tag{7.12}$$

where $Z_0 = Tk/\omega$.

Imposing the boundary condition $Z(L) = Z_L$ enables A_R to be written in terms of A_I,

$$A_R = A_I \left[\frac{Z_0 - Z_L}{Z_0 + Z_L}\right] \exp(i2kL). \tag{7.13}$$

Then substituting Equation (7.13) into Equation (7.12) eliminates the amplitudes of the waves and gives the input impedance of the string at any point to the right of $x = x_0$,

$$Z(x) = Z_0 \left\{ \frac{Z_L cos[k(L-x)] - iZ_0 sin[k(L-x)]}{Z_0 cos[k(L-x)] - iZ_L sin[k(L-x)]} \right\}. \tag{7.14}$$

From standard transmission-line theory, the input impedance to the left of $x = x_0$ is that of a finite-length string (Fletcher and Rossing 1998),

$$Z(x) = iZ_0 cot(kx)\,. \tag{7.15}$$

These two sections of string have the same displacement and velocity at $x = x_0$ but in general have a different slope. This discontinuity produces a restoring force that is balanced by the driving force. The input impedance at $x = x_0$ is thus given by the sum of Equation (7.14) and Equation (7.15), which reduces to

$$Z(x_0) = \frac{Z_0 Z_L sin(kL) - iZ_0^2 cos(kL)}{Z_0 cos[k(L-x_0)] - iZ_L sin[k(L-x_0)]} \frac{1}{sin(kx_0)}. \tag{7.16}$$

Next we want to find the transfer impedance given by Equation (7.8). Comparing this expression to the input impedance in Equation (7.7), we see that $Z_T(x) = Z(x_0)\dot{y}(x_0)/\dot{y}\,(x)$. Combining Equations (7.10) and (7.13) we get

$$\frac{\dot{y}(x_0)}{\dot{y}(x)} = \frac{Z_0 cos[k(L-x_0)] - iZ_L sin[k(L-x_0)]}{Z_0 cos[k(L-x)] - iZ_L sin[k(L-x)]}, \tag{7.17}$$

then multiplying Equations (7.16) and (7.17) gives

$$Z_T(x) = \frac{Z_0 Z_L sin(kL) - iZ_0^2 cos(kL)}{Z_0 cos[k(L-x)] - iZ_L sin[k(L-x)]} \frac{1}{sin(kx_0)}. \tag{7.18}$$

Finally, inverting this equation and setting $x = L$ gives the desired transfer admittance,

$$Y_T(L) = \frac{sin(kx_0)}{Z_L sin(kL) + iZ_0 cos(kL)}. \tag{7.19}$$

Now that the transfer admittance has been obtained, damping and dispersion is added to the string. The damping comes in the form of a viscous damping force (containing the internal damping and air damping of the string) that is included in the impedance of the string and wavenumber, in the latter case giving a complex wave-vector. The damping force is given by $\gamma = \beta/\mu$, where β is the mechanical resistance per unit length and μ is the mass per unit length, modifying k,

$$k \to \frac{\omega}{c}\left(1 + \frac{i\gamma}{\omega}\right)^{1/2}. \tag{7.20}$$

It is more convenient to use the Q value of the string rather than the damping force, these are related like so, $Q_s = \omega/\gamma$. A similar modification is made to the characteristic impedance of the string,

$$Z_0 \to Z_0 \left(1 + \frac{i}{Q_s}\right)^{1/2} . \tag{7.21}$$

The Q value itself can take different forms depending on the type of string being used. A simple frequency dependent scheme for the Q value of the string is used here where Equation (7.22) is used for wound nylon strings and Equation (7.23) is used and for plain nylon strings. These equations were derived by Bernard Richardson as simple equations to fit data by Valette (1995).

$$Q_s(\omega) = 2000 + 0.1\left(1 - \frac{\omega}{2\pi}\right), \tag{7.22}$$

$$Q_s(\omega) = \frac{3\omega}{2\pi}\exp\left(-\frac{0.0005}{\pi}\omega\right) + 200 . \tag{7.23}$$

Dispersion is also included in the model by modifying c in Equation (7.20) to include the dispersion coefficient, α,

$$c \to v(1 + \alpha\omega^2) , \tag{7.24}$$

where v is the wave velocity given by $v = \sqrt{T/\mu}$.

7.1.3 Comparison of models

The modal superposition model (MSM) and transmission-line model (TLM) were implemented to get the velocity response of the body from a force applied to the string. A sampling frequency of 22050 Hz was chosen and a signal of 2^{16} points generated a tone of 2.97 s. The calculation involved seven low-order body modes and 70 string partials (the number of string partials must be stated in the MSM whereas string partials are generated up to the Nyquist frequency in the TLM), with string parameters corresponding to the note D_3. The calculation using the MSM typically took around 6.7 s whereas using the TLM took around 4.1 s. The time evolutions of the two tones are shown in Figure 7.2.

The time-domain graphs of the two synthesised tones are not equivalent, but show good agreement in general trend, as does the frequency spectrum, shown in Figure 7.3. Note that the spectrum for the MSM tone has been shifted 15 Hz to the right in order to see the two curves more clearly.

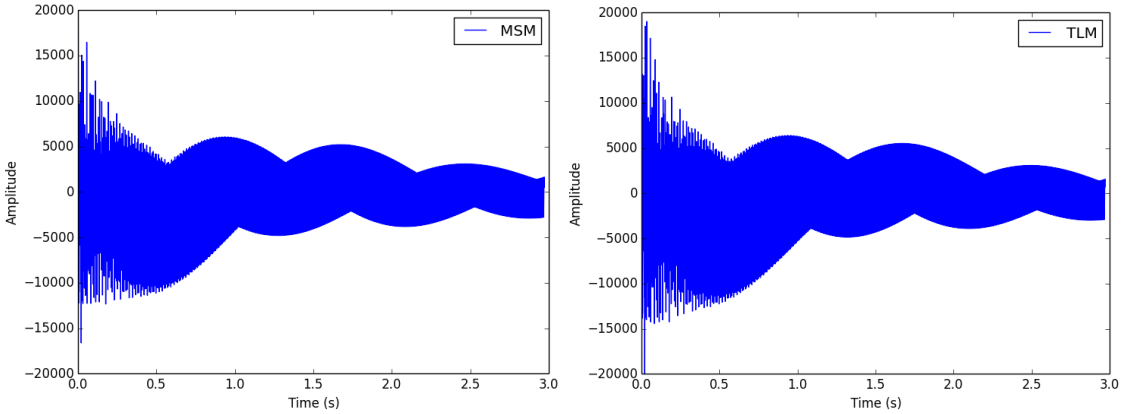

Figure 7.2: Time evolution of a guitar pluck using MSM (left) and TLM (right).

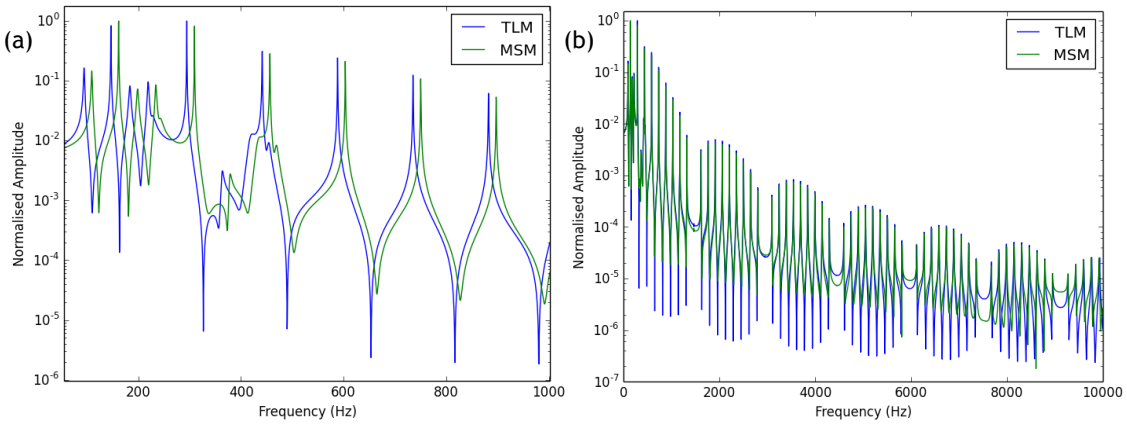

Figure 7.3: Spectra of guitar pluck using two different models. (a) 0-1kHz with MSM shifted 15 Hz to the right (b) 0-10kHz.

The peaks of the body components line up nicely as do the string components. There is some discrepancy in the anti-resonances though these are of little importance.

The parameters of string partials were extracted from both tones as described in Chapter 3 to find whether the difference between the two tones are likely to be perceivable. This is done because it is difficult to say whether a slight difference in comparing two FFTs is something significant or not.

Figure 7.4a shows the Q values of string partials of the note D_3 using both synthesis methods. Note that the Q values of the first nine partials are virtually identical. The large error bars of every tenth partial are due to the fact that the string excitation was at one tenth of its length from the bridge. This results in every tenth partial having very low amplitude to the point where it can be considered to be noise. The Q value fits deteriorate with frequency, hence the partials do not match up as well towards higher frequency.

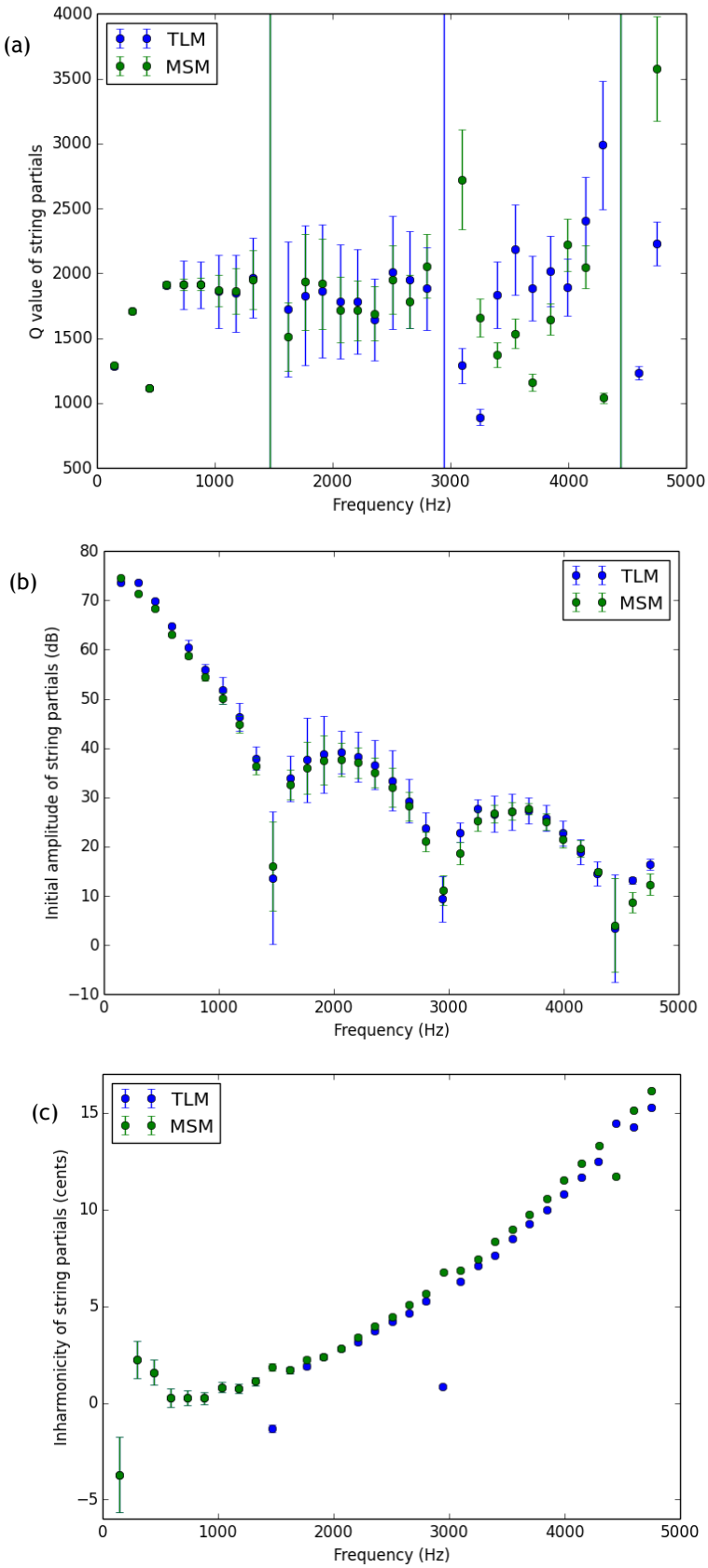

Figure 7.4: Graphs of (a) Q values (b) initial amplitudes and (c) inharmonicities of string partials of the note D_3 generated using the transmission-line model (TLM) and modal superposition model (MSM).

Figure 7.4b shows the initial amplitudes of string partials from both models. These match up very well up to 5 kHz, as do the frequencies in Figure 7.4c, shown as the inharmonicity from the estimated 'true' fundamental. It is obvious that not quite the same dispersion value was used in both synthesis methods; this does not matter at this point. It is unlikely that any difference in tone quality could be heard between these two tones, and so there is no preference in terms of synthesis accuracy.

It seems that both models give similar results for the velocity response from a string pluck, and that the difference between them is not likely to be perceivable. However a choice must be made between them. For the purpose of synthesising tones in an adaptive listening test it is important for the synthesis method to be fast. The fastest method here is the TLM. This is probably because very large matrices must be created for the MSM due to the high number of degrees of freedom. If the requirements of the model were a few string modes coupled to a few body modes then the MSM would perhaps be faster than the TLM. However, there will be as much as 60 string modes and perhaps even more body components, therefore the MSM is likely to be too slow to use in listening tests.

7.2 Coupling the instrument to the surrounding air

A simple derivation of the sound pressure from a monopole source was given in Section 2.4 along with the expression for a dipole sources derived by Hill et. al. (2004). The reader is advised to see the paper by Hill et. al. for further details of the reconstruction of the monopole and dipole sound-field. The sound pressure is specified in spherical polar coordinates $p(r, \theta, \varphi)$ for a given excitation force F. Using spherical-harmonic decomposition on the measured sound-field of the instrument allows separation of the sound-field into monopole and dipole contributions. Higher multi-pole sources are excluded due to their negligible contribution to the overall sound pressure. The monopole and dipole contribution of each mode is given by the source strengths: G_{00} for monopoles and G_{1x}, G_{1y}, and G_{1z} for dipoles (simply named S_ω and D_ω in Chapter 2). The pressure at a point in space due to a single radiating mode is then found by firstly getting rid of the time dependence in the finite-sized monopole expression, Equation (2.9). Then the sum of the monopole and dipole contributions is taken and multiplied by $F\,Y(\omega)$ to yield

$$p(\omega) = -\frac{i\rho_0 \omega F}{4\pi r} Y(\omega) e^{ikr} \left[G_{00} \frac{e^{-ika_0}}{1 - ika_0} + \left(\frac{1}{r} - ik\right)\left(\frac{2e^{-ikd_0}}{2 - 2ikd_0 - k^2 d_0^2}\right)\left(G_{1x} \sin\theta \cos\varphi + G_{1y} \sin\theta \sin\varphi + G_{1z} \cos\theta\right)\right], \tag{7.25}$$

where the monopole source size, a_0, and dipole source size, d_0, are assumed to be the same with a value of 50 mm (Hill et al. 2004). The above equation is then summed over all modes of interest.

The problem of coupling the three sub-systems (string, body and surrounding air) now becomes apparent. The transfer admittance calculation requires the load to include all body modes to be summed, whilst the radiation calculation requires the response of each mode to be calculated one at a time. However, dividing Equation (7.25) by Equation (7.5), both summed over all body modes of interest, gives the sound pressure per unit velocity at the bridge. A good approximation to the transfer function, $H(\omega)$, representing the sound pressure response at a given point in space from a force applied to the string at the plucking point, is then given by

$$H(\omega) = \frac{p(\omega)}{Y(\omega)} Y_T. \tag{7.26}$$

Finally, the inverse Fourier transform of $H(\omega)$ gives the time-domain radiated sound signal generated by a delta-function force. For a string released from a stable equilibrium, i.e. a step force function, $H(\omega)$ is by multiplied by $1/\omega$ prior to the Fourier transform.

7.3 Modelling the sound pressure response of a classical guitar

The overall goal here is to model the sound pressure response of a classical guitar up to 5 kHz. Only one string position is modelled and a single string polarisation is used.

The first part of this section describes the type of measurements that were necessary to obtain data for the modelling process. The latter part of this section demonstrates the modelling procedure showing the accuracy of the model at various stages.

7.3.1 Data from measurements

There are a number of measurements needed in order to obtain an accurate model of the sound pressure from a classical guitar. These include calibrated input admittance and sound pressure responses, a full sound-field measurement and the velocity and sound pressure response to a wire-break of the string. A detailed description of the apparatus and method is not given here because the measurements were mostly carried out by another PhD student, Ian Perry. However, a brief account was given in Section 3.6.

Guitar BR2 was chosen to be modelled because the mechanical and acoustic properties of this instrument have been investigated extensively in the past. The apparatus for all the above-mentioned measurements was calibrated by Ian Perry. All the measurements took place in a anechoic chamber, which is not strictly necessary for the input admittance measurement. What is necessary is that the instrument was under the same conditions for each measurement. The reason for this is that changes in the supports or restraints of the instrument or humidity in the room could influence the vibrational behaviour of the instrument making the modelling procedure much more difficult. Therefore the input admittance and sound pressure response were taken at the same time, and the velocity and sound pressure response from a wire-break excitation were taken at the same time, all four of these measurements were taken within ten minutes of each other with the instrument under the same conditions throughout.

The admittance and sound pressure results were averaged over five measurements. The averaging process gave poor results for the wire-break measurements so they were not averaged. The reason for the poor averaging result is likely to be due to slightly different plucking conditions for each wire-break. An effort was made to pluck at the same location on the string and at the same angle away from the instrument, but small variations, such as the wire getting stuck in the windings of the string, can lead to slight changes in the recorded signal that results in poor averaging.

The string was plucked one-tenth of the length of the string from the nut rather than the bridge. This was done to avoid the string hitting the fretboard creating what is sometimes called ‘fret-buzz’. Plucking near the nut of the guitar also prevents the plucking force being applied at the bottom of the instrument where the minimum amount of restraints as possible is used.

The guitar was suspended by rubber bands, a thin piece of string was tied around the body across the centre of the lower bout; this is not ideal as it will affect the vibration of the body but the instrument had to be held firmly in place to resist

the pulling involved with the wire-break measurement. The strings were damped using a cloth, apart from during the wire-break measurements of course in which case all strings apart from one were damped. Only one string position was chosen for the modelling process, which was the open fifth string. The reason for this choice is because the admittance measured at the termination point of this string on the bridge gives a good average level for the admittance at each string position, it is also assumed to give a similar average level of the sound pressure.

The sound-field measurement and subsequent spherical-harmonic decomposition was done as part of Ian Perry's doctorate work. This means that the sound-field data was not tailored for this work and compromises had to be made. The measurement was done in the range 0-2 kHz, therefore not covering the whole frequency range of interest here. Also the striking position of the impact hammer was at a different position from the other measurements taken here. The sound-field data was taken with the striking position at the top E string, whereas here the striking position was chosen to be at the A string. Nevertheless, the full range was not absolutely necessary and is it assumed that the difference in striking position would not yield a substantial difference in the spherical-harmonic decomposition results.

7.3.2 Modelling procedure

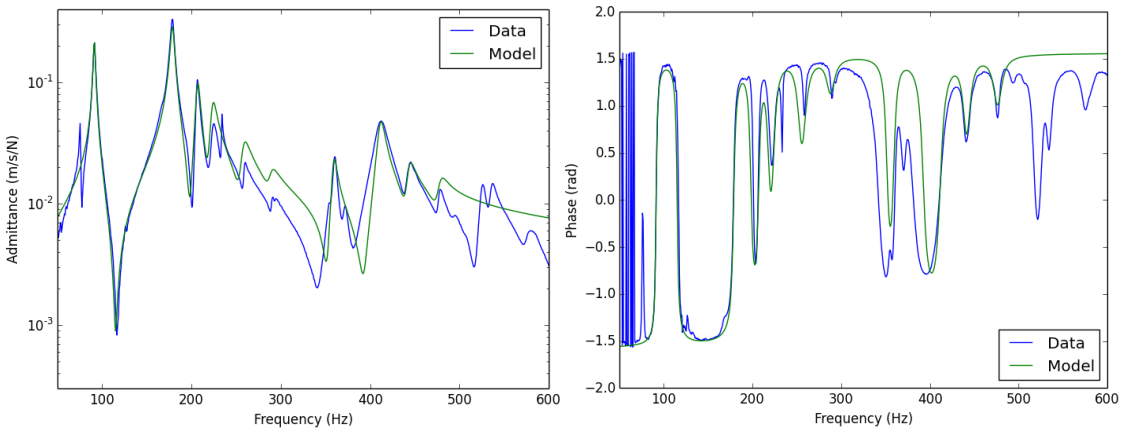

Figure 7.5: Magnitude (left) and phase (right) of admittance fit of modes up to 500 Hz.

The modelling procedure starts by modelling the input admittance. Here the admittance was modelled up to 500 Hz using the simple peak-picking method. This range includes the important low-order modes and so it is important to model the modes in this range accurately. The magnitude and phase of the admittance fits are shown in Figure 7.5. Some peaks were ignored; this is because their absence improved the fit of the velocity response from the TLM to a wire-break

measurement. Also note that this is not the best possible fit to the admittance, compromises were made at several points in the modelling procedure as the final pressure response was the most important fit.

The velocity response from a wire-break pluck of the fifth string was then compared with the TLM model up to 500 Hz to check for consistency, this is shown in Figure 7.6. The spectrum of the synthesised tone has been shifted 10 Hz to the right to see each curve more clearly. It is clear that all of the peaks do not match up; in particular the fundamental string component is much weaker in the model than in the measurement. Later findings showed that the fundamental was over-estimated in the modelled pressure response therefore the weak fundamental here was ignored.

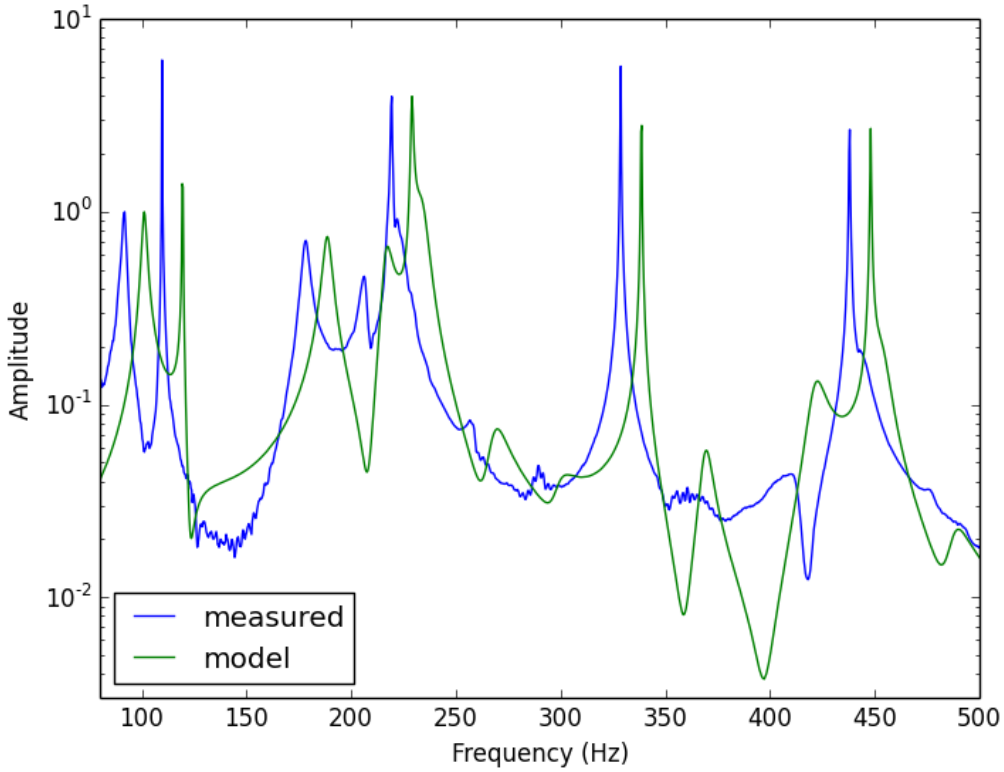

Figure 7.6: Comparing the velocity response from a wire-break for string 5 of guitar BR2 with result from the TLM. Both curves are normalised to the height of the first peak, the model has been shifted 10 Hz to the right.

The next step was to model the sound pressure of the monopole and three orthogonal dipole components using the sound-field data post-SHD. As mentioned previously, this is a necessary step as modelling the sound pressure accurately using monopoles and dipoles is nearly impossible without the sound-field data.

The monopole fit and three dipole fits are shown in Figure 7.7. One of the reasons that this step is so difficult is that each of the four parameters for a single mode can be either positive or negative. Using the same convention as Hill et al., the

polarity of the most strongly-radiating mode, the $T(1,1)_2$ mode, is assumed positive and the polarities of other modes are then set to give the correct relative phases.

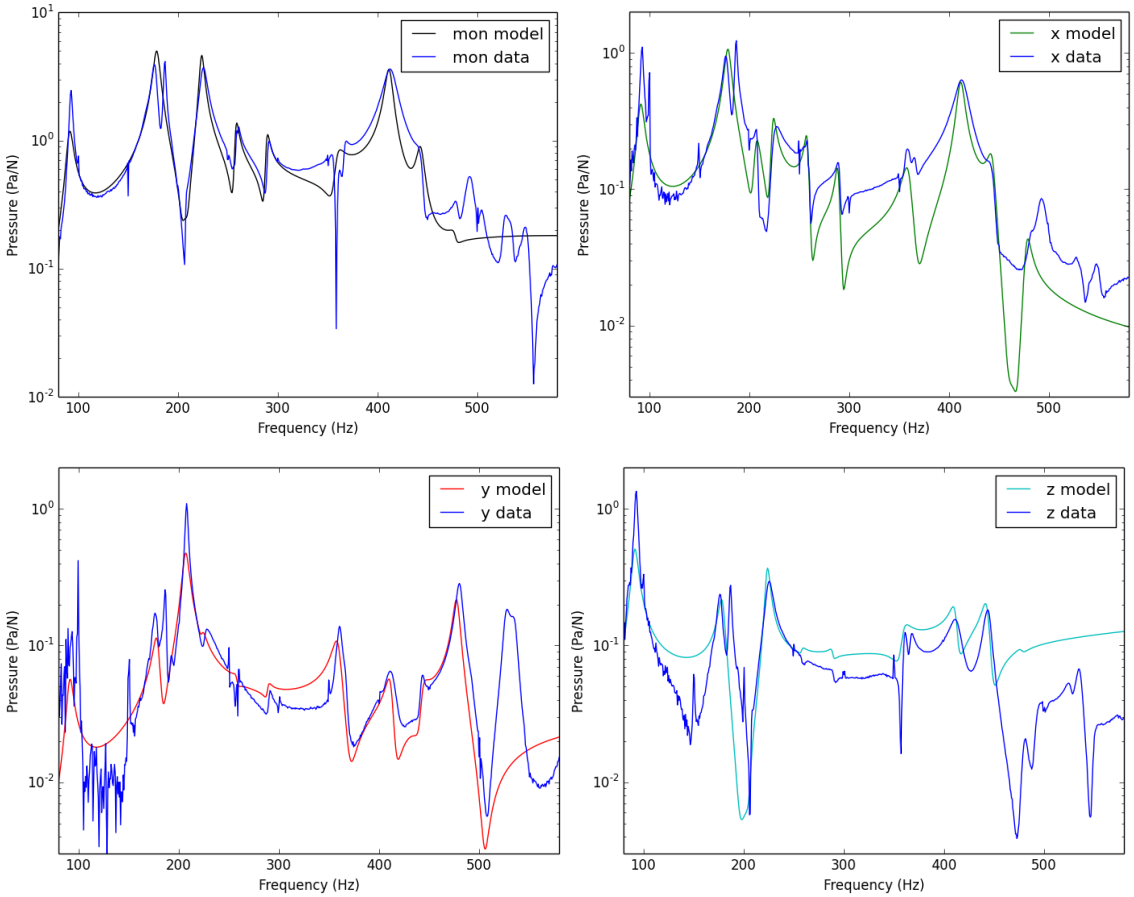

Figure 7.7: Individual fits of the monopole component and three orthogonal dipole components. This is made possible from a SHD calculation on the sound-field of the instrument.

Note that Hill et al. determined these parameters from the calculated spherical harmonics, whereas here the parameters were fitted by trial and error. The quality of fit shown by Hill et al. is therefore better but not by a substantial amount.

The first mode of the guitar, associated with the Helmholtz resonance of the cavity, is of opposite polarity to the $T(1,1)_2$. This is because the $T(1,1)_1$ mode radiates most of its sound through the sound-hole and the $T(1,1)_2$ radiates sound from the lower bout of the soundboard. At the instant when the strings apply a downward force on the bridge, the $T(1,1)_1$ is radiating sound as air rushes out through the sound-hole, but at the same time the $T(1,1)_2$ mode is not pushing the air outside the instrument, hence the two modes are of opposite polarity. In fact, the radiation from the $T(1,1)_1$ has been shown to have a strong dipole moment, again, this is because when a downward force is applied on the bridge, air will rush out of the sound-hole (Weinreich 1985).

Using Equation (7.25) the sound pressure response is then reconstructed and compared with the measurement; this is shown in Figure 7.8. There are a number of

possible reasons why there is discrepancy between measurement and model here. One reason could be the fact that the monopole and dipole parameters were fitted to measurements made with the impact hammer exciting a different position along the bridge to the sound pressure measurement. Also, the two measurements were made on different days, so changes in humidity could lead to changes in the pressure response of the instrument.

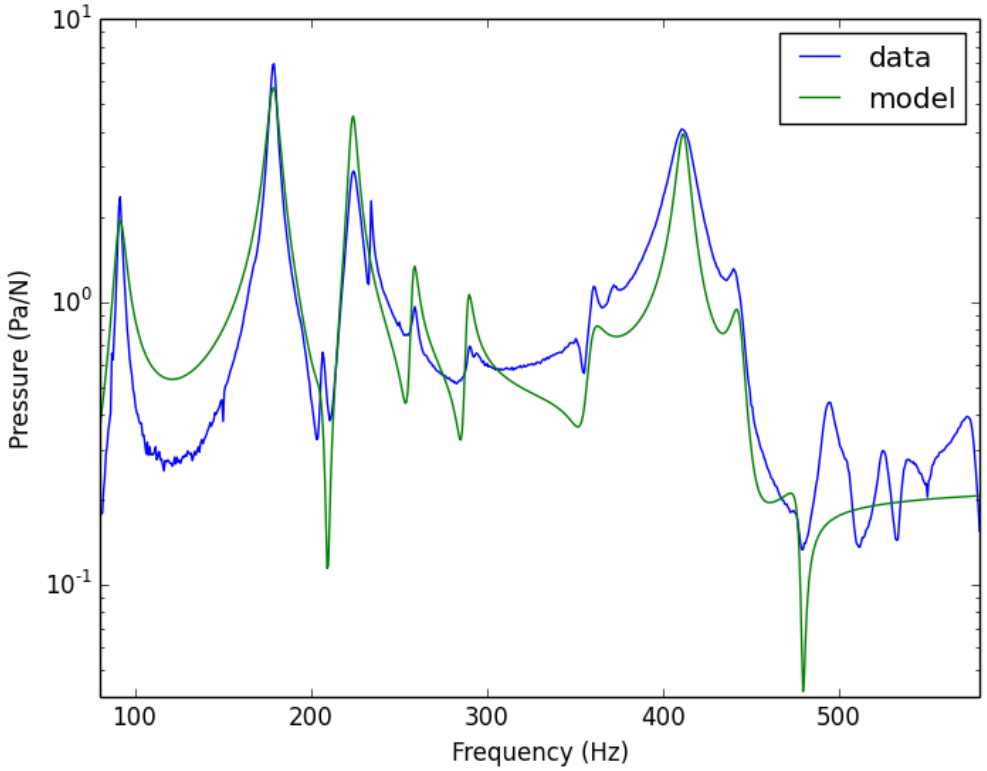

Figure 7.8: Sound pressure of guitar BR2 along with the modelled sound pressure using Equation (7.25).

Finally, the sound pressure response from a wire-break excitation of the string is compared with the model up to 500 Hz, this comparison is shown in Figure 7.9.

It is clear to see that the fit to the string partials are better than the body components of the radiated sound. Compromises were made to try and rectify this. Note that in the pressure response curve in Figure 7.8, the amplitude of the first two peaks and the peaks at about 350 and 400 Hz are underestimated. These peaks are overestimated in the sound pressure response from a wire-break in Figure 7.9. The reason for this cannot be explained here. It is possible that the model of the sound pressure might improve with adjusting other parameters in the model, such as monopole and dipole source sizes. However, it is unlikely that these parameters would have enough influence over such a small frequency range as the results shown so far.

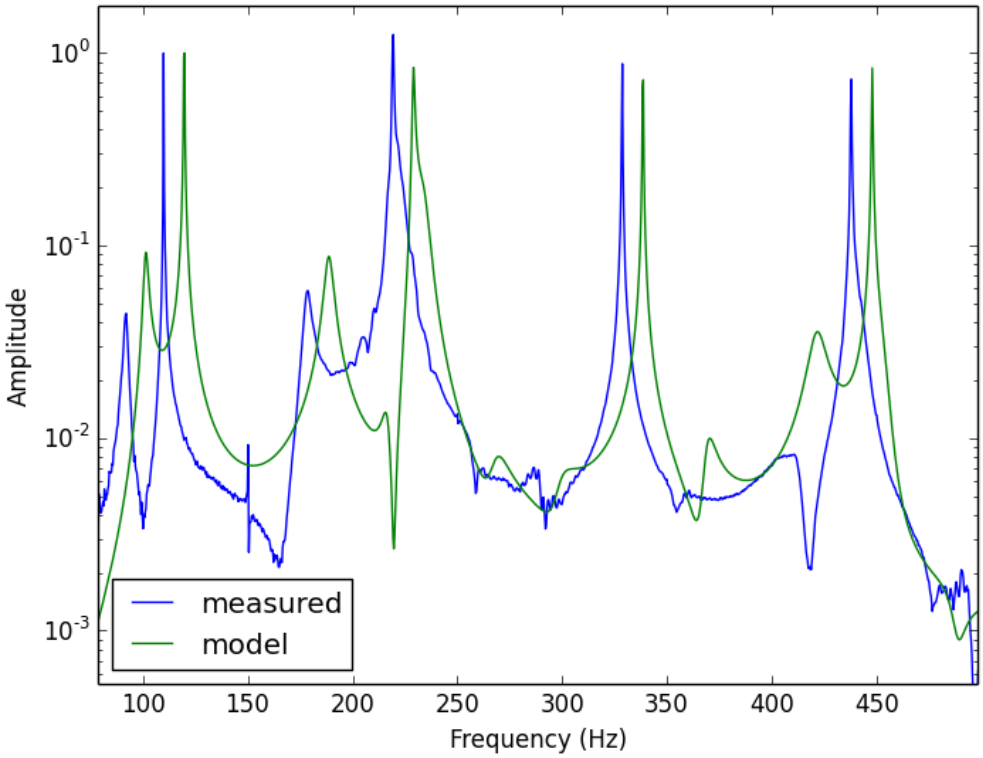

Figure 7.9: FFT of sound pressure due to a wire-break of the fifth string of guitar BR2 along with result from TLM (shifted 10 Hz to the right). Both curves are normalised to the fundamental.

7.4 Extending the model

As stated previously, it is important to obtain the most accurate model as possible for the pressure response from an instrument for the use of psychoacoustical tests. Including higher-order modes, along with their sound-pressure source strengths, opens the opportunity to extend the model and achieve a more accurate synthesis of an instrument. This means that certain listening tests can be designed that have not been carried out previously. It is therefore important to develop the model as far as possible whilst retaining comparable accuracy to measurement.

Weinreich introduced the idea of adding modes above the frequency where modal overlap occurs in order to make the synthesised sound of a violin more credible (Weinreich 1993) . There was no intention of fitting the mechanical response accurately; he added modes that were nearly equally spaced in frequency and used randomly generated numbers according to some set of statistics to set the modal parameters. He called it a fictitious instrument. Woodhouse went on to carry out this method in more detail and applied it to the guitar, calling it a ‘statistical guitar’. He

then used the statistical guitar to carry out listening tests on some of the string and body parameters (Woodhouse et al. 2012). Note that the model used by Woodhouse included a very simple method of modelling the radiation properties of the instrument. The modelling method here is similar but with a far more detailed method of modelling the radiation properties of the instrument. Here the classical guitar is modelled up to 5 kHz and includes both monopole and dipole source contributions.

7.4.1 Fitting the mechanical response

Modal density for a guitar body should include modes of the soundboard, air cavity and back-plate, although the latter two tend to be very weak with increasing frequency. Therefore, as Weinreich (1995) suggested, it is sufficient to treat it as a single plate having constant modal spacing.

Woodhouse (2004b) generated modal frequencies in the following way to obtain the acceleration response from his 'statistical' guitar. Firstly the number of peaks in a given range is counted and the average modal spacing is calculated, which Woodhouse found to be 38 Hz on his guitar. Then he applied the following equation, $\Delta f = 38(2/\pi)\sqrt{r_1^2 + r_2^2}$, where $r_1$and r_2 are randomly chosen numbers from a Gaussian distribution with a mean of zero and standard deviation of one. For the guitar modelled here, BR2, the average modal spacing up to 2 kHz was found to be 40 Hz, therefore the modal frequencies in the model were generated using this equation,

$$\Delta f = 40\,\frac{2}{\pi}\sqrt{r_1^2 + r_2^2}\,, \tag{7.27}$$

where $r_1$and r_2 are randomly chosen numbers from a Gaussian distribution with mean of zero and standard deviation of one.

The modes were then split into bands corresponding to the frequencies where the general shape of the input admittance changed (this will become clearer shortly). The frequency bands, along with the ranges of the uniform distributions used to generate modal parameters, are listed in Table 7.1.

The Q values were calculated using randomly chosen numbers from uniform distributions. The limits of the distributions were the same as Woodhouse (2004b), which are similar to those measured in 15 guitars in a later paper by Woodhouse (2012). The limits of band 4 were decreased slightly because the peaks in this range were initially judged to be too sharp (see Table 7.1).

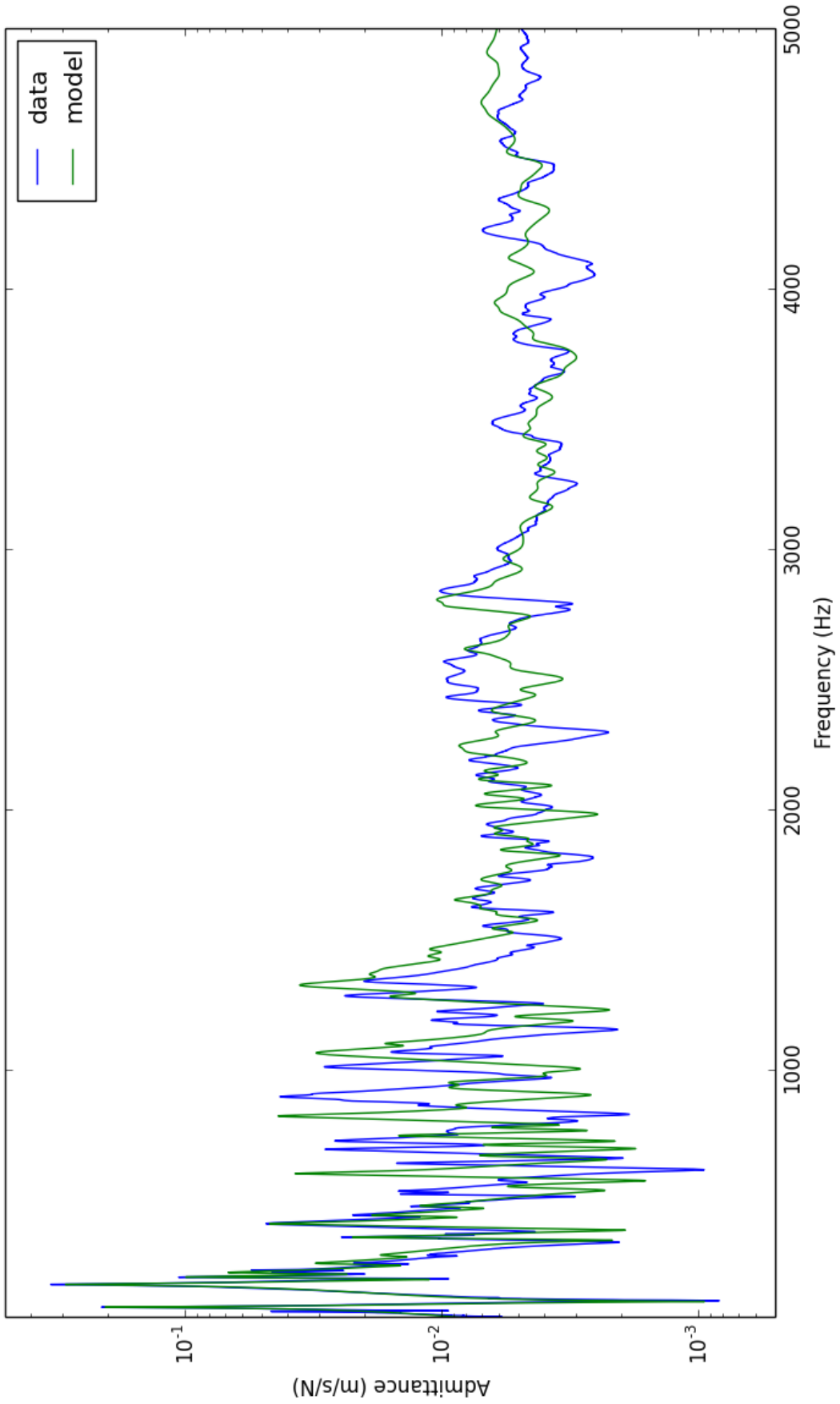

Figure 7.10: Input admittance of guitar BR2 along with the admittance of the statistical guitar. This is shown on a linear frequency scale because the low-frequency fit was shown in Figure 7.5.

The final part of the jigsaw in modelling the admittance was to model the effective masses. These were adjusted until the level of the modelled response matches that of the data. The limits of the uniform distributions used are also shown in Table 7.1. Note that, from a theoretical point of view, the minimum that the effective mass can be is half of the combined mass of the soundboard and bridge, which makes the lower boundary for Band 4 seem a bit high. However, towards higher-frequencies nodal lines get closer together and so the measurement position is more likely to be nearer a nodal line resulting in increasing effective masses.

The magnitude of the complex input admittance of guitar BR2 is plotted up to 5 kHz in Figure 7.10, along with the admittance of the 'statistical guitar'. This is shown on a linear frequency scale because the low-frequency fit was shown in Figure 7.5. The phase of the admittance is not shown here because it is not particularly useful in this case. From inspection of this graph it is obvious to see the reasons for splitting up the curve into certain bands for the fitting process. A clear change can be seen between the limits of the bands 0-500 Hz, 500-1500 Hz, 1.5-3 kHz and 3-5 kHz.

	Band 2 (0.5-1.5 kHz)	Band 3 (1.5-3 kHz)	Band 4 (3-5 kHz)
Q value	30-80	30-80	25-75
Effective mass (kg)	0.13-3	0.7-3.4	1.2-4
Monopole (m^2)	±0.04	±0.012	±0.01
Dipole x (m^3)	±0.002	±0.0015	±0.0013
Dipole y (m^3)	±0.002	±0.0015	±0.0013
Dipole z (m^3)	±0.002	±0.0015	±0.0013

Table 7.1: Limits of uniform random number distributions chosen for modal parameters of the 'statistical guitar'. Note that Band 1 includes modes from 0-500 Hz that were fitted more in a more accurate manner.

7.4.2 Fitting the pressure response

As mentioned in Chapter 2, the theory of a point source radiating sound as monopoles and dipoles should not be applied when the wavelength of the radiated sound is larger than the source size. Although this limiting condition is relaxed by changing the source to a finite-sized source, it is unlikely that this change extends the frequency range up to 5 kHz for the guitar. However, as will be shown in this section, applying spherical-harmonic decomposition to the sound-field from a guitar results in curves representing the monopole and dipole sound pressure responses of

the guitar. Modelling these response curves as monopole and dipole radiation from a finite-size source and combining them using Equation (7.25) yields the modelled sound pressure, which fits the measured sound pressure from the instrument reasonably well. Therefore this shows that the sound pressure response from a guitar can be modelled to a good approximation as the sum of monopole and dipole sources of finite size.

The exact values and polarity of each source strength component above 500 Hz is assumed to be less important, therefore randomly chosen numbers from uniform distributions were used to estimate these values. The overall contribution of each parameter was plotted on top of the spherical-harmonic decomposition data and the limits of the distributions were adjusted to give reasonable results. Note there is equal probability for each parameter to be positive or negative.

As mentioned previously, the SHD data only went up to 2 kHz, therefore the individual components from the spherical-harmonic decomposition data were extrapolated up to 5 kHz. Then a reasonable fit to the sound pressure up to this range was reached by adjusting the limits of the uniform distributions of Bands 2 and 3 to what is shown in Table 7.1.

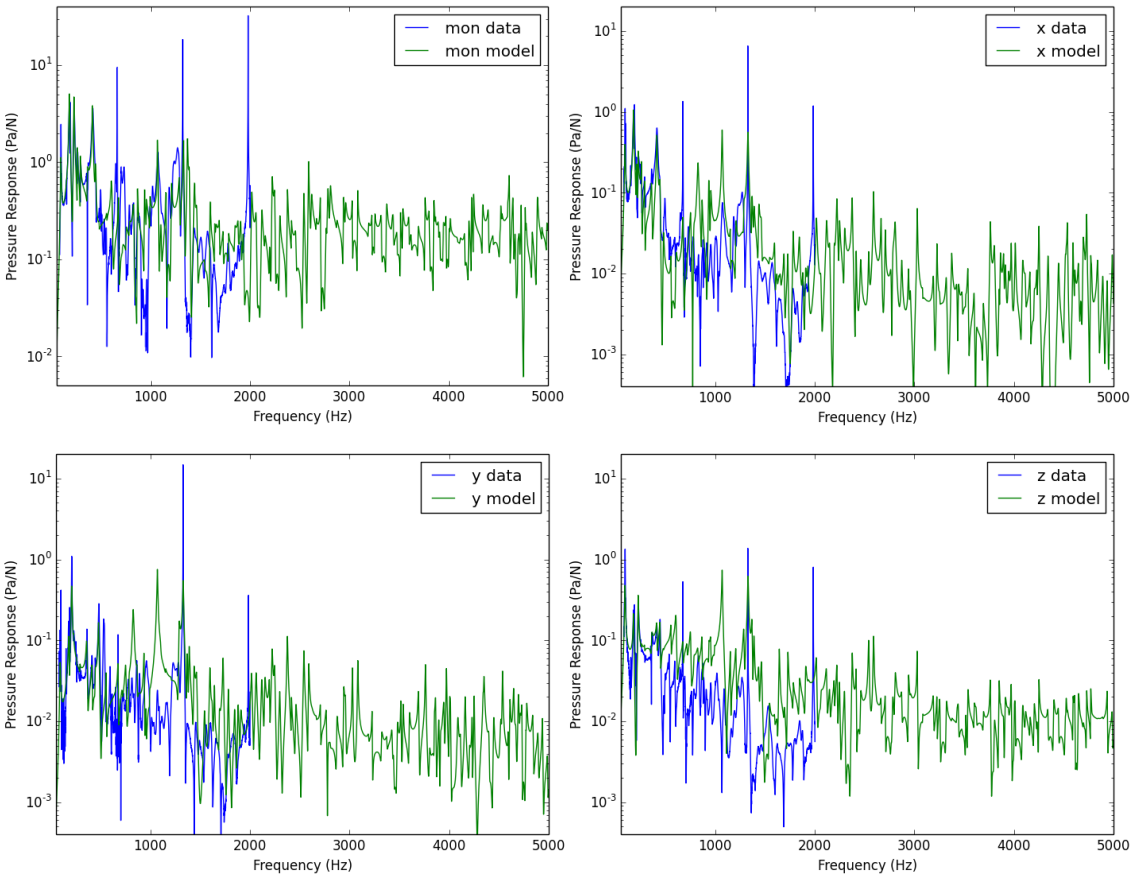

Figure 7.11: Monopole and three dipole pressure response curves for guitar BR2. The measured data only goes up to 2 kHz so an estimate was made for the response between 2-5 kHz.

Some considerable time was spent on adjusting the parameters of the individual dipole source strengths without achieving an acceptable fit. At this point a decision was made to look elsewhere in the model for possible reasons why the model did not fit the spherical harmonic decomposition curves. The problem was towards higher frequencies, the base level of the curves would increase so that the response was at a higher level at 1.5 kHz than the level at 200 Hz, where the most strongly radiating modes are. Closer inspection of Equation (7.25) shows that towards higher frequencies, and therefore larger k values, the term $k^2 d_0^2$ tends to dominate the magnitude of the dipole pressure response. Therefore the dipole source size, d_0, was increased in order to get the base level to decrease towards higher frequencies rather than increase. A size of 150 mm gave a suitable fit to the data. In turn this affected the total sound pressure so that the base level of the model was below that of the measurement. Therefore the monopole source size, a_0, was decreased to a value of 10 mm as to raise the base level of the sound pressure at higher frequencies. Following the discussion of Hill et al. (2004), a better fit might be achieved by setting individual source radii so that they are frequency dependent. This might be a promising avenue for future work.

The individual monopole and three dipole sound pressure responses are shown in Figure 7.11 along with fits using the corresponding terms of Equation (7.25). The first things to note are the large peaks in the data at multiples of 660 Hz. This is due to the spherical harmonic decomposition calculation breaking down at frequencies corresponding to when multiples of half-wavelengths of the sound are equal to the distance between the two microphones used for the measurement. Assuming the speed of sound in air to be 343 m/s, the microphone separation works out to be 26 cm; this is consistent with the positioning of the two microphones in the anechoic chamber. The reader should ignore these peaks as they do not represent anything real about the pressure response.

The graphs in Figure 7.11 show a reasonable fit up to 2 kHz, although perhaps frequency dependent source radii would yield a more accurate base level for these responses, or at least, a different source radius for each dipole direction. Also the accuracy of the higher-frequency end of the model would obviously be improved greatly having data up to 5 kHz.

The individual radiation components were then summed using Equation (7.25) to get the total sound pressure response of the instrument, as is shown in Figure 7.12. Perhaps the base level of the sound pressure response is a little low at some points but increasing the base level of the individual components would give poorer fits to the individual responses shown in Figure 7.11.

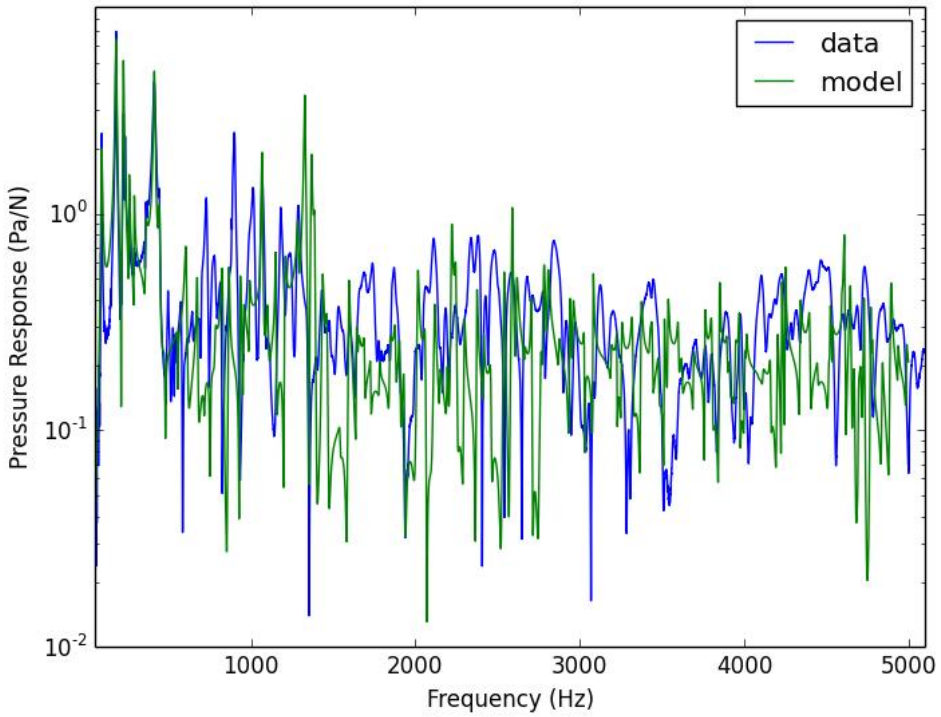

Figure 7.12: Measured pressure response of guitar BR2 along with the modelled pressure response.

The final stage to the modelling process was to generate a guitar tone from the TLM and compare it with the measured sound pressure response from a wire-break excitation of the open fifth string. An FFT of the sound pressure from a wire-break is shown in Figure 7.13 along with the result from the TLM.

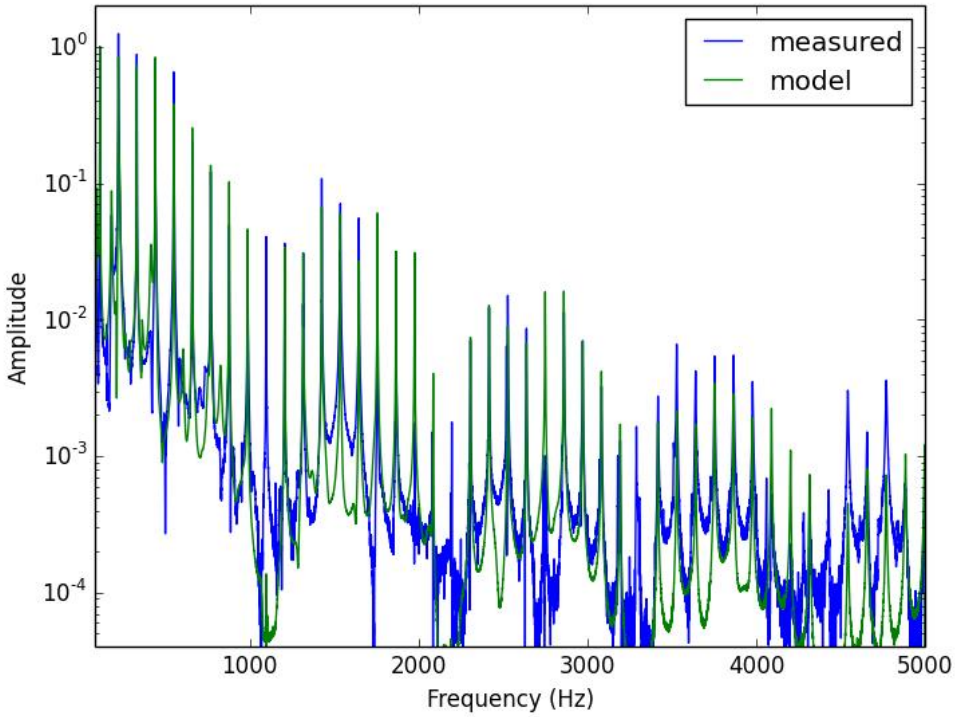

Figure 7.13: FFT of the radiated sound from a wire-break excitation of the fifth string of guitar BR2, along with the sound pressure response from the TLM. Both curves are normalised to the fundamental.

This graph shows good agreement between measurement and model. Yet it is difficult to determine the accuracy of the model by comparing just FFTs of the radiated sound. Therefore the parameters of the string partials were extracted from the measured radiated sound and modelled sound pressure response using the STFFT method described in Chapter 3. This gives a much clearer analysis of the accuracy of the model. A comparison of the parameters of the string partials between a measured wire-break and synthesised tone using the model is shown in Figure 7.14. Note that the data points corresponding to every tenth partial have been omitted because the plucking position was one tenth the length of the string and so these components are poorly represented.

The general trends of the initial amplitudes agree well between measurement and model. However, there is a relatively poor agreement at low frequencies. Perhaps this could have been improved by spending more time on making small adjustments to the model, but it is likely that this would compromise the fit to the input admittance or pressure response. Considering results presented in Section 5.4, it is likely that there is a perceivable difference between initial amplitudes of the measured radiated sound and synthesised tone because of the poor fit of the fundamental.

The general trend of the Q values is not quite as good as the fit of the initial amplitudes, but a good match between measurement and model is not as important here as was demonstrated in Section 5.4. The discrepancy in Q values could be the result of only including one string polarisation in the model. It is difficult to assess whether there is a perceivable difference in the decays of the partials because one set of data is not consistently greater than the other. The average Q values are 1985 for the measured tone and 2300 for the synthesised tone, which is 16% greater. This is not likely to be a perceivable difference.

The general trend of the inharmonicity of string partials show a decent fit, which is expected, because the value of the dispersion of the string in the model was determined using this method. The fundamental shows a very good fit, but the second partial does not. This suggests that the frequency and effective mass of the $T(1,1)_1$ mode was accurately fitted, therefore perturbing the frequency of the fundamental, but these parameters were not so well fitted for the modes surrounding the second partial around 220Hz. Although the difference in inharmonicity between the second partials looks large here it is actually only 0.3 Hz, which is 13 times smaller than the JND quoted in the literature (Moore et al. 1985). Therefore it is unlikely that the difference in inharmonicity of the string partials of the measured tone and synthesised tone are perceivable.

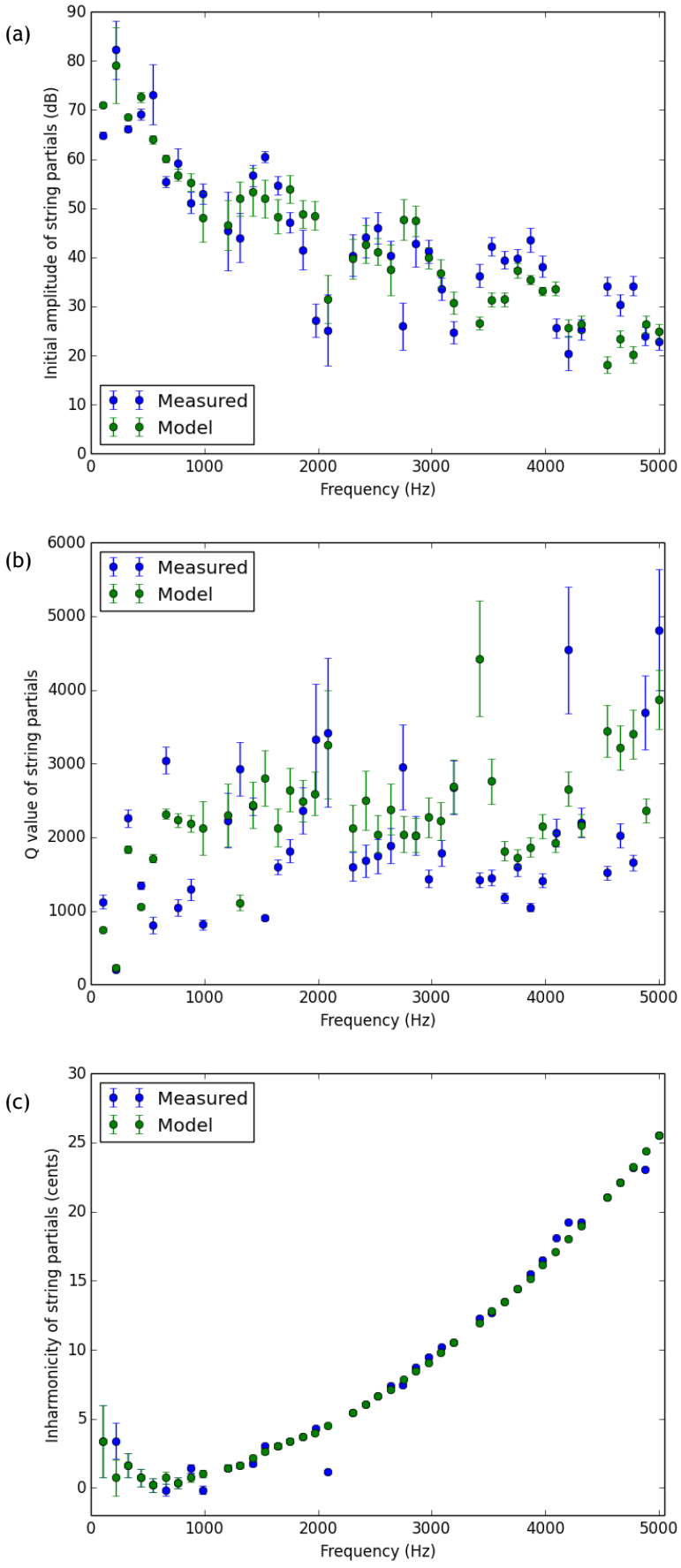

Figure 7.14: Comparing the difference in a) initial amplitude b) Q value and c) inharmonicity of string partials between measured wire-break and TLM guitar tone.

Thus, after comparing the parameters of the string partials, it seems that only a small perceivable difference lies between the measured radiated sound and synthesised tone. This difference is due to the initial amplitude of the fundamental. Although it is possible to go back and make small adjustments to the model to try and rectify this problem, it is not completely clear at what stage it would be best to intervene. It is therefore best to make do with an overly-strong fundamental in the low-range of the statistical guitar.

7.5 Modelling other plucked-string instruments

Differences in the radiated sound and mechanical response of the bodies of a classical guitar, folk guitar and banjo were discussed in Chapter 4, along with a comparison between modal parameters of their low-order modes. A further interesting point that aids in confirming previous suppositions is to apply modelling techniques used previously for the classical guitar to the folk guitar and banjo. The hope is that doing this will uncover key features in the vibrational behaviour of these instruments that are essential to perceptually accurate modelling.

The modelling procedure for these two instruments is the same as that for guitar BR2 described in Section 7.3.2 and Section 7.4.1. This time only the acceleration response of the bridge to a step force function applied to the string was modelled as there was no available sound-field data for these instruments. As mentioned previously, sound-field data is essential when it comes to modelling the sound pressure response of the instrument as monopole and dipole sources. The modelled acceleration was later converted into velocity as it gave a more realistic sound.

7.5.1 Simon and Patrick folk guitar

The admittance at the bridge was measured at the position of the fifth string for the folk guitar and the eight lowest peaks in the admittance were fitted up to 500 Hz. This string was chosen as it is neither at the edge or middle of the bridge, therefore a good candidate for a sort of ‘mean’ admittance along the bridge. A measurement of the velocity response to a wire-break was then used to check the accuracy of the model up to 500 Hz. The admittance was then modelled up to 5 kHz in a similar manner to guitar BR2.

The average modal spacing for the folk guitar up to 2 kHz was found to be 45 Hz and a similar equation to Equation (7.27) was used to determine the resonance frequencies for the body modes. Q values were estimated by initially using the STFFT technique on modes with the highest peaks every 110 Hz up to 5 kHz. This method is likely to yield the maximum Q values as a function of frequency, because the modes with the highest peaks are likely to have the largest Q values, although this depends also on the effective mass of the mode. Similar Q values to the classical guitar were found for the folk guitar as would be expected. Effective masses were estimated, as before, by matching the height of the admittance curve of the model with that of the measurement. The limits of the uniform distributions used to model the input admittance of this instrument are shown in Table 7.2, along with the frequency bands used to split up the response curve. The resulting modelled admittance curve is shown in Figure 7.15 along with the measured admittance for the Simon and Patrick folk guitar.

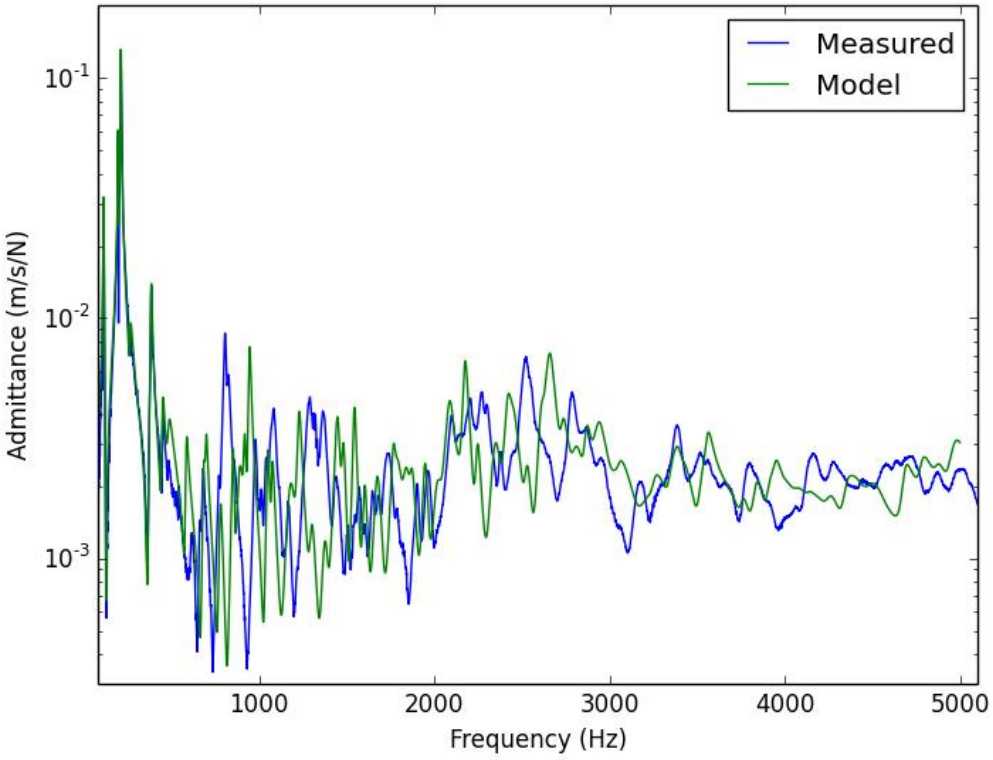

Figure 7.15: Measured and modelled input admittance of Simon and Patrick folk guitar using randomly chosen numbers from uniform distributions to generate modal parameters.

At this point the velocity response to a wire-break up to 5 kHz was compared with the model and string-partial parameters extracted to check the accuracy of the model. It was found that the model gave insufficient strength to higher-order partials and much lower Q values than measured from wire-break measurements. This could be due to overestimated effective masses between 1-4 kHz, but decreasing this

parameter in the stated frequency range led to a deterioration in the fit to the measured admittance response. Therefore the attention was turned towards the string parameters.

The tension and mass per unit length of the string were taken from the D'addario website (D'addario 2015) as for the classical guitar model. The problem was that the frequency-dependent Q value function used to model the classical guitar was not suitable to be used for the steel-string guitar. Therefore, data from previous experiments carried out at Cardiff were used where the vibration of an isolated steel string was recorded from a wire-break excitation. The string was attached to a heavy steel bar with a mounted force transducer. The signal from the force transducer was put through the STFFT program to yield Q values as a function of frequency. An equation for the frequency-dependent Q value of a string from Valette (1995) was then used to fit the measured Q values from the steel bar experiment. This equation has many parameters, therefore it was simplified by grouping terms according to their relation to frequency. The equation then takes the following form,

$$Q(\omega) = \left(\frac{2\pi c_1}{\omega} + \frac{\omega c_2}{2\pi} + c_3\right)^{-1}, \tag{7.28}$$

where c_1, c_2 and c_3 are constants that were estimated to be 4.3 x 10^{-2}, 3.3 x 10^{-12} and 1.1 x 10^{-4} respectively using scipy's least-squares curve-fitting function. The measured Q values and line of best fit are shown in Figure 7.16.

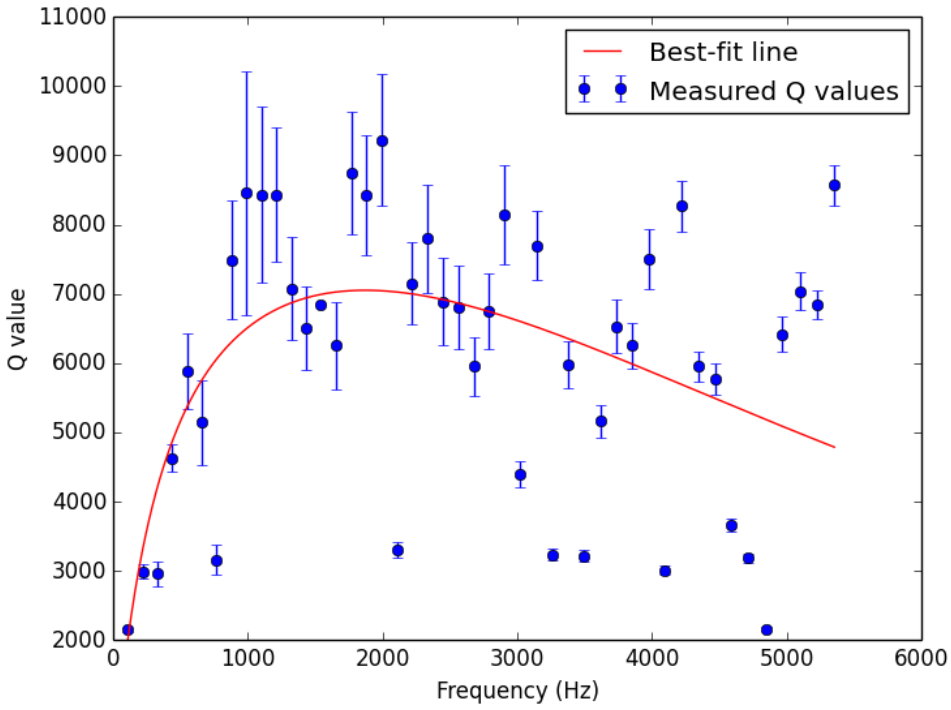

Figure 7.16: Measured Q values for an A_2 steel string attached to a steel bar. The best-fit line was calculated using Equation (7.28) and scipy's least-squares curve fitting function.

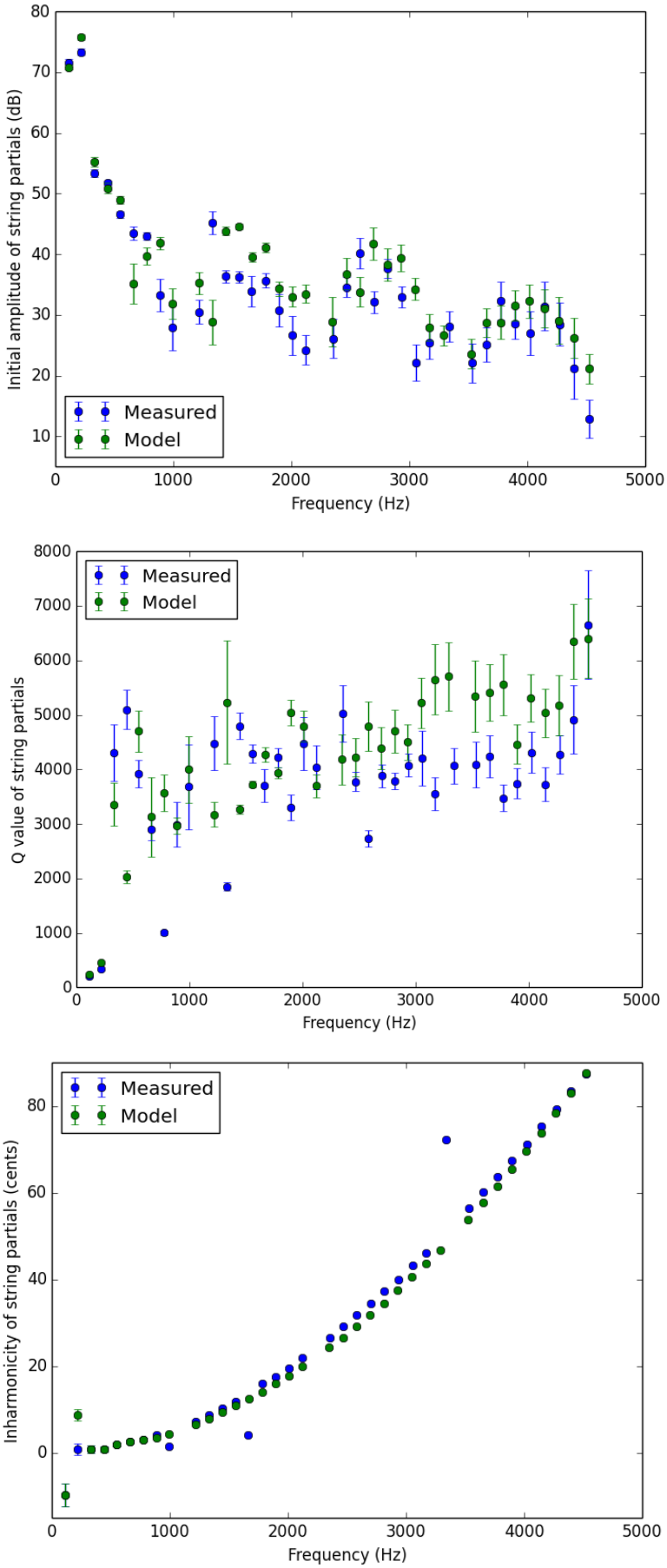

Figure 7.17: Comparing parameters of string partials between measurement and model for Simon and Patrick folk guitar.

Although the fit in Figure 7.16 is not particularly good, using Equation (7.28) with the estimated parameters greatly improved the accuracy of the model. The initial amplitudes, Q values and frequencies of string partials up to 5 kHz were extracted from the velocity response to a wire-break excitation of the note A_2, and from the synthesised tone using the TLM; these are compared in Figure 7.17.

The low-order partials of the synthesised tone fit the measurement well, with a slight discrepancy in the second partial, though not likely to be perceivable. Higher-order partials also show a good fit, which was greatly improved by the string Q value modification discussed above.

7.5.2 Gretsch Broadkaster banjo

The admittance at the bridge of the banjo was measured at its fourth string. Once again, the eight lowest peaks in the admittance were fitted, this time up to 800 Hz. A measurement of the velocity response to a wire-break was then used to check the accuracy of the model up to 800 Hz. The admittance was then modelled up to 5 kHz in a similar manner to the two guitars.

There were two important differences in the modelling procedure when it came to modelling the banjo. First of all the procedure used to calculate modal frequencies could not be applied to the banjo because the head of the banjo is a membrane rather than a plate, giving a modal spacing that decreases with frequency, like $1/\omega$ (Weinreich 1995). To find a reasonable spacing, the frequencies of all peaks up to 5 kHz were measured roughly by eye and a plot of modal spacing against frequency showed the expected relation. A curve was fitted to these points to yield the following equation for the modal frequencies in Hz, indexed i,

$$f_i = \left(\frac{50000}{f_{i-1}} + 10\right)\frac{2}{\pi}\sqrt{r_1^2 + r_2^2}\,, \tag{7.29}$$

where $r_1$and r_2 are randomly chosen numbers from a Gaussian distribution with mean of zero and standard deviation of one.

The second major difference in the case of the banjo was the pattern found for the modal Q values. As shown in Figure 7.18 the Q values follow a trend of roughly a straight line from 0.2-5 kHz, with a region of large variation between 1-3 kHz. This region of large variation was ignored because these vibrations were related to the after-length of the string rather than the banjo-head. The modelled Q values therefore used the line of best fit shown in Figure 7.18, where the intercept was replaced by a randomly chosen number from a normal distribution with mean and standard deviation of 20 (see Table 7.2).

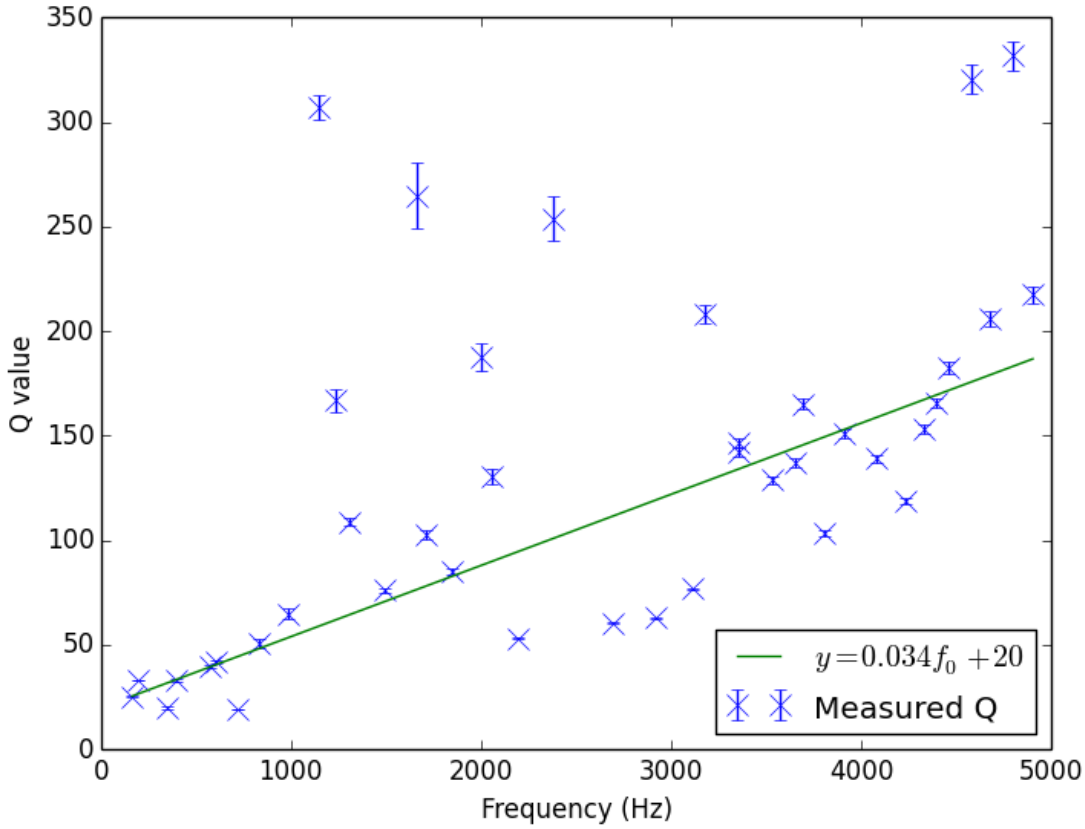

Figure 7.18: Q values of body modes measured at regular intervals (about 120 Hz) from the input admittance of the Gretsch banjo. The line of best fit, judged by eye rather than by least-squares fit, is plotted as the green line.

The input admittance of the banjo along with the modelled admittance response is shown in Figure 7.19. A decent fit was achieved using the above modifications to the modelling procedure, although the Q values around 1.2 kHz look very much underestimated due to the after-length section of the strings being free to vibrate, and Q values above 3.5 kHz look a little overestimated.

The string Q value function used for the classical guitar again gave unsatisfactory results for the banjo model. This time there was no banjo string data available to model the Q values, therefore the same parameters as for the steel guitar string were used.

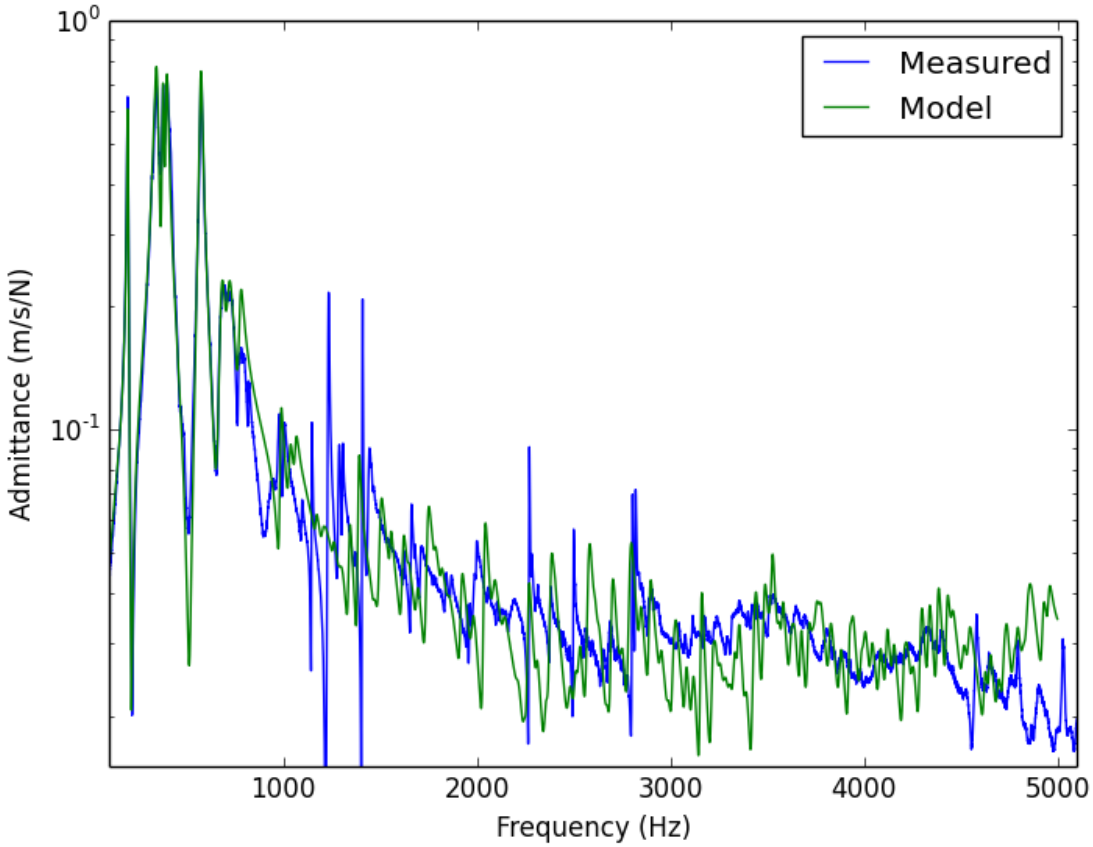

Figure 7.19: Measured and modelled input admittance of Gretsch banjo using randomly chosen numbers from certain distributions to generate modal parameters.

As before, the initial amplitudes, Q values and inharmonicity of string partials from measurement and model were extracted. These are compared in Figure 7.20. The initial amplitudes agree very well for both low- and high-order string partials. The Q values of the low-order partials also agree well, but between 1-3 kHz the measured Q values are about twice the Q values of the synthesised tone. This frequency range matches up with the region of large Q values of the body modes from the admittance measurement shown in Figure 7.18, and can also be seen in the form of sharp peaks in the input admittance in Figure 7.19. This is likely to be the result of the string's after-length interacting with the playing-length of the string. This interaction that was not included in the model and so is not expected to be reproduced in the results. It perhaps would be interesting to find out whether this effect is perceivable, and if so, it should be included in future banjo models.

The inharmonicity fit shown in Figure 7.20c shows that perhaps the string in the model was tuned slightly sharp and there was not enough dispersion in the string.

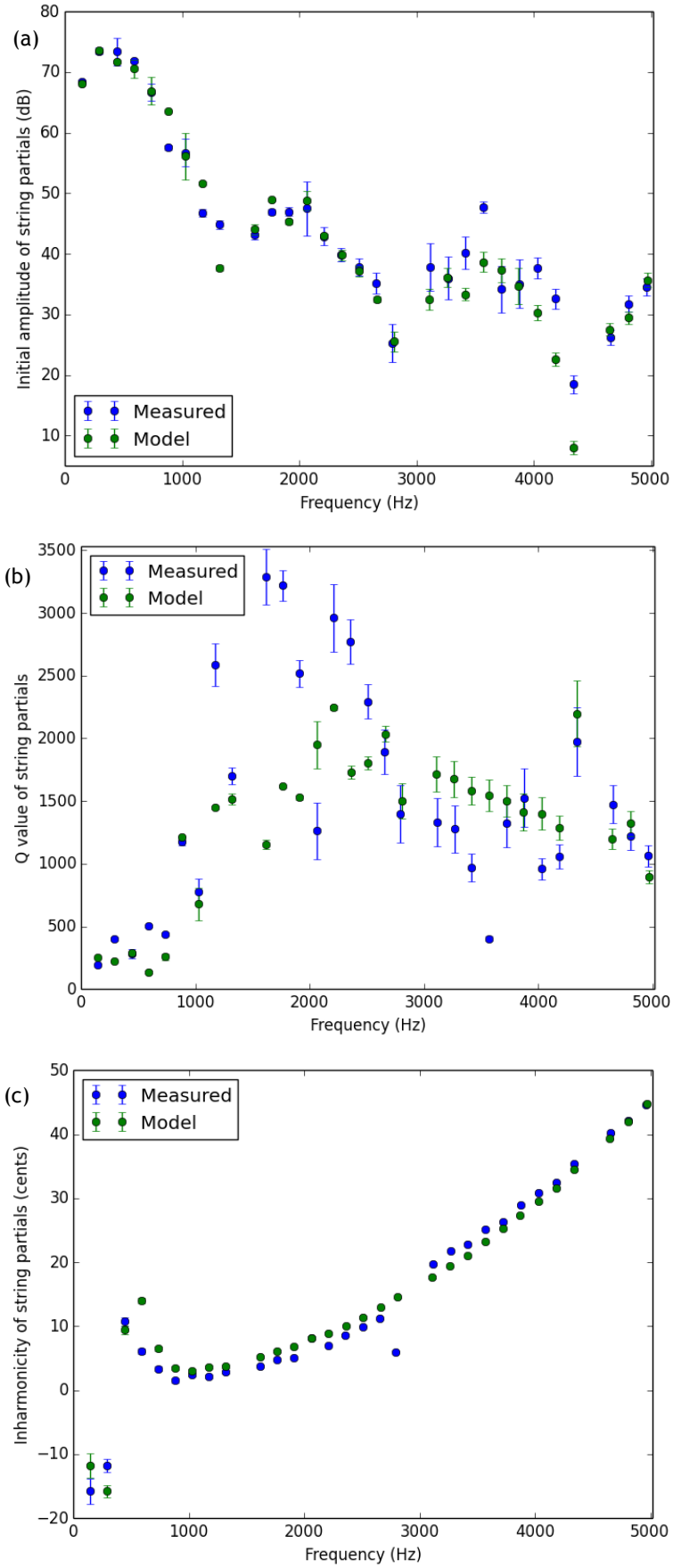

Figure 7.20: (a) Initial amplitudes (b) Q values and (c) inharmonicity plots comparing string partial parameters between measurement and model for Gretsch banjo.

7.5.3 Comparison between instruments

	Folk guitar			Banjo		
	Band 2 0.5-2 kHz	Band 3 2-3 kHz	Band 4 3-5 kHz	Band 2 0.8-1.1 kHz	Band 3 1.1-3 kHz	Band 4 3-5 kHz
Q	20-75	25-75	25-75	0.034 f_0 + r		
M_{eff} (kg)	1.5-6	0.8-3.5	2-6	0.05-0.5	0.04-1	0.3-1.7

Table 7.2: Limits of uniform distributions used to generate modal parameters for modelling the admittance of the Simon and Patrick folk guitar and the Gretsch banjo. Note that the Q value for the banjo were modelled as being proportional to the frequency plus *r*, which is a randomly chosen number from a normal distribution with mean 20 and standard deviation of 20.

The modal parameters of low-order modes for classical guitar BR2, the Simon and Patrick folk guitar and the Gretsch banjo were compared in Section 4.3.5. Measuring these parameters of higher-order modes directly becomes impossible using techniques described in this thesis. However, by modelling the admittance and generating synthesised sounds from these instruments to check the accuracy of the model, it is possible to estimate the modal parameters of higher-order modes.

When comparing modal parameters of these three instruments in different frequency bands it is important to note that the bands are not the same for all instruments. This is because the bands were chosen as to reflect how the admittance of each instrument changed with frequency.

The first thing to note here is the modal spacing of the instruments. The two guitars have a uniform modal spacing whereas in the banjo it decreases with frequency. This is because the head of the banjo is a membrane rather than a plate. The mean modal spacing found in the classical guitar and folk guitar here were 40 and 45 Hz respectively, which is not a significant difference.

The Q values of high-order modes of the two guitars are not significantly different, but the general trend of the Q values of the banjo is different and is proportional to frequency.

The mean effective mass of the high-order modes of the classical guitar increased with frequency, having mean values of 1.57, 2.05 and 2.60 kg in bands 2, 3 and 4. The same is not true for the folk guitar, with mean effective masses of 3.75, 2.15 and 4.00 kg in bands 2, 3 and 4. This dip in effective mass in band 3 could be an important feature of the sound quality of the folk guitar as it would modify the balance between the low and high-frequency partials. The mean effective mass of the banjo does increase with frequency, with values of 0.28, 0.52 and 1.00 kg in bands 2, 3 and 4.

Chapter 8 JND in parameters of a classical guitar model

Using the classical guitar model described in the previous chapter, listening tests were carried out to measure the just noticeable differences (JNDs) in certain parameters of the model. The scope for different tests is huge because there are five parameters per body mode and over 100 modes to choose from, but as mentioned previously, the number of subjects available to take the tests is limited due to resources. Therefore care must be taken here in designing listening tests that play to the strengths of the synthesis model.

In Chapter 1 previous work by Wright (1996) and Woodhouse et. al. (2012) was discussed where, in both cases, a physical model of a classical guitar was used for psychoacoustical work. Wright found that low-order modes are most influential in changing the tone quality of the instrument and that the Q value is the least influential parameter. He also concluded that the effective mass is a global parameter because changes in this parameter causes perceivable changes high above the resonance frequency of the mode, whereas resonance frequency of a mode is local parameter, affecting only notes that are nearby in frequency. It is worth reminding the reader here that Wright's model described the modes of the body up to 700 Hz but no effort was made to model the modes above 700 Hz. In three different listening tests Woodhouse et. al. measured JNDs in frequency of all modes in their model, modes in the range 150-250 Hz and modes in the range 500-1000 Hz, yielding results of 0.92%, 1.87% and 1.53% respectively. They also measured the JND

in Q value of all modes by increasing and decreasing the parameter, yielding results of 19% and 22% respectively.

Considering the above findings and previously published models on the classical guitar it was decided that the first listening experiment here should be on finding the relative significance of monopole and dipole radiation of the instrument. With detailed experiments having been carried out on the frequency and Q value of body modes it was decided that the second experiment here would concern the effective masses of modes. As Wright found the low-order modes more influential than higher-order modes, the second experiment here would compare JNDs of effective masses of low-order to high-order modes, both for low-pitch notes and high-pitch notes on the instrument.

In all tests in this chapter the modification, MOD, is defined as a percentage of the modelled values, MV, such that the parameter value for the modified tone, PV, is $PV = MV(1 + MOD/100)$. Hence a modification of 100 corresponds to doubling the value of the parameter.

8.1 Experiment I: Monopole and dipole source strengths

The aim of the first experiment described in this chapter was to quantify the significance of monopole and dipole contributions to the radiated sound from the instrument. This experiment involved two listening tests; one measured the JND in monopole source strength of all body modes in the guitar model and the other test measured the JND in dipole source strengths of all modes.

For this experiment, eight subjects were recruited to take the two tests. The subjects were third-year undergraduate physics students and therefore not considered to be musicians; where 'musician' is used in the same sense as in other published work (Fritz et. al. 2007). The group were a mix of keen music listeners that played at least one musical instrument to varying standards. All subjects were given a five-minute presentation on the procedure of the test and given the same instructions prior to the test; they were not told what type of modification they were listening for in each test.

The stimulus was a short musical phrase consisting of three different octaves of the note G; G_2, G_3 and G_4 having fundamental frequencies of 98.0, 196.0 and 392.0 Hz respectively. The first two notes were generated using 2^{13} points at a sampling frequency of 11025 Hz, producing 0.74 s of each note. The third note was generated

using 2^{12} points at the same sampling frequency, producing a 0.37 s tone. The three tones were then added together such that the second tone started 0.186 s after the first tone and the third tone started a further 0.186 s after the second tone. The resulting tone was a broken chord with overlapping notes. It was truncated to 0.74 s and a steep exponential decay was added to the last 50 samples of the tone to avoid clicks or pops at the end of the tones. Each stimulus took around 3.2 s to generate.

The tests took place in a quiet room that is sound-insulated. The program for the listening tests ran on a laptop and the stimuli were played through Sennheiser HD 495 headphones.

8.1.1 Results and discussion

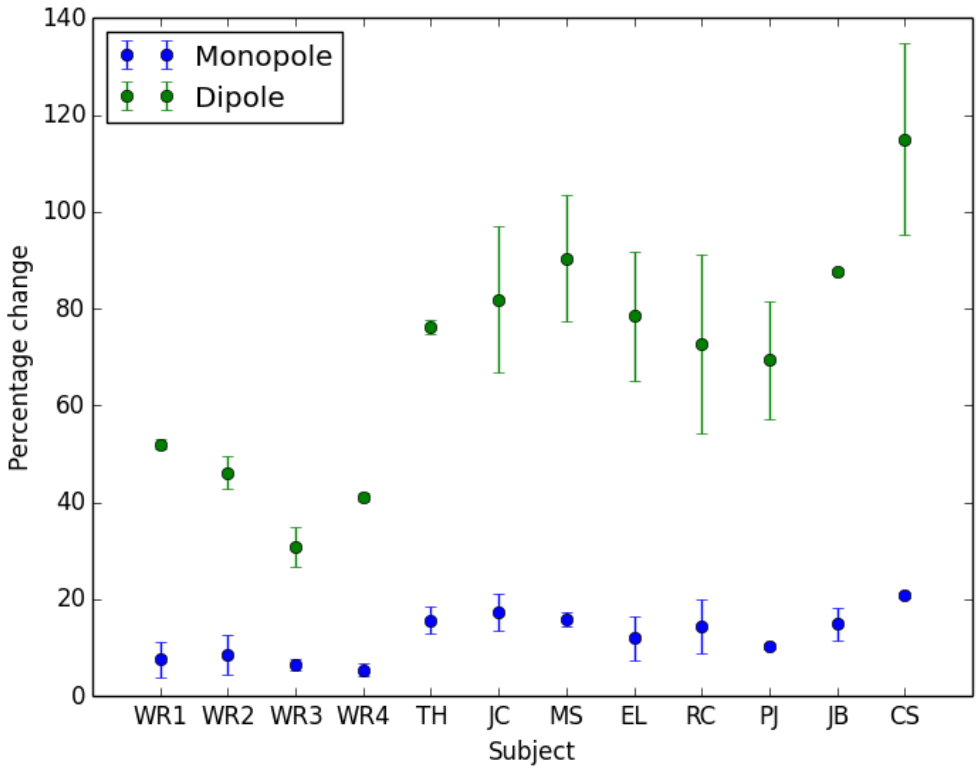

Figure 8.1: Results for eight subjects and the author WR (repeated three times) for the two listening tests discussed in this section. Averages between eight listeners are 15% and 84% for monopole and dipole changes respectively. Averages between my tests are 7% and 43% for monopole and dipole changes respectively. Error bars refer to error in JND measured in each listening test.

The results from the two listening tests for the eight subjects are shown in Figure 8.1, along with results from when I took these tests four times. The mean between the eight listeners are 15% and 84% for monopole and dipole changes respectively. My averages are roughly half these values. In the students' results and

my results the JND in monopole source strength is 5.6 and 6.1 times smaller than the JND in dipole source strengths respectively.

Note that in the dipole source strength test the result refers to the same increase to all three orthogonal dipole source strengths, i.e. an 84% increase to all three parameters. Is is also worth noting that the point in space chosen as the 'listening point' for the listening tests was with the parameters θ and φ from Equation (7.25) equal to 45 degrees and r equal to 0.45 metres (see Figure 2.4 for definitions of these parameters).

These results show that the monopole source strength is a much more influential parameter on the perceived sound than the dipole source strengths. This is to be expected when looking back at Figure 7.11 and comparing the level of the monopole sound pressure relative to the three dipole sound pressure levels. The mean of the measured monopole sound pressure from the sound-field data is 0.47 Pa/N whereas the sum of the three means of the dipole sound pressures is 0.14 Pa/N. Therefore a small percentage increase in the monopole source strength will be a greater increase in the total sound pressure than the equivalent percentage change in the dipole source strengths.

An increase of 15% in the monopole source strength of all modes in the guitar model corresponds to an increase in the mean total sound pressure response of the instrument from 0-5 kHz of 1.1 dB. The equivalent calculation for an 84% increase in dipole source strengths corresponds to an increase in mean total sound pressure response of 0.6 dB. Repeating the above calculation for the frequency band 0-1.5 kHz results in an increase of 1.1 dB for both monopole and dipole results. This can be explained in the following way. Increasing the monopole source strengths shifts the total sound pressure response curve upwards evenly across its frequency range because it is the strongest component at all frequencies. On the other hand increasing the dipole source strengths tends to boost the total sound pressure response below 1.5 kHz much more than those above 1.5 kHz. Thus, this fact suggests that the main cue for perceiving an increase to all dipole source strengths is a boost in frequencies below 1.5 kHz whereas the main cue for perceiving an increase in all monopole source strengths is more like a broadband change in loudness.

It is worth noting that the above discussion depends heavily on the source size parameters of the model, which tend to influence the balance between low and high-frequency base level of the individual sound pressure response curves.

8.2 Experiment II: Importance of effective masses of low-order modes

This experiment was designed to evaluate the relative importance of low-order modes, i.e. weigh-up the sensitivity of changes to modes with $\omega_0/2\pi$<400 Hz and modes with $\omega_0/2\pi$>400 Hz. This was done by carrying out a total of four listening tests: two measuring JNDs in effective masses of all modes below 400 Hz and two tests measuring JNDs in effective masses of modes from 400-5000 Hz. The stimulus of one test in each category was a chord of low notes and the other test had a stimulus of higher notes. The notes were chosen such that the fundamentals of the low notes were all below 400 Hz and the fundamentals of all the high notes were above 400 Hz.

Six subjects took the four tests here, this time the listeners were all amateur musicians. The stimuli were constructed in a similar manner described in the previous section, but this time using different notes. Two tests used low-pitch notes in the E major chord, which were B_2, E_3, and $G\#_3$ with fundamental frequencies of 123.5, 164.8 and 207.7 Hz respectively. The other two tests used high-pitch notes in the E major chord, which were $G\#_4$, B_4, and E_5 with fundamental frequencies of 415.3, 493.9 and 659.3 Hz respectively.

The tests were taken in the same room as before using the same laptop and headphones.

8.2.1 Results and discussion

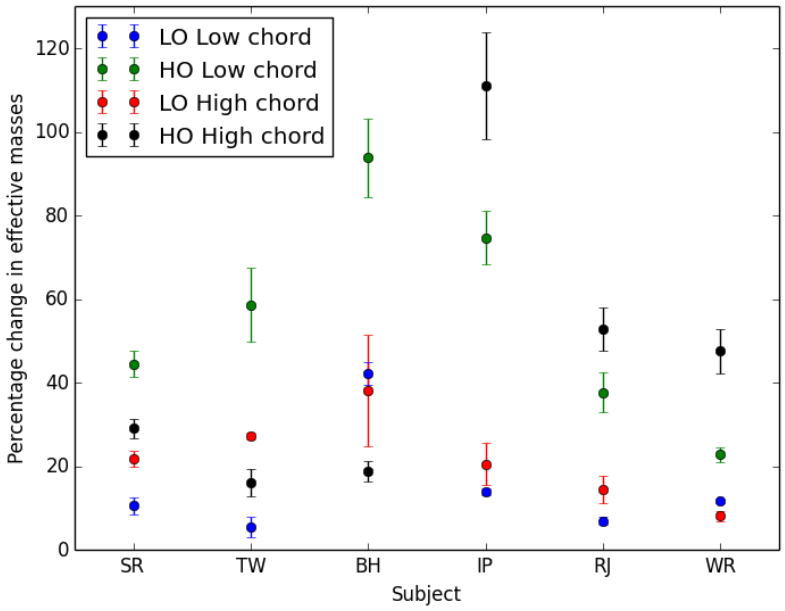

Figure 8.2: Results for six subjects in four listening tests. LO and HO refer to modifications to low-order and high-order modes, low chord refers to low-pitch notes and high chord refers to high-pitch notes.

Figure 8.2 shows the results for the second experiment in this chapter. The results of 'IP' and 'RJ' are the only ones that appear in the same order. Although not all listeners are sensitive to the same changes, the mean results help to show, on average, how much the effective mass must be modified to produce a perceivable change.

Test	Mean %	Standard error of the mean %
Low-order modes, low-pitch chord	15	5
High-order modes, low-pitch chord	55	9
Low-order modes, high-pitch chord	22	4
High-order modes, high-pitch chord	46	13

Table 8.1: Averages and standard deviations of the results shown in Figure 8.2.

Table 8.1 summarises the results showing averages and standard errors of each test. These values show that changes to low-order modes are about twice as easy to detect as changes to high-order modes for high-pitch notes, and about four times as easy for low-pitched notes. They also show that changes in the vibrational properties of an instrument are more obvious if the modes that undergo the change have a similar frequency to the fundamental frequency of the notes in the listening test. The above statements are consistent with previous work at Cardiff (Wright 1996; Richardson et. al. 2008), but the results presented here help to quantify more accurately the perceived difference in the radiated sound due to changes in the vibrational behaviour of the instrument.

It is interesting to note that according to some of the listeners, the main cue for the third listening test listed in Table 8.1 was the loudness of the 'thud' of the body noise in the low-frequency range, which was below the frequency of the lowest fundamental. Although low-order modes with low effective masses are generally thought of as a 'good' quality to a classical guitar, these modes also add a percussive element to high-pitch notes on the instrument. The added percussive element may be an unwanted quality by some players but perhaps is a desirable quality for other players.

In retrospect, it would have been interesting to ask each listener to write down and describe how they perceived the difference between the reference and modified tones in each test. Alternatively, using a short list of commonly used words to

describe the tone quality of a classical guitar, each subject could point out what change they could hear in the modified sound, similar to the work of Fritz et. al. (2012). This extra information would have been useful in analysing the results and helpful to inform the instrument maker of the type of change that results from modifying the vibrational behaviour of a guitar.

Chapter 9 Discussions and Conclusions

In this chapter the results from Chapters 4, 6, 7 and 8 will be discussed and the main conclusions of the research are given. Ways of improving certain methods used in this research are suggested as well as possible future work. It is more convenient however to organise this chapter according to the three aims of the work. Therefore this chapter is split into three sections: comparison between plucked-string instruments, wolf notes on the classical guitar and JND in parameters of a classical guitar model.

9.1 Comparison between plucked-string instruments

The first measurements carried out to compare the three plucked-string instruments studied in this thesis were of the radiated sound of a classical guitar, folk guitar and banjo. The initial amplitudes, Q values and frequencies of string partials were extracted from the radiated sound and the following observations were made.

The balance of initial amplitudes between low- and high-order partials, shown in Figure 4.4a, was most even for the folk guitar and least even for the banjo. This is likely to result in the folk guitar having a brighter tone quality and the banjo having a duller tone quality with the classical guitar somewhere in between. The underlying reason behind these different tone qualities was demonstrated in Figure 4.16, showing the mean admittance in octave bands relative to the mean admittance up to

5 kHz. Here it was shown that above 1.3 kHz the folk guitar has the highest relative admittance level and the banjo has the lowest relative admittance level.

Comparing the Q values of the string partials showed that the folk guitar had the longest sustain, especially the plain strings on the instrument. The slightly lower string-body coupling level of the folk guitar may contribute towards its longer sustain, but the main reason is because of the low internal damping of the strings themselves. The plain nylon strings of the classical guitar had a relatively short sustain due to a larger amount of internal damping. Although the banjo's strings are made of steel the low-order partials of the banjo had the smallest Q values. This is because of the strong string-body coupling in the banjo's low-frequency range resulting in the energy of the string being rapidly transferred to the banjo-head. Towards higher-frequencies the string-body coupling of the banjo decreases and the level of the Q values of the string partials raises above that of the classical guitar.

Fitting a simple model for the inharmonicity of the strings due to their stiffness, given by Equation (4.1), showed good agreement for the two guitars, but a poorer fit was found for the banjo. This was because of the strong string-body coupling in the banjo that was not taken into account in the simple inharmonicity model. Similar results for the inharmonicity factor B were found here to that reported by Woodhouse et al. (2012). The one result that stood out from the rest here was the inharmonicity of the G string on the classical guitar. This was found to be around twice the value of any other string on the instrument and creates an uneven tone quality between the strings that is well-known to classical and flamenco guitarists. A possible avenue for a small future project would be to find out to what extent guitarists, general musicians and non-musicians can hear the difference between the inharmonicity of the G string and other strings on the classical guitar. The results would be of interest to string manufacturers and challenge their current solutions to produce a string that has a more acceptable level of inharmonicity such as nylon-wound nylon strings.

The program that was developed to extract the parameters of string partials (described in Section 3.1) was imperative for the above analysis and proved useful throughout this work for comparing tones. The accuracy of initial amplitude measurements have been greatly improved here by addressing the problem of leakage error (described in Section 3.2).

The analysis mentioned above did not yield conclusive evidence of the difference in tone quality between these types of instruments because of the lack of data. To take this work further data from many classical guitars, folk guitars and banjos should be collected. Using larger sample groups it would become clearer

whether the above observations are consistent for many instruments within the same category.

Although it was shown through waterfall plots that the string components clearly dominate the radiated sound from plucked-string instruments, for a more comprehensive comparison it would be interesting to extract and compare the parameters of the body thud for each instrument as well as the string partials. It is likely that the stronger the string-body coupling of the instrument, the stronger the presence of the body thud. Hence the banjo has a more percussive element than that of the folk guitar. The thud is analogous to a consonant sound at the beginning of words like “buy” and “die”; they have a similar vowel sound that dominates the sound of the word but it is the short-lived transient at the beginning that tells us the identity of the word. It is likely that a similar auditory process aids us to distinguish between the sounds of two instruments within the same family.

After measuring the characteristic impedance of the strings on each instrument and the admittance of the bodies, the global coupling level could be computed, shown in Figure 4.17. Woodhouse (2004b) made a similar calculation for three classical and flamenco guitars and five violins. He found a very strong family resemblance for the guitars and for the violins, but they were very different from each other. It was therefore not a surprising result to see that the banjo produced a very different curve from that of the two guitars, but a larger difference was expected between the classical and folk guitars. As mentioned previously, the higher coupling level of the banjo is because its head is much more flexible than the wooden soundboards of the guitars. The most significant difference between the global coupling curves of the two guitars was the frequencies of the two lowest-frequency peaks rather than coupling level itself. This result suggests that there is little difference between the two instruments and so the global coupling level is not very useful to distinguish between these two types of guitar.

The coupling level of the banjo was much higher than that of the two guitars, which means that the banjo is very susceptible to wolf notes. It was shown in Section 4.3.3 that the admittance curves of the two banjos measured in this thesis were very similar. The lowest resonance of the two banjos was within 1 Hz of the fundamental of the note G_3. The next resonance on these instruments was also tuned to roughly the same frequency, which was less than 1 Hz from the note F_4. Given the findings and discussion on wolf notes it seems incongruous that a banjo player would set up their instrument such that the frequencies of the body modes would coincide with notes played on the instrument. However, it seems that many notes on the banjo undergo perceivable frequency and Q value perturbations to the point where the

perturbations of one note do not stand out from others. These perturbations are a general characteristic of the sound of the instrument and are a part of its acoustical signature.

The next comparison to make between the classical guitar, folk guitar and banjo is their modal parameters. In the low-frequency region of the mechanical responses of these instruments (eight lowest-frequency body modes) no significant difference was found between their modal spacing measured in cents. There was no real difference in Q values of the low-order modes between the two guitars. The Q values of the guitars were around 1.6 times larger than the modal Q values of the banjo. Woodhouse et al. (2012) found the JND in Q value of all modes of a guitar model to be a scale factor of 1.2, therefore this difference is possibly perceivable but perhaps not particularly obvious, as was found by Richardson et al. (2008).

The main difference between the parameters of low-order modes of these instruments was the effective masses, with an average of 0.83, 1.93 and 0.03 kg for the classical guitar, folk guitar and banjo respectively. In Chapter 8 the JND for the effective masses of low-order modes of a guitar model was measured to be around 18% or a scale factor of 1.2. With a difference of a factor of two between the effective masses of the two guitars and nearly three orders of magnitude between the guitars and the banjo, this parameter is the obvious choice for the instrument maker as the most important one to control.

At the beginning of the study modelling the three instruments was not considered to be useful in highlighting further differences between the instruments. However, applying the same synthesis model to all three instruments led to estimates of modal parameters up to 5 kHz. This also highlighted the importance of an accurate model for the damping of the different types of strings. It was found that the mean modal spacing of the two guitars was approximately constant with increasing frequency, as is expected for a plate-like structure (Fletcher and Rossing 1998), having an average spacing of around 43 Hz. On the other hand, the head of the banjo acts more like a membrane than a plate and so the modal spacing decreases with frequency. It is difficult to tell whether this is perceptually important to the banjo's acoustical signature because the effective masses of the banjo's higher-order modes are substantially higher than the lower-order ones, therefore unlikely to contribute much to the radiated sound.

The Q values of the guitars were again very similar, although slightly lower for the folk guitar. The Q values of the banjo seemed to follow quite a different trend as they were roughly proportional to frequency. There was a region of large variation between 1-3 kHz that corresponded to the frequencies of the after-lengths. Once again the banjo held some interesting effects towards higher-frequencies, but these

are unlikely to affect the tone quality of the instrument because of the low output level towards higher-frequency.

The pattern of mean effective masses used to fit the admittance curves of the three instruments was very different. The mean effective masses of modes in frequency bands are plotted against the band's central frequency in Figure 9.1. In the case of the classical guitar and banjo the effective mass increases with frequency. A logarithmic curve seemed to fit the effective masses of the classical guitar better than a linear fit, where a linear fit suited that of the banjo better. Note that one could not expect the effective masses of the banjo to increase indefinitely, but this relation seems to hold for the frequency range studied here.

The effective masses of the folk guitar do not seem to have any simple relation with frequency. This is reflected in the mean admittance in bands relative to total mean admittance graph in Figure 4.16 and its effect on the radiated sound has been discussed in an early paragraph in the section. The lowest relative admittance for this folk guitar calculated in octave bands is around 1 kHz, which corresponds to large effective masses in Figure 9.1 around this frequency. There is then an increase in relative admittance level around 2 kHz corresponding to the decrease in effective mass seen below.

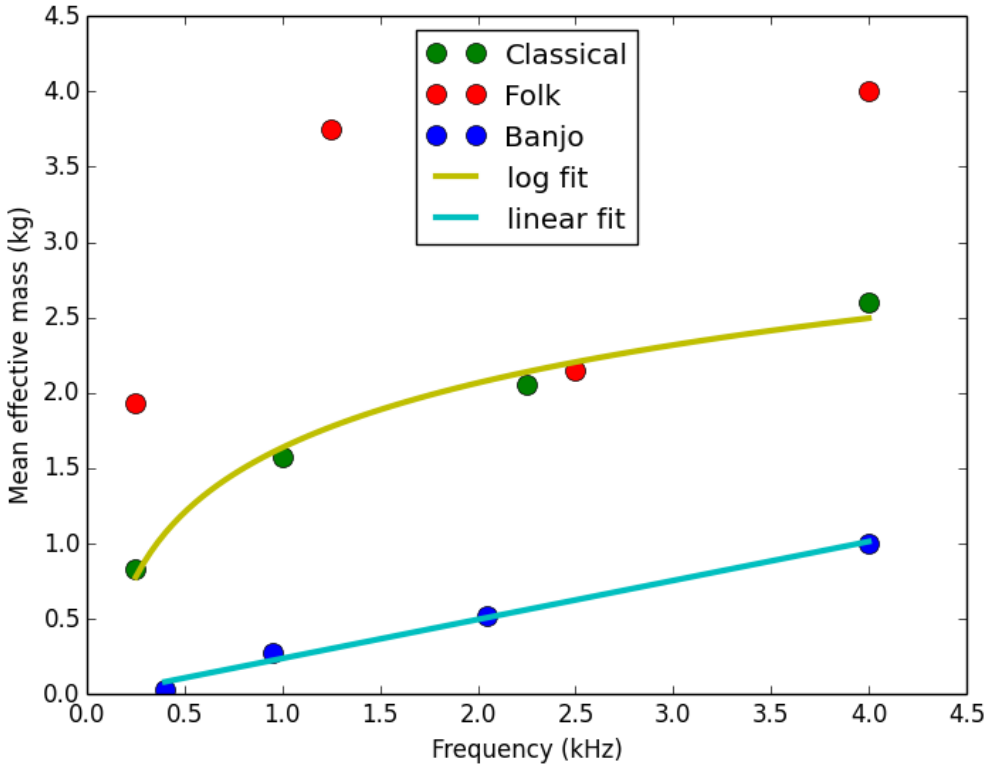

Figure 9.1: Mean effective masses of frequency bands used for physical modelling plotted against central frequency of the band in kHz. A log fit suited the trend of the classical guitar data points and a linear fit was best suited to the banjo data. No simple fit suited the trend of the effective masses of the modes of the folk guitar.

It would be well worth making similar investigations on other folk guitars, as well as classical guitars and banjos, to see whether these are common traits of instruments in their respective families or if they are unique to the instruments studied here.

A brief investigation into the modal shapes of two classical guitars, two steel-string guitars and a banjo highlighted the following observations. Given the shape of the outline of the guitar body it is important to have a strut, or struts, below the sound hole that will restrict the T(1,1) modes to the lower bout, where the strings are coupled to the body. In the case of the classical guitar this comes in the form of a basic horizontal strut below the sound hole and for the folk guitar the X-shaped struts works to the same effect. A more symmetric design can lead to poor radiation from the T(2,1) mode in front of the instrument, but can also gain from a more strongly radiating $T(1,1)_2$ mode. The large tension of steel strings mean that a strong X-shaped strutting pattern is used for the folk guitar; this means that some modes that are important for the radiation of sound in the classical guitar, such as the T(3,1), are less important for the folk guitar. The fine detail of the strutting seems to have a greater effect on higher-order modes, which have less influence over the overall tone quality (see Section 8.2.1).

Considering the apparent drop in effective masses of modes between 2-3 kHz on the folk guitar, perhaps the fine detail of the strutting gives this instrument a more balanced tone quality between low and high-order partials. Once again, data from more instruments would help support this hypothesis. If this lower effective mass region is consistent for this type of guitars, some psychoacoustical work would also be useful in determining whether this drop in effective mass is perceivable.

The folk guitar was chosen to compare with the classical guitar because it has a thicker soundboard and a more robust bracing therefore the string-body coupling was expected to be much lower than that of the classical guitar. The measured difference in coupling level was much smaller than anticipated, but further investigations carried out on the folk guitar led to the following conclusions that should be of interest to instrument makers. It is the smaller damping in the steel strings that result in the folk guitar having a longer sustain. The higher tension steel strings have led to a different bracing design being employed in the folk guitar that seems to contribute towards a brighter tone quality by decreasing the effective masses of modes between 2-3 kHz. The classical guitar studied here had a better bass response because its low-order modes are lower in frequency. There was no significant difference in modal spacing or Q values between the folk and classical guitars. This information may help instrument makers carry out better-informed

strategies to control the balance in tone quality between lower and higher-frequencies.

The banjo was chosen to compare with the classical guitar because the level of coupling between the string and the body is much higher in the banjo. The difference was obvious this time from the global coupling graphs. The very high coupling level leads to many wolf notes on the banjo, yet this is not considered a problem on this instrument because so many notes undergo these perturbation effects, these are a part of the instrument's acoustical signature. There were some interesting effects towards the higher-frequencies in the mechanical response of the banjo such as decreasing modal spacing and increasing Q values. These effects are the result of the banjo having a membrane instead of a plate as its main radiating component. Although the higher-frequency region on the banjo follows a different tend from other plucked-string instrument studied in the literature, it is unlikely that these characteristics play a significant role in the instrument's acoustical signature and are therefore not particularly useful for the maker.

9.2 Wolf notes on the classical guitar

The work on wolf notes here carried on from the work of Gough (1982), who derived a model to describe the dynamics of a coupled string-body system. The emphasis here was put on finding out whether perturbations to frequency and Q value of coupled string-body modes on the classical guitar are perceivable.

Gough's formulation was used and detailed expressions were derived for frequency and Q value perturbations. The model was compared with real data showing good agreement for string-body modes within around 10 Hz of each other. It was then possible to explore the dynamics of the coupled system and predict the amount of perturbation for a given interaction between a string partial and body mode as a function of coupling strength. Exploring the model in this way would be insightful for instrument makers because they could estimate the amount of perturbation that will occur if they built an instrument in a certain way.

This work was then taken further by carrying out psychoacoustical work to find the JND in frequency and Q value to a typical fundamental of a low-range note on the guitar. The results from these listening tests were then fed back into the model along with some measurements on a real guitar to yield coupling threshold curves that show the perceivable wolf notes on the instrument.

Previous investigations on the guitar studied at Cardiff (Wright 1996) found that frequencies of body modes are liable to shift as much as 5% due to atmospheric changes. This suggests that a more insightful measure of the wolf note is to measure the width of the coupling threshold curves at the coupling level of the string-body system and to quote this width in units of cents. This is called the width of the wolf note. It was also discussed in Chapter 6 that the results for frequency perturbation should be treated with more credibility than the result for Q value perturbation because of the parameters chosen for the reference sounds in the listening tests.

The width of wolf notes on a classical guitar could perhaps be treated as a measure of quality of the instrument. As mentioned previously, a high-quality instrument will be very responsive to the player's touch. This means the low-order modes should have a low effective mass, but of course this can lead to over-coupling of the string to the body. Therefore the width of the wolf note on a classical guitar can indicate the trade-off between responsiveness and perceivable wolf notes.

To eliminate an existing wolf note on an instrument the coupling strength must be decreased. This can be done by decreasing the mass of the string or increasing the effective mass of the body mode. In Section 4.3.2 the results of an experiment were presented where mass was added to the anti-nodal region of a mode of a guitar. Although a relatively straightforward relation was found between mass loading and effective mass of the body mode, adding mass to the soundboard of a guitar is not a wise method of eliminating a wolf note. For the case described in Section 6.2.4 it was shown that choosing a slightly lighter string on that particular guitar would reduce the wolf note width by 20%, which is at least worth a try from the player's point of view.

To take this work further it would firstly be useful to carry out more listening tests. Persuading a group of professional guitarists as well as a group of general musicians to take the tests would put this work into a clearer context by clarifying the amount of perturbation that is perceivable to each group. Secondly it would be interesting to build up a data bank of modal parameters of low-order modes on a range of guitars, and to ask players whether they think the most severe wolf note on the instrument is acceptable or not. These two points would make the problem of wolf notes on the classical guitar clearer so that instrument makers would better understand the severity of the problem and also the boundaries of an acceptable string-body coupling level.

Christensen (1980) was the first to point out the importance of the ratio A/M, which is the effective area (or source strength used in this thesis) divided by the effective mass of a mode. A large value of this ratio leads to a strongly radiating mode, hence a strongly radiating instrument. The work carried out on wolf notes in

this thesis indicates that there is a minimum cut-off point for the value of the effective mass of certain modes. Therefore future work should perhaps concentrate on the effective area of modes to try and maximise the sound output from the instrument.

A final piece of advice that could help instrument makers in this area is to take into consideration the strings that will be used on an instrument before starting the building process. If the player intends to use lighter strings (lower tension) then the maker can make the soundboard thinner, the heavier the strings the thicker the soundboard should be. Instrument makers probably use this rule of thumb to some extent because a larger tension is needed for heavier strings so a stronger soundboard is needed. However, this tip is useful for fulfilling tonal objectives as well as structural ones.

9.3 JNDs in parameters of a classical guitar model

Results were given in Chapter 8 from two psychoacoustical experiments using the guitar model developed for this research. The first experiment was to evaluate the relative importance of monopole and dipole radiation from the classical guitar by measuring the JNDs in their respective source strengths. The two listening tests in the first experiment were taken by a group of eight people, whom, for the purpose of comparing these results with those from the literature, are labelled as non-musicians. The JND in monopole source strength of all modes of the instrument was 15%, and the JND in dipole source strengths was 84%. These results indicate that the monopole component of the radiated sound is much more influential to the overall sound output than dipole components. It is worth reminding the reader that the modelled instrument had a traditional fan or Torres bracing pattern and the quoted results might be slightly different if the guitar model was based on an instrument with an asymmetrical bracing pattern. It was noted in Section 8.1.1 that increasing the dipole source strength tended to boost the sound pressure below 1.5 kHz much more than above this frequency. Therefore, for this particular guitar model, the main cue for the JND in dipole source strength was an increase in sound pressure below 1.5 kHz.

Comparing the above results with similar experiments in the literature, the JNDs found here are larger than expected. As previously mentioned, Woodhouse et al. (2012) found the JND in Q value of all modes to be 20%. Wright (1996) found that changes to effective masses and effective areas led to large changes in the perceived

sound quality whereas changes to the Q values of modes led to much more subtle changes in the sound quality. A similar conclusion was reached by Richardson et al. (2008). Therefore one would expect the JND in monopole source strength to be much less than the JND in Q values. As this is not the case one must compare the details of the tests carried out by Woodhouse with the tests carried out here. Woodhouse used musicians as well as non-musicians to take his listening tests, where the former have been shown to achieve smaller JNDs than the latter. Perhaps more significantly Woodhouse's result was the average of the four best results from a larger group of 13 listeners. Therefore no real comparison can be made between the two experiments because one is the average of eight non-musicians and the other is the average of four musicians who performed the best out of a larger sample group.

The second experiment here was on changing the effective masses of low-order modes (below 400 Hz) and higher-order modes (above 400 Hz). For this experiment it was decided that it would be worth using both low-frequency notes and higher-frequency notes as the stimulus, resulting in a total of four listening tests. These tests were taken by six amateur musicians. The results indicated that it is easier to achieve smaller JNDs in a test where the frequencies of the modes undergoing the change are within the vicinity of the notes of the stimulus. Also, it is easier to achieve smaller JNDs in tests where changes are made to low-order modes rather than higher-order modes regardless of the pitch of the stimulus. The latter point supports the notion that effective mass is a global parameter (Wright 1996), because the JND for low-order modes with a high-pitch stimulus was less than half the JND of high-order modes using a low-pitch stimulus, that is, the effective mass of low-order modes have significant influence over notes well above their resonant frequencies.

The results of the second experiment are difficult to relate to the findings of Fritz et al. (2007), who carried out similar listening tests using a violin model. The changes in amplitude of the admittance implemented by Fritz were made by applying a Fourier filter directly to the admittance rather than changing modal parameters and generating the admittance curve from these parameters, as was done here. However, it is possible to approximate the conversion from admittance increase to the decrease in effective mass. The JND in amplitude of the admittance in the range 190-650 Hz, which includes the violin's low-order modes, was found to be around 3.7 dB and 6 dB for musicians and non-musicians respectively. This corresponds roughly to a scale factor of 1.5 and 2 respectively, which is much larger than the result found for the classical guitar here. The lowest JND in amplitude found in the admittance of the violin was between 1.3-4.2 kHz, yielding a JND of 3 dB and 5 dB for musicians and non-musicians respectively. This corresponds to a scale factor of about 1.4 and 1.8

respectively, still larger than the smallest results found here. One important difference between the experiments carried out here and those carried out by Fritz et al. is that the loudness of the stimuli used by Fritz were kept roughly constant so that the main cue for the listener was a change in tone quality rather than loudness. In the experiments carried out here the main aim was to find JNDs in the sound from any cue caused by a given parameter change, including loudness.

It is also worth mentioning that Fritz and Woodhouse both used a three-up one-down routine for their adaptive listening tests rather than the two-up one-down routine used here. This means that the experiments by Fritz and Woodhouse measured the 79% point on the psychometric function whereas the experiments carried out in this research measured the 71% point on the psychometric function. This discrepancy means that the experiments carried out here are likely to yield slightly smaller JNDs. The significance of choosing a two-up one-down test rather than a three-down one-up test is considered to be negligible compared with the significance of the points outlined above.

The JND found here in effective mass of all modes below 400 Hz was 15% using low-pitch notes as the stimulus. This is a reasonable result in comparison with the result of JND in monopole source strength from the first experiment. This is because the sound pressure, given by Equation (7.25), is proportional to monopole source strength for a point source (with only a small difference to a finite-sized source below 400 Hz) and is inversely proportional to the effective mass of a mode. Hence, as pointed out by Christensen (1984) and others at Cardiff (Wright 1996; Hill et al. 2004; Richardson et al. 2008), the value of the effective area is just as important as the value of the effective mass, and it is the value of the ratio A/M of a mode which is most important.

There is potential for a significant amount of further research to be done in this area. First of all there are many possible improvements to be made on the modelling side of the work. The model developed here seemed to have a weak fundamental in the transfer response at the bridge, yet the modelled sound pressure response had a fundamental that was too strong. The explanation for this was not found. Also, there were a few issues with the sound-field data. The sound-field measurement was made on a different day from the rest of the measurements meaning that atmospheric changes could have affected the pressure response of the instrument. The sound-field measurement was made with the hammer at a different striking position to the rest of the measurements. Also the sound-field data only went up to 2 kHz and had to be extrapolated up to 5 kHz. A purpose-made measurement of the sound-field would have improved some imprecise fits. Further attention could be given to the source

radius parameter, which has a strong influence over the balance between low and high frequency in the spherical-harmonic decomposition fits. Better fits would be possible by considering frequency-dependent source radii, or at least a different source radius for each of the three dipole orientations. As a final note on the modelling process it seemed that after moving on to other plucked-string instruments it became apparent that the process, including the fitting, becomes easier with a little practice.

There is not much to be said about improving the listening test procedure, the weakness here was the lack of subjects to take the tests, in particular the lack of musicians. Taking the mean of a sample of ten for a given test would be sufficient, but motivating ten musicians to take such tests would more than likely involve a financial contribution.

Some useful listening tests have been mentioned above, but there is further potential. It has been established through this work and previous work at Cardiff that the effective area and effective mass of low-order modes are the most influential parameters for the classical guitar. However, as mentioned above, these experiments have allowed loudness to be a cue in the listening experiments. Keeping the loudness constant, it would be possible to determine the frequency band of the guitar's response that is most influential on tone quality, similar to work carried out by Dünnwald (1991) and Fritz et al. (2007) for the violin. Perhaps then a different balance would be seen between the JND in effective masses of low-order modes and higher-order modes. The first step in doing this would be to look at the admittance of many classical guitars and decide on the different frequency bands to split up the response as well as judge the tonal difference in changing the amplitude of each band, as was done by Dünnwald (1991). Information from these tests would give instrument makers a target for making a 'brighter' sounding instrument, for example, or to give a guitar sound more 'clarity'.

Simpler listening tests that do not necessitate a physical model would also be of use to makers and musical acousticians. One example would be to explore the relation between JND in Q value of an exponentially decaying pure tone and the length of the stimulus. As mentioned previously in this thesis, experiments on damping of signals are much rarer in the literature than loudness and frequency.

References

Caldersmith, G. (1978) Guitar as a reflex enclosure. *Journal of the Acoustical Society of America* **63**(5), 1566-1575.

Christensen, O. (1983) Response of Played Guitars at Middle Frequencies. *Acustica* **53**(1), 45-48.

Christensen, O. (1984) Oscillator Model for Analysis of Guitar Sound Pressure Response. *Acustica* **54**(5), 289-295.

Christensen, O. and Vistisen, B. (1980) Simple model for low-frequency guitar function. *J. Acoust. Soc. Am.* **68**(3), 758-766.

Čížek, V. (1986) *Discrete Fourier Transforms and their Applications*. Bristol, Adam Hilger.

Craig, R. R. (1981) *Structural Dynamics, An Introduction to Computer Methods*. New York, Wiley.

D'addario. (2015) *D'addario tension chart* (Online). Available at: http://daddario.com/upload/tension_chart_13934.pdf (Accessed: 16/07/2015).

Darwin, C. J. et al. (1972) An auditory analogue of the sperling partial report procedure: Evidence for brief auditory storage. *Cognitive Psychology* **3**(2), 255-267.

Dickey, J. (2003) The structural dynamics of the American five-string banjo. *Journal of the Acoustical Society of America* **114**(5), 2958-2966.

Dünnwald, H. (1991) Deduction of objective quality parameters on old and new violins. *Catgut Acoustical Society* **1**(7), 1-5.

Ewins, D. J. (1985) *Modal Testing: Theory and Practice*. Research Studies Press Ltd.

Firth, I. M. (1978) Action of the cello at the wolf tone. *Acustica* **39**(4), 252-263.

Fletcher, N. H. and Rossing, T. D. (1998) *The Physics of Musical Instruments*. 2nd ed. New York, Springer.

Fritz, C. et al. (2012) Exploring violin sound quality: Investigating english timbre descriptors and correlating resynthesized acoustical modifications with perceptual properties. *Journal of the Acoustical Society of America* **131**(1), 783-794.

Fritz, C. et al. (2007) Perceptual thresholds for detecting modifications applied to the acoustical properties of a violin. *J. Acoust. Soc. Am.* **122**(6), 3640-3650.

Gough, C. (1984) The nonlinear free vibration of a damped elastic string. *Journal of the Acoustical Society of America* **75**(6), 1770-1776.

Gough, C. E. (1980) Resonant response of a violin G-string and the excitation of the wolf-note. *Acustica* **44**(2), 113-123.

Gough, C. E. (1981) Theory of String Resonances on Musical Instruments. *Acustica* **49**(2), 124-141.

Gura, P. and Bollman, J. (1999) *America's Instrument: The Banjo in the Nineteenth Century*. University of North Carolina Press.

Higgins, R. J. (1976) Fast Fourier transform: An introduction with some minicomputer experiments. *American Journal of Physics* **44**(8), 766-773.

Hill, T. J. W. et al. (2004) Acoustical parameters for the characterisation of the classical guitar. *Acta Acustica united with Acustica* **90**(2), 335-348.

Järveläinen, H. and Karjalainen, M. (2006) Perceptibility of inharmonicity in the acoustic guitar. *Acta Acustica united with Acustica* **92**(5), 842-847.

Kay, S. M. (1987) *Modern Spectral Estimation: Theory and Application*. New Jersey, Prectice Hall.

Kinsler, L. E. et al. (2000) *Fundamentals of Acoustics*. 4th ed. New York, Wiley.

Kock, W. E. (1937) The Vibrating String Considered as an Electrical Transmission Line. *The Journal of the Acoustical Society of America* **8**, 227-233.

Kreiman, J. and Gerratt, B. R. (2010) Perceptual sensitivity to first harmonic amplitude in the voice source. *The Journal of the Acoustical Society of America* **128**(4), 2085-2089.

Laroche, J. (1993) The use of the matrix pencil method for the spectrum analysis of musical signals. *The Journal of the Acoustical Society of America* **94**(4), 1958-1965.

Le Carrou, J. L. et al. (2009) Sympathetic string modes in the concert harp. *Acta Acustica united with Acustica* **95**(4), 744-752.

Le Carrou, J. L. et al. (2007) Experimental study of A0 and T1 modes of the concert harp. *The Journal of the Acoustical Society of America* **121**(1), 559-567.

Levitt, H. (1971) Transformed up-down methods in psychoacoustics. *J. Acoust. Soc. Am.* **49**(2), 467-477.

Lynn, P. A. (1977) *An Introduction to the Analysis and Processing of Signals*. The Macmillan Press.

Meyer, J. (1983a) The function of the guitar body and its dependence upon constructional details. In: *Function, Construction and Quality of the Guitar*. Ed: Jansson, E.V., Vol. 38. Royal Swedish Academy of Music, 77-109.

Meyer, J. (1983b) Quality aspects of the guitar tone. In: *Function, Construction and Quality of the Guitar*. Ed: Jansson, E.V., Vol. 38. Royal Swedish Academy of Music, 51-76.

Moore, B. C. J. (1997) *An Introduction to the Psychology of Hearing*. 4th ed. London, Academic Press.

Moore, B. C. J. et al. (1985) Thresholds for the detection of inharmonicity in complex tones. *J. Acoust. Soc. Am.* **77**(5), 1861-1867.

Morse, P. M. and Ingard, K. U. (1968) *Theoretical Acoustics*. 1st ed. McGraw-Hill.

Mostowski, A. and Stark, M. (1964) *Introduction to Higher Algebra*. New York, Pergamon Press.

Newland, D. E. (1989) *Mechanical Vibration Analysis and Computation*. New York, Wiley.

Perry, I. (2014) *Sound radiation measurements on guitars and other stringed musical instruments*. PhD Thesis, Cardiff University.

Porat, B. and Friedlander, B. (1987) On the Accuracy of the Kumaresan-Tufts Method for Estimating Complex Damped Exponentials. *IEEE Transactions on Acoustics, Speech, and Signal Processing* **35**(2), 231-235.

Rae, J. (2010) Banjo. In: *The Science of String Instruments*. Ed: Rossing, T.D. London, Springer, 59-75.

Rae, J. and Rossing, T. D. (2004) The acoustics of the banjo. In: *Proceedings of the ISMA conference*, Japan.

Richardson, B. E. (1982) *A physical investigation into some factors affecting the musical performance of the guitar*. PhD Thesis, University College, Cardiff.

Richardson, B. E. (1994) The Acoustic Development of the Guitar. *Catgut Acoustical Society* **2**(5), 1-10.

Richardson, B. E. et al. (2008) Plucked String Sound Analysis and Perception. In: *Proceedings of the Institute of Acoustics conference*. 437.

Richardson, B. E. et al. (2012) The three-mass model for the classical guitar revisited. In: *Proceedings of the Acoustics 2012 conference*, Nantes.

Richardson, S. J. (2001) *Acoustical Parameters for the Classical Guitar*. PhD Thesis, Cardiff University.

Rossing, T. D. et al. (2002) *The Science of Sound*. 3rd ed. London, Addison Wesley.

Schelleng, J. C. (1962) The Violin as a Circuit. *J. Acoust. Soc. Am.* **35**(3), 326-338.

Sloane, I. (1976) *Classical guitar construction*. London, Omnibus Press.

Stephey, L. A. and Moore, T. R. (2008) Experimental investigation of an American five-string banjo. *Journal of the Acoustical Society of America* **124**(5), 3276-3283.

Thompson, J. K. and Tree, D. R. (1980) Leakage Error in Fast Fourier Analysis. *Journal of Sound and Vibration* **71**(4), 531-544.

Valette, C. (1995) The Mechanics of Vibrating Strings. In: *Mechanics of Musical Instruments*. Ed: Hirschberg, A. et al. Vienna, Springer-Verlag.

Weinreich, G. (1977) Coupled piano strings. *J. Acoust. Soc. Am.* **62**(6), 1474-1484.

Weinreich, G. (1985) Sound hole sum rule and the dipole moment of the violin. *Journal of the Acoustical Society of America* **77**(2), 710-718.

Weinreich, G. (1993) Radiativity revisited: theory and experiment ten years later. In: *Proceedings of the SMAC93 conference*, Stockholm. 432-427.

Weinreich, G. (1995) Vibration and Radiation of Structures with Application to String and Percussion Instruments. In: *Mechanics of muscial instruments*. Ed: Hirschberg, A. et al. Vienna, Springer-Verlag.

Weinreich, G. and Arnold, E. B. (1980) Method for Measuring Acoustic Radiation Fields. *Journal of the Acoustical Society of America* **68**(2), 404-411.

Woodhouse, J. (2004a) On the synthesis of guitar plucks. *Acta Acustica* **90**(5), 928-944.

Woodhouse, J. (2004b) Plucked guitar transients: Comparison of measurements and synthesis. *Acta Acustica united with Acustica* **90**(5), 945-965.

Woodhouse, J. and Langley, R. S. (2012) Interpreting the input admittance of violins and guitars. *Acta Acustica united with Acustica* **98**(4), 611-628.

Woodhouse, J. et al. (2012) Perceptual thresholds for acoustical guitar models. *Acta Acustica united with Acustica* **98**(3), 475-486.

Wright, H. (1996) *The Acoustics and Psychoacoustics of the Guitar*. PhD Thesis, Cardiff University.